Proceedings of the Mini-Workshop

Advances in Hadronic Resonances

Bled, Slovenia, July 2 – 9, 2017

Edited by

Bojan Golli

Mitja Rosina

Simon Širca

University of Ljubljana and Jožef Stefan Institute

The Mini-Workshop *Advances in Hadronic Resonances*

Organizing Committee

Mitja Rosina, Bojan Golli, Simon Širca

List of participants

Marko Bračko, Ljubljana, `marko.bracko@ijs.si`
Bojan Golli, Ljubljana, `bojan.golli@ijs.si`
Viktor Kashevarov, Mainz, `kashev@kph.uni-mainz.de`
Itaru Nakagawa, RIKEN, `itaru@bnl.gov`
Hedim Osmanović, Tuzla, `hedim.osmanovic@untz.ba`
Willi Plessas, Graz, `willibald.plessas@uni-graz.at`
Saša Prelovšek, Ljubljana, `sasa.prelovsek@ijs.si`
Nikita Reichelt, Graz, `nikita.reichelt@uni-graz.at`
Mitja Rosina, Ljubljana, `mitja.rosina@ijs.si`
Helios Sanchis Alepuz, Graz, `helios.sanchis-alepuz@uni-graz.at`
Andrey Sarantsev, Bonn & Gatchina, `andsar@hiskp.uni-bonn.de`
Wolfgang Schweiger, Graz, `wolfgang.schweiger@uni-graz.at`
Simon Širca, Ljubljana, `simon.sirca@fmf.uni-lj.si`
Jugoslav Stahov, Tuzla, `jugoslav.stahov@untz.ba`
Igor Strakovsky, Washington, `igor@gwu.edu`
Yasuyuki Suzuki, Niigata, `yasuyuki_suzuki@riken.jp`
Alfred Švarc, Zagreb, `svarc@irb.hr`
Lothar Tiator, Mainz, `tiator@kph.uni-mainz.de`
Yannick Wunderlich, Bonn, `wunderlich@hiskp.uni-bonn.de`

Contents

Preface

Resonances remain an important tool to study the structure and dynamics of hadrons and an efficient catalyst for our traditional Mini-Workshops at Bled. The many ideas, questions and responses presented at our meeting should not fade away and we thank the participants for submitting their contributions to the Proceedings as a permanent reminder of our common interests and discussions.

An important aspect of the talks was the bridge between the phenomenological phase shift analyses and the theoretical interpretation of resonances. Attempts were shown to relate experimental data to pole parameters in a model-independent way, introducing additional constraints to obtain a unique solution. This year, the emphasis was on meson photoproduction, in particular of η and η′, as well as doubly-polarized pion electroproduction. Of interest was also pion photoproduction on bound neutrons and the forward neutron asymmetry in proton-nucleus collisions.

The Roper resonance is still a challenge. It is not clear to which extent it is predominantly a three-quark system or a dynamically generated resonance. The dynamics of other baryons also requires an extension beyond the valence quark configurations. The knowledge of the baryon form-factors has improved both due to new experimental analyses as well due to new theoretical perspectives, especially regarding transition form-factors.

It was interesting to learn about the cluster separability in relativistic few body problems, about phase rotation ambiguities, and about the progress in understanding strength functions in hadronic and nuclear dynamics.

The third emphasis was on new resonances in the charm sector. The meson and baryon resonances discovered at the Belle detector at KEKB are still being analysed in order to determine their quantum numbers and their double-$q\bar{q}$ or "molecular" dimeson structure. In view of the forthcoming Belle2 upgrade it is time to analyse the prospects of identifying the double charm baryons and the DD^* dimesons (tetraquarks).

We were very happy to host such enthusiastic participants. We do hope to meet you at Bled again soon and that you will enjoy reading these Proceedings and refresh your memories of the subjects of our common interest. Perhaps you might wish to offer these Proceedings to your colleagues as a temptation to join us at Bled in the near future.

Ljubljana, November 2017 B. Golli, M. Rosina, S. Širca

The full color version of the Proceedings are available at `http://www-f1.ijs.si/BledPub`, and the presentations can be found at `http://www-f1.ijs.si/Bled2017/Program.html`.

Predgovor

Resonance so še vedno pomembno orodje za študij zgradbe in dinamike hadronov, pa tudi učinkovit katalizator za naše tradicionalne Blejske delavnice. Mnoge zamisli, vprašanja in odzivi, ki smo jih predstavili na našem srečanju, ne smejo oveneti, zato se zahvaljujemo udeležencem, da so poslali svoje prispevke kot trajen spomin na naša skupna zanimanja in razprave.

Pomemben vidik predavanj je bil most med fenomenološko analizo faznih premikov in teoretičnim tolmačenjen resonanc. Predstavljeni so bili poskusi, kako povezati eksperimentalne podatke s parametri polov na modelsko neodvisen način, s tem da se vpeljejo dodatni pogoji, ki vodijo do enolične rešitve. Letos je bil poudarek na fotoprodukciji mezonov, zlasti η in η′, pa tudi na elektroprodukciji dvojno polariziranih pionov. Zanimiva je bila tudi fotoprodukcija pionov na vezanih nevtronih ter asimetrija nevtronov, ki letijo naprej pri trkih protonov na jedrih.

Roperjeva resonanca predstavlja še vedno izziv. Ni še jasno, do katere mere je pretežno sistem treh kvarkov ali dinamično povzročena resonanca. Dinamika mnogih drugih barionov tudi zahteva razširitev modelov na konfiguracije, ki presegajo zgolj valenčne kvarke. Poznavanje barionskih oblikovnih faktorjev se je izpopolnilo zaradi novih eksperimentalnih analiz kakor tudi zaradi novih teoretičnih pogledov, zlasti v zvezi z oblikovnimi faktorji za prehode.

Zanimiv je bil vpogled v ločljivost gruč pri relativističnem problemu malo teles, v mnogoličnost rotacije faz, pa tudi napredek pri razumevanju jakostnih funkcij v hadronski in jedrski dinamiki.

Tretji poudarek je bil na novih resonancah v čarobnem sektorju. Mezonske in barionske resonance, ki so jih odkrili na detektorju Belle na pospeševalniku KEKB, še vedno analizirajo, da bi določili njihova kvantna števila in njihovo "molekularno" dimezonsko zgradbo v zvezi z dvojnimi pari qq̄. V perspektivi skorajšnjega povečanja detektorja Belle2 je čas, da prevetrimo možnosti identifikacije dvojno čarobnih barionov ter dimezonov (tetrakvarkov) DD∗.

Čutimo se srečne, da smo se družili s tako navdušenimi udeleženci. Upamo, da vas bomo spet kmalu videli na Bledu in da boste uživali branje tega Zbornika in osvežili spomine na probleme našega skupnega zanimanja. Morda boste ponudili ta Zbornik svojim kolegom kot vabo, da se nam v bližnji prihodnosti pridružijo na Bledu.

Ljubljana, november 2017   B. Golli, M. Rosina, S. Širca

Barvno verzijo lahko dobite na `http://www-f1.ijs.si/BledPub` in prosojnice predavanj na `http://www-f1.ijs.si/Bled2017/Program.html`.

Workshops organized at Bled

▷ *What Comes beyond the Standard Model*
　　　(June 29–July 9, 1998), Vol. **0** (1999) No. 1
　　　(July 22–31, 1999)
　　　(July 17–31, 2000)
　　　(July 16–28, 2001), Vol. **2** (2001) No. 2
　　　(July 14–25, 2002), Vol. **3** (2002) No. 4
　　　(July 18–28, 2003), Vol. **4** (2003) Nos. 2-3
　　　(July 19–31, 2004), Vol. **5** (2004) No. 2
　　　(July 19–29, 2005), Vol. **6** (2005) No. 2
　　　(September 16–26, 2006), Vol. **7** (2006) No. 2
　　　(July 17–27, 2007), Vol. **8** (2007) No. 2
　　　(July 15–25, 2008), Vol. **9** (2008) No. 2
　　　(July 14–24, 2009), Vol. **10** (2009) No. 2
　　　(July 12–22, 2010), Vol. **11** (2010) No. 2
　　　(July 11–21, 2011), Vol. **12** (2011) No. 2
　　　(July 9–19, 2012), Vol. **13** (2012) No. 2
　　　(July 14–21, 2013), Vol. **14** (2013) No. 2
　　　(July 20–28, 2014), Vol. **15** (2014) No. 2
　　　(July 11–20, 2015), Vol. **16** (2015) No. 2
　　　(July 11–19, 2016), Vol. **17** (2016) No. 2
　　　(July 10–18, 2017), Vol. **18** (2017) No. 2
▷ *Hadrons as Solitons* (July 6–17, 1999)
▷ *Few-Quark Problems* (July 8–15, 2000), Vol. **1** (2000) No. 1
▷ *Statistical Mechanics of Complex Systems* (August 27–September 2, 2000)
▷ *Selected Few-Body Problems in Hadronic and Atomic Physics* (July 7–14, 2001),
　　　Vol. **2** (2001) No. 1
▷ *Studies of Elementary Steps of Radical Reactions in Atmospheric Chemistry*
　　　(August 25–28, 2001)
▷ *Quarks and Hadrons* (July 6–13, 2002), Vol. **3** (2002) No. 3
▷ *Effective Quark-Quark Interaction* (July 7–14, 2003), Vol. **4** (2003) No. 1
▷ *Quark Dynamics* (July 12–19, 2004), Vol. **5** (2004) No. 1
▷ *Exciting Hadrons* (July 11–18, 2005), Vol. **6** (2005) No. 1
▷ *Progress in Quark Models* (July 10–17, 2006), Vol. **7** (2006) No. 1
▷ *Hadron Structure and Lattice QCD* (July 9–16, 2007), Vol. **8** (2007) No. 1
▷ *Few-Quark States and the Continuum* (September 15–22, 2008),
　　　Vol. **9** (2008) No. 1
▷ *Problems in Multi-Quark States* (June 29–July 6, 2009), Vol. **10** (2009) No. 1
▷ *Dressing Hadrons* (July 4–11, 2010), Vol. **11** (2010) No. 1
▷ *Understanding hadronic spectra* (July 3–10, 2011), Vol. **12** (2011) No. 1
▷ *Hadronic Resonances* (July 1–8, 2012), Vol. **13** (2012) No. 1
▷ *Looking into Hadrons* (July 7–14, 2013), Vol. **14** (2013) No. 1
▷ *Quark Masses and Hadron Spectra* (July 6–13, 2014), Vol. **15** (2014) No. 1
▷ *Exploring Hadron Resonances* (July 5–11, 2015), Vol. **16** (2015) No. 1
▷ *Quarks, Hadrons, Matter* (July 3–10, 2016), Vol. **17** (2016) No. 1
▷ *Advances in Hadronic Resonances* (July 2–9, 2017), Vol. **18** (2017) No. 1

η and η′ photoproduction with EtaMAID including Regge phenomenology⋆

V. L. Kashevarov, L. Tiator, M. Ostrick

Institut für Kernphysik, Johannes Gutenberg-Universität, D–55099 Mainz, Germany

Abstract. We present a new version of the EtaMAID model for η and η′ photoproduction on nucleons. The model includes 23 nucleon resonances parameterized with Breit-Wigner shapes. The background is described by vector and axial-vector meson exchanges in the t channel using the Regge cut phenomenology. Parameters of the resonances were obtained from a fit to available experimental data for η and η′ photoproduction on protons and neutrons. The nature of the most interesting observations in the data is discussed.

EtaMAID is an isobar model [1,2] for η and η′ photo- and electroproduction on nucleons. The model includes a non-resonant background, which consists of nucleon Born terms in the s and u channels and the vector meson exchange in the t channel, and s-channel resonance excitations, parameterized by Breit-Wigner functions with energy dependent widths. The EtaMAID-2003 version describes the experimental data available in 2002 reasonably well, but fails to reproduce the newer polarization data obtained in Mainz [3]. During the last two years the EtaMAID model was updated [4–6] to describe the new data for η and η′ photoproduction on the proton. The presented EtaMAID version includes also η and η′ photoproduction on the neutron.

At high energies, $W > 3$ GeV, Regge cut phenomenology was applied. The models include t-channel exchanges of vector (ρ and ω) and axial vector (b_1 and h_1) mesons as Regge trajectories. In addition to the Regge trajectories, also Regge cuts from rescattering $\rho\mathbb{P}$, ρf_2 and $\omega\mathbb{P}$, ωf_2 were added, where $\mathbb{P}$ is the Pomeron with quantum numbers of the vacuum $0^+(0^{++})$ and f_2 is a tensor meson with quantum numbers $0^+(2^{++})$. The obtained solution describes the data up to $E_\gamma = 8$ GeV very well. For more details see Ref. [7]. Energies below $W = 2.5$ GeV are dominated by nucleon resonances in the s channel. All known resonances with an overall rating of two stars and more were included in the fit. To avoid double counting from s and t channels in the resonance region, low partial waves with L up to 4 were subtracted from the t-channel Regge contribution.

The most interesting fit results are presented in Figs. 1-5 together with corresponding experimental data.

In Fig. 1, the total $\gamma p \to \eta p$ cross section is shown. A key role in the description of the investigated reactions is played by three s-wave resonances N(1535)1/2−,

---

⋆ Talk presented by V. Kashevarov
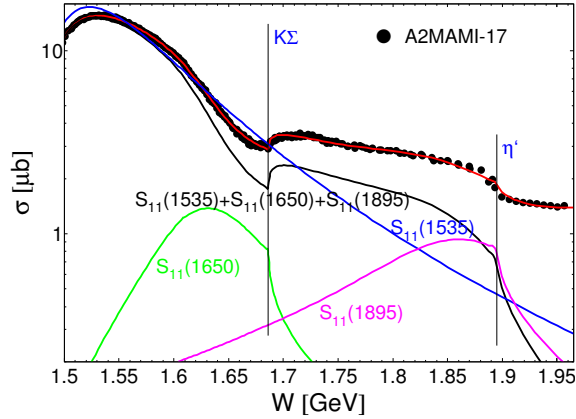
Fig. 1. (Color online) Total cross section of the $\gamma p \rightarrow \eta p$ reaction with partial contributions of the main nucleon resonances. Red line: New EtaMAID solution. Vertical lines correspond to thresholds of $K\Sigma$ and $\eta' N$ photoproduction. Data: A2MAMI-17 [6].
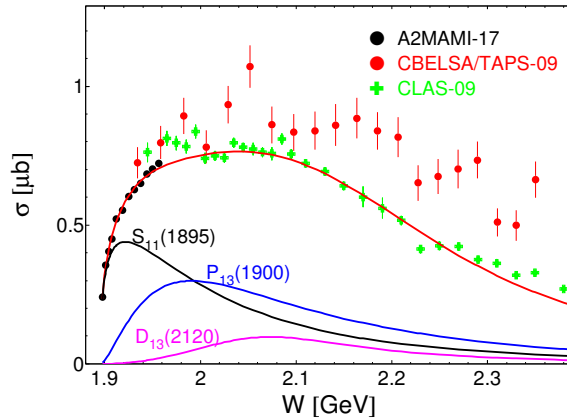
Fig. 2. (Color online) Total cross section of the $\gamma p \rightarrow \eta' p$ reaction with partial contributions of the main nucleon resonances. Red line: New EtaMAID solution. Data: A2MAMI-17 [6], CBELSA/TAPS-09 [9], and CLAS-09 [10].

$N(1650)1/2^-$, and $N(1895)1/2^-$, see partial contributions of these resonances in Fig. 1. The first two give the main contribution to the total cross section and are known very well. An interference of these two resonances is mainly responsible for the dip at $W = 1.68$ GeV. However, the narrowness of this dip we explain as a threshold effect due to the opening of the $K\Sigma$ decay channel of the $N(1650)1/2^-$ resonance. The third one, $N(1895)1/2^-$, has only a 2-star overall status according to the PDG review [10]. But we have found that namely this resonance is responsible for the cusp effect at $W = 1.96$ GeV (see magenta line in Fig. 1) and provides a fast increase of the total cross section in the $\gamma p \rightarrow \eta' p$ reaction near threshold (see black line in Fig. 2). A good agreement with the experimental data was

obtained for the cross sections of the $\gamma p \rightarrow \eta'p$ reaction, Fig. 2. The main contributions to this reaction come from $N(1895)1/2^-$, $N(1900)3/2^+$, and $N(2130)3/2^-$ resonances.
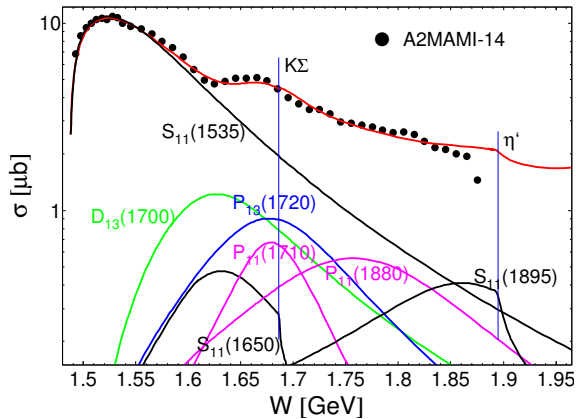

Fig. 3. (Color online) Total cross section of the $\gamma n \rightarrow \eta n$ reaction with partial contributions of the main nucleon resonances. Red line: New EtaMAID solution. Data: A2MAMI-14 [11].

Very interesting results were obtained during the last few years for the $\gamma n \rightarrow \eta n$ reaction. The excitation function for this reaction shows an unexpected narrow structure at $W \sim 1.68$ GeV, which is not observed in $\gamma p \rightarrow \eta p$. As an example, the total cross section measured with highest statistics in Mainz [11] is shown in Fig. 3. The nature of the narrow structure has been explained by different authors as a new exotic nucleon resonance, or a contribution of intermediate strangeness loops, or interference effects of known nucleon resonances, see Ref. [12]. In our analyses, the narrow structure is explained as the interference of s, p, and d waves, see partial contributions of the resonances in Fig. 3. Our full solution, red line in Fig. 3, describes the data up to $W \sim 1.85$ GeV reasonably well and shows a cusp-like structure at $W = 1.896$ GeV similar as in Fig. 2 for the $\gamma p \rightarrow \eta p$ reaction. However, the data demonstrate a cusp-like effect at the energy of ~ 50 MeV below. This remains an open question for our analyses as well as for the final state effects in the data analysis.

Recently, the CLAS collaboration reported a measurement of the beam asymmetry Σ for both $\gamma p \rightarrow \eta p$ and $\gamma p \rightarrow \eta'p$ reactions [13]. At high energies, $W > 2$ GeV, the $\gamma p \rightarrow \eta p$ data have maximal Σ asymmetry at forward and backward directions, see Fig. 4. We have found that an interference of $N(2120)3/2^-$ and $N(2060)5/2^-$ resonances is responsible for such an angular dependence. The data was refitted excluding the resonances with mass around 2 GeV. The most significant effect we have found by refitting without $N(2120)3/2^-$ (black line) and $N(2060)5/2^-$ (blue line). The red line is our full solution.

The beam asymmetry Σ for $\gamma p \rightarrow \eta'p$ reaction is presented in Fig. 5 with the GRAAL data [14] having a nodal structure near threshold. Such a shape of the an-
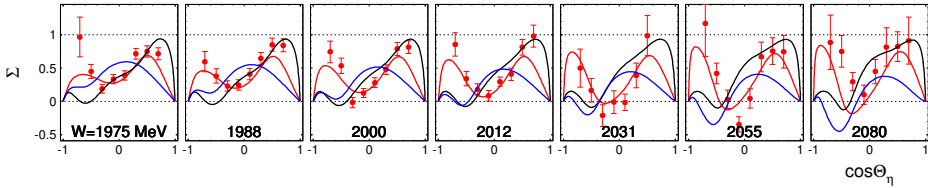
Fig. 4. (Color online) Beam asymmetry Σ for the $\gamma p \rightarrow \eta p$ reaction. Red line: New Eta-MAID solution. Results of the refit to the data without $N(2120)3/2^-$ are shown by the black lines and without $N(2060)5/2^-$ - blue lines. Data: CLAS-17 [13],
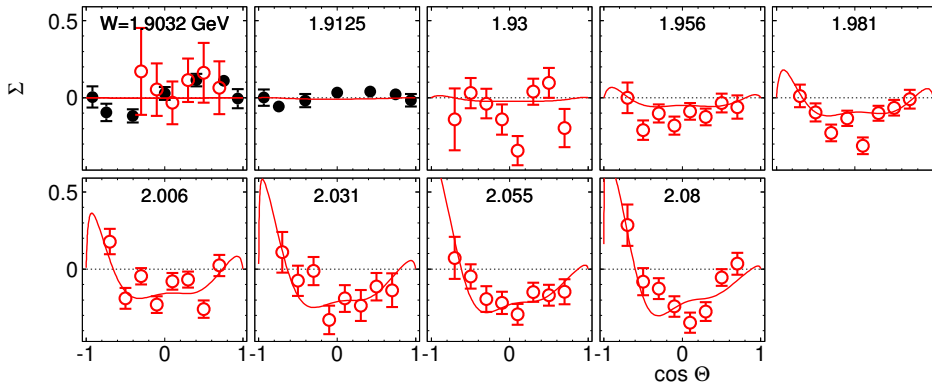
Fig. 5. Beam asymmetry Σ for the $\gamma p \rightarrow \eta' p$ reaction. Red line: New EtaMAID solution. Data: GRAAL-15 [14] (black), CLAS-17 [13] (red).

gular dependence could be explained by interference of s and f or p and d waves. However, the energy dependence is inverted in all models. The EtaMAID-2016 solution [5] describes the shape of the GRAAL data for Σ, but not the magnitude. The new CLAS data [13] can not solve this problem because of poor statistics new threshold. Our new solution describes the Σ data well at $W > 1.95$ GeV.

In summary, we have presented a new version ηMAID-2017n updated with new resonances and new experimental data. The model describes the data currently available for both η and η' photoproduction on protons and neutrons. The cusp in the η total cross section, in connection with the steep rise of the η' total cross section from its threshold, is explained by a strong coupling of the $N(1895)1/2^-$ to both channels. The narrow bump in ηn and the dip in ηp channels have a different origin: the first is a result of an interference of a few resonances, and the second is a threshold effect due to the opening of the $K\Sigma$ decay channel of the $N(1650)1/2^-$ resonance. The angular dependence of Σ for $\gamma p \rightarrow \eta p$ at $W > 2$ GeV is explained by an interference of $N(2120)3/2^-$ and $N(2060)5/2^-$ resonances. The near threshold behavior of Σ for $\gamma p \rightarrow \eta' p$, as seen in the GRAAL data, is still an open question. A further improvement of our analysis will be possible with additional polarization observables which soon should come from the A2MAMI, CBELSA/TAPS, and CLAS collaborations.

References

1. W. -T. Chiang, S. N. Yang, L. Tiator, and D. Drechsel, Nucl. Phys. **A700**, 429 (2002).
2. W.-T. Chiang, S. N. Yang, L. Tiator, M. Vanderhaeghen, and D. Drechsel, Phys. Rev. C **68**, 045202 (2003).
3. J. Akondi *et al.* (A2 Collaboration at MAMI), Phys. Rev. Lett. **113**, 102001 (2014).
4. V. L. Kashevarov, M. Ostrick, L. Tiator, Bled Workshops in Physics, Vol.**16**, No.1, 9 (2015).
5. V. L. Kashevarov, M. Ostrick, L. Tiator, JPS Conf. Proc. **13**, 020029, (2017).
6. V. L. Kashevarov *et al.* (A2 Collaboration at MAMI), Phys. Rev. Lett. **118**, 212001 (2017).
7. V. L. Kashevarov, M. Ostrick, L. Tiator, Phys. Rev. C **96** 035207 (2017).
8. C. Patrignani *et al.* (Particle Data Group), Chin. Phys. C **40**, 100001 (2016).
9. V. Crede *et al.* (CBELSA/TAPS Collaboration), Phys. Rev. C **80**, 055202 (2009).
10. M. Williams *et al.* (CLAS Collaboration), Phys. Rev. C **80**, 045213 (2009).
11. (A2 Collaboration at MAMI), D. Werthmüller *et al.* , Phys. Rev. C **90**, 015205 (2014).
12. (A2 Collaboration at MAMI), L. Witthauer *et al.* , Phys. Rev. C **95**, 055201 (2017).
13. P. Collins *et al.*, (CLAS Collaboration), Phys. Lett. B **771** , 213 (2017).
14. P. Levi Sandri *et al.* (GRAAL Collaboration), Eur. Phys. J. A **51** , 77 (2015).

The role of nucleon resonance via Primakoff effect in the very forward neutron asymmetry in high energy polarized proton-nucleus collision

I. Nakagawa for the PHENIX Collaboration

RIKEN, 2-1 Hirosawa, Wako, Saitama 351-0198, Japan

Abstract. A strikingly strong atomic mass dependence was discovered in the single spin asymmetry of the very forward neutron production in transversely polarized proton-nucleus collision at $\sqrt{s} = 200$ GeV in PHENIX experiment at RHIC. Such a drastic dependence was far beyond expectation from conventional hadronic interaction models. A theoretical attempt is made to explain the A-dependence within the framework of the ultra peripheral collision (Primakoff) effect in this document using the Mainz unitary isobar (MAID2007) model to estimate the asymmetry. The resulting calculation well reproduced the neutron asymmetry data in combination of the asymmetry comes from hadronic amplitudes. The present EM interaction calculation is confirmed to give consistent picture with the existing asymmetry results in $p^{\uparrow} + Pb \rightarrow \pi^0 + p + Pb$ at Fermi lab.

1 Nuclear Dependence of Spin Asymmetry of Forward Neutron Production

Large single spin asymmetries in very forward neutron production seen [1] using the PHENIX zero-degree calorimeters [2] are a long established feature of transversely polarized proton-proton collisions at RHIC in collision energy $\sqrt{s} = 200$ GeV. Neutron production near zero degrees is well described by the one-pion exchange (OPE) framework. The absorptive correction to the OPE generates the asymmetry as a consequence of a phase shift between the spin flip and non-spin flip amplitudes. However, the amplitude predicted by the OPE is too small to explain the large observed asymmetries. A model introducing interference of pion and a_1-Reggeon exchanges has been successful in reproducing the experimental data [3]. The forward neutron asymmetry is formulated as

$$A_N \propto \phi_{\text{flip}} \phi_{\text{non-flip}} \sin \delta \qquad (1)$$

where ϕ_{flip} ($\phi_{\text{non-flip}}$) is spin flip (spin non-flip) amplitude between incident proton and out-going neutron, and δ is the relative phase between these two amplitudes. Although the OPE can contribute to both spin flip and non-flip amplitudes, resulting A_N is small due to the small relative phase. The decent amplitude can be generated only by introducing the interference between spin flip π exchange and spin non-flip a_1-Reggeon exchange which has large phase shift in between [3].

During the RHIC experiment in year 2015, RHIC delivered polarized proton collisions with gold (Au) and aluminum (Al) nuclei for the first time, enabling the exploration of the mechanism of transverse single-spin asymmetries with nuclear collisions. The observed asymmetries showed surprisingly strong A-dependence in the inclusive forward neutron production [4] and the data even change the sign of A_N from p + p to p + A as shown in Fig.1, while the existing framework which was successful in p + p only predicts moderate A-dependence and does not have any mechanism to flip the sign of A_N in any p + A collision systems [5]. Thus the observed data are absolutely unexpected and unpredicted. The p + Au data point shows magnificently large A_N of about 0.18 which is three times larger than that of p + p in absolute amplitude.
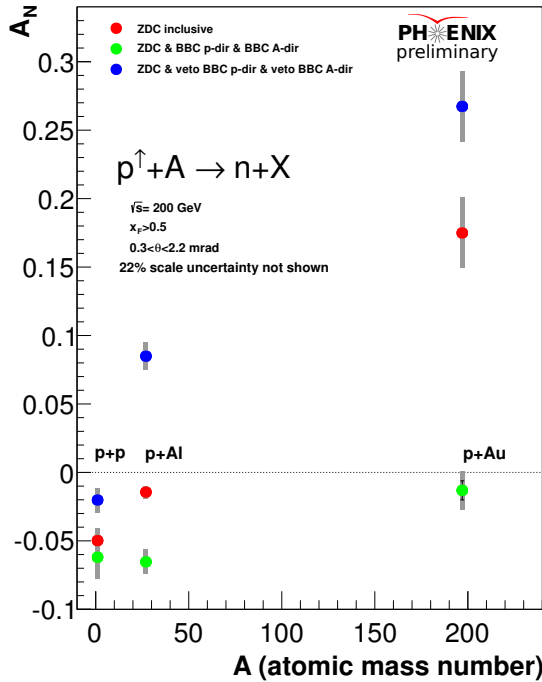
Fig. 1. (Color online) Observed forward neutron A_N in transversely polarized proton-nucleus collisions [4]. Data points are A=1, A=27, and A=197 are results of p + p, p+Al, and p+Au, respectively. Red, Blue and Green data points are neutron inclusive, neutron + BBC veto, and BBC tagged events, respectively.

More interestingly, another drastic dependence of A_N was observed in correlation measurements in addition to the inclusive neutron. In these measurements, another out-going charged particle was either tagged or vetoed within the acceptance of the beam-beam counter (BBC) in both North and South arms which covers $3.1 \leq |\eta| \leq 3.9$. The BBCs cover such a limited acceptance, but the resulting asymmetries behaved remarkably contradicts. Once BBC hits (BBC tagging) are

required in both arms (green data points), the drastic behavior of inclusive A_N is vanished and no flipping sign was observed between p + p and p + Au. On the contrary, the asymmetries are pushed even more positive for p + Al and p + Au data points once no hits in BBC are required (BBC vetoed) as represented by blue data points. Further details of the experiment are discussed in reference [4].

2   Ultra-Peripheral Collision (Primakoff) Effects

Due to the smallness of the four momentum transfers of the present kinematics, i.e. $-t \leq 0.5$ (GeV/c)^2, the EM interaction may play a role which becomes increasingly important in large atomic number nucleus. The EM field of the nucleus becomes rich source of exchanging photons between the polarized proton. This is known as the ultra-peripheral collision (UPC) in heavy ion collider experiments. In the UPC process, there is no charge exchange at the collision vertex unlike π or a_1 meson exchange.

The description of A_N is thus extended from Eq. (1) to Eqn. (2), which includes not only hadronic but also EM amplitudes:

$$
\begin{aligned}
A_N \propto\ & \phi_{\text{flip}}^{\text{had}} \phi_{\text{non-flip}}^{\text{had}} \sin \delta_1 + \phi_{\text{flip}}^{\text{EM}} \phi_{\text{non-flip}}^{\text{had}} \sin \delta_2 \\
& + \phi_{\text{flip}}^{\text{had}} \phi_{\text{non-flip}}^{\text{EM}} \sin \delta_3 + \phi_{\text{flip}}^{\text{EM}} \phi_{\text{non-flip}}^{\text{EM}} \sin \delta_4
\end{aligned}
\tag{2}
$$

where 'EM' and 'had' stand for electromagnetic and hadronic interactions, and $\delta_1 \sim \delta_4$ are relative phases, respectively. The second and the third terms are known as Coulomb nuclear interference (CNI), which is observed to cause $< 5\%$ asymmetry of elastic scattering in p + p, and p+ C processes [6]. However the known asymmetry induced by the CNI is not sufficient enough to explain the present large asymmetry as large as 18%. The main focus of this document is thus the fourth term, namely the EM interference term. Before starting discussion on the EM interaction in the present neutron asymmetry, another asymmetry experiment in Fermi Lab is to be introduced in the next section.

3   Fermi's Primakoff Experiment

Here I introduce one interesting experiment which may be related with the present forward neutron asymmetry. The experiment [7] was executed in Fermi laboratory using the high energy 185 GeV transversely polarized proton beam. A large analyzing power observed in π^0 production from Pb fixed nuclear target in $|t'| < 1 \times 10^{-3}$ (GeV/c)^2 where Coulomb process is expected to play predominant role. Shown in the left panel of Fig. 2 is the invariant-mass spectrum of the $\pi^0 p$ system in $p^\uparrow + Pb \rightarrow \pi^0 + p + Pb$ for $|t'| < 1 \times 10^{-3}$ (GeV/c)^2. The prominent peak in region I ($W < 1.36$ GeV/c) is the $\Delta(1232)$ and the second bump is due to $N^*(1520)$ resonances. The large negative analyzing power $A_N \sim -0.57 \pm 0.12$ was observed in the region II of the invariant mass 1.36 to 1.52 GeV, while A_N was consistent with zero in the lower mass $W < 1.36$ GeV region. The authors claim

this is due to the interference between the spin-flipping Δ(P33) and spin non-flipping N*(P11) resonance amplitudes as shown in the panel (a) and (b) in Fig. 3 via the Primakoff (electro-magnetic EM interaction) effect. The P11 resonance can be N*(1440) and higher resonances.
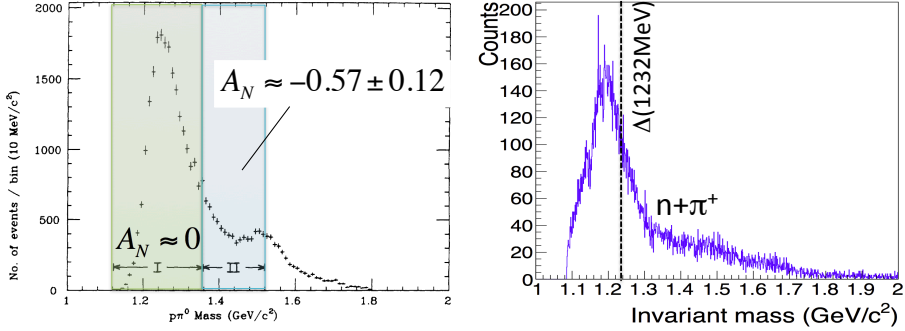
Fig. 2. (Left) The invariant-mass spectrum of the $\pi^0 + p$ system in $p^\uparrow + Pb \to \pi^0 + p + Pb$ for $|t'| < 1 \times 10^{-3}$ $(GeV/c)^2$ [7]. Peaks due to the $\Delta^+(1232)$ and N*(1520) resonances are shown. (Right) The Invariant mass spectrum of the Monte-Carlo simulation of the EM effect for RHIC experiment.
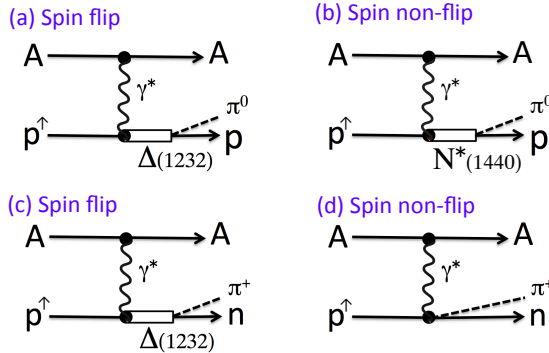
Fig. 3. The Feynman diagrams of possible spin flip and spin non-flipping amplitudes which may play key roles to produce large asymmetries in π^0 (top row) and π^+ (bottom row) productions. (d) is non-resonant π^+ production as known as Kroll-Rudermann term [14].

There are non-trivial differences between the present neutron production at RHIC and the above π^0 production at Fermi experiments. Some key experimental conditions are listed in Table 1. Due to coincidence detection of π^0 and p in the Fermi experiment, the invariant mass W of $\pi^0 p$ system is determined experimentally, while only neutron is detected in RHIC experiment. Therefore the invariant mass of $\pi^+ n$ system can only be predicted by the Monte-Carlo. Shown in the right panel of Fig. 2 is the invariant mass spectrum of $\pi^+ n$ system predicted by the Monte-Carlo assuming EM interaction for the RHIC experiment [10]. The nuclear photon yield is calculated by STARLIGHT model [8] while

unpolarized $\gamma^* p \rightarrow \pi^+ n$ is calculated using SOPHIA model [9]. The neutron energy cut $x_F = E_n/E_p > 0.4$ is applied to be consistent with the experiment [4] where E_n is the energy of the outgoing neutron and E_p is the incident proton beam energy. As can be seen, the prominent peak is located slightly below $\Delta(1232\text{MeV})$ peak since the equivalent photon yield is weighted to lower energy in the nuclear Coulomb field [10]. The momentum transfer are defined $t' = t - (W^2 - m^2)^2/4P_L^2$ for the Fermi experiment[1], whereas t is defined as $-t = m_n^2(1 - x_F)^2/x_F + p_T^2/x_F$ for the RHIC experiment, where m_n is neutron mass, and p_T is the transverse momentum of neutron. Unfortunately, the momentum transfers are not defined consistently between two experiments due to undetected π^+ in the RHIC experiment.
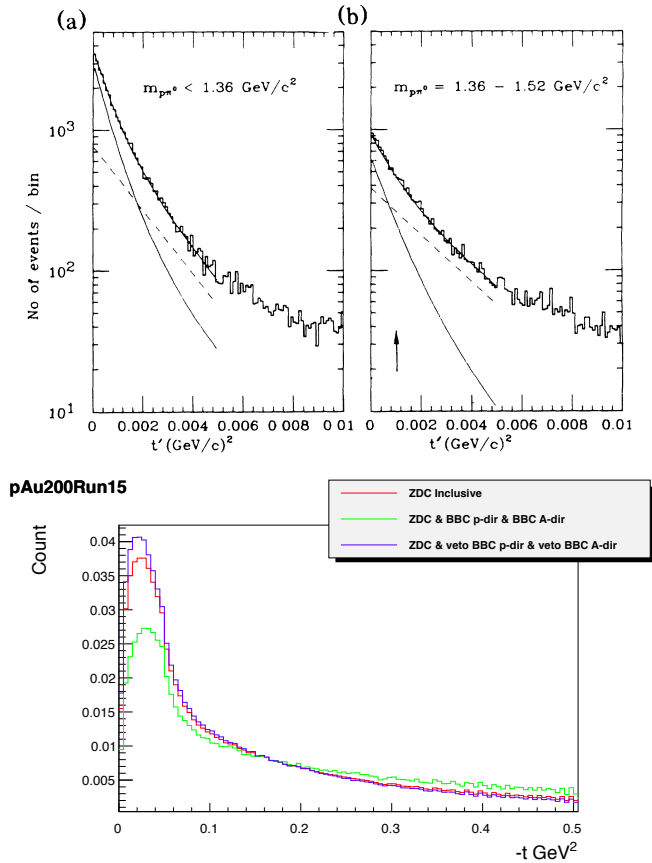
Fig. 4. (Top) The t' distributions of the $\pi^0 p$ system in $p^\uparrow + Pb \rightarrow \pi^0 + p + Pb$ for $W < 1.36$ GeV and $1.36 < W < 1.52$ GeV, respectively. The finite asymmetry was observed in the region $|t'| < 1 \times 10^{-3}$ $(\text{GeV/c})^2$ of panel (b) [7]. (Bottom) The experimental momentum transfer distributions of the RHIC experiment for 3 different trigger selections. (Color online)

---

[1] See reference [7] for the definition.

Table 1. The difference of experimental conditions between RHIC [4] and Fermi [7] experiments.

	Fermi	RHIC
Beam Energy E_p [GeV]	185	100
$\sqrt{s}$ [GeV]	19.5	200
Target nucleus	Pb	Au
Detected particle(s)	$p + \pi^0$	n
Momentum transfer $(GeV/c)^2$	$|t'| < 0.001$	$0.02 < -t < 0.5$
Invariant mass W [GeV]	$1.36 < W < 1.52$	
A_N	$-0.57 \pm (0.12)_{sta} + 0.21 - 0.18$	$+0.27 \pm 0.003$

4 Asymmetry Induced by Photo-Pion Production

Pion production reaction from nucleon are intensely studied in various medium energy real photon and electron beam facilities. See reference [11] as one of review articles. The present forward neutron asymmetries via UPC effect corresponds to the photo-pion production from a transversely polarized fixed target. The polarized γ^*p cross section is given as Eq. (4):

$$\frac{d\sigma_{\gamma^*p^\uparrow \to \pi^+ n}}{d\Omega_\pi} = \frac{|q|}{\omega_{\gamma^*}}\{R_T^{00} + P_y R_T^{0y}\} \tag{3}$$

$$= \frac{|q|}{\omega_{\gamma^*}}[R_T^{00}\{1 + P_2 \cos\phi_\pi T(\theta_\pi^*)\}] \tag{4}$$

where R_T^{00} is the unpolarized, while R_T^{0y} is target polarized response functions, respectively. $T(\theta_\pi^*)$ corresponds to the definition of the present analyzing power $A_N = T(\theta_\pi^*) = R_T^{0y}/R_T^{00}$. θ_π^* represents production angle of π in the center-of-mass system. There are several theoretical/phenomenological fitting models available to describe photo-pion production observables. Here I quote Mainz unitary isobar model, namely MAID2007 [12] to calculate the asymmetries in the present kinematics.

Shown in Fig. 5 is the MAID prediction of the unpolarized response function R_T^{00} plotted as a function of the invariant mass W of pion and nucleon systems at $Q^2 = 0(GeV/c)^2$ and $\theta_\pi^* = 40°$. The multipoles are weak function of $Q^2(= -t)$ and only moderately change within our kinematic coverage $-t < 0.5 \ (GeV/c)^2$. The leading order multipole decomposition following the notation of reference [13] is given in Eq. (5):

$$R_T^{00} = \frac{5}{2}|M_{1+}|^2 + M_{1+}^* M_{1-} + 3M_{1+}^* E_{1+} + ... \tag{5}$$

where M_{1+} is famous magnetic dipole transition amplitude from the nucleon ground state to the $\Delta(P33)$ resonance state. As blue curve indicates, the $\gamma^*p \to$

R00 (Q2=0, theta*pi=40deg)
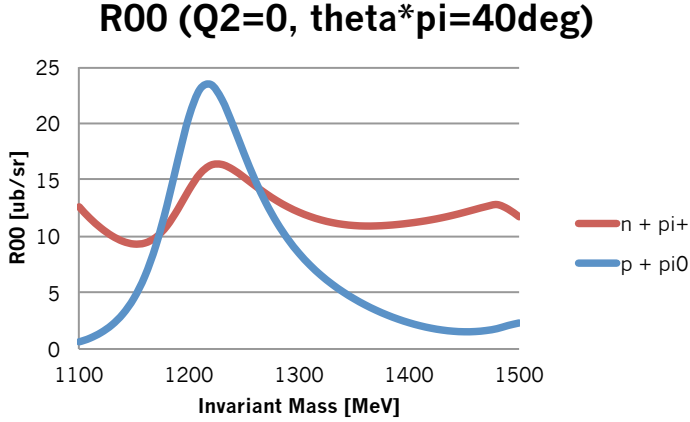
Fig. 5. (Color online) Unpolarized $R_T^{00}(W)$ response function at $Q^2 = 0(\text{GeV}/c)^2$ and $\theta_\pi^* = 40°$ plotted as a function of the invariant mass W [MeV]. Red and blue curves represent MAID predictions for $\gamma^*p \to \pi^+ + n$ and $\gamma^*p \to \pi^0 + p$ decay channels, respectively.

$\pi^0 p$ channel shows distinctive peak around well known Δ resonance region ($W = 1232$ MeV) in Fig. 5. This is mainly driven by the dominant $|M_{1+}|^2$ term in Eq. (5). On the contrary, the Δ peak is not as distinctive as π^0 channel for the π^+ channel and shows rather larger cross section in the threshold pion production region below Δ. This is due to enhanced charge coupling of photon to the pion field in the target proton which doesn't exist for π^0 channel. This is known as Kroll-Rudermann term [14] as shown in the diagram (d) in Fig. 3.

Shown in Fig. 6 is the target polarization response function $R_T^{0y}(W)$ of the MAID predictions for $\gamma^*p^\uparrow \to \pi^+n$ (red) and $\gamma^*p^\uparrow \to \pi^0p$ (blue) decay channels, respectively. The leading order multipole decomposition of R_T^{0y} is denoted as Eq. (6):

$$R_T^{0y} = \text{Im}\{E_{0+}^*(E_{1+} - M_{1+}) - 4\cos\theta_\pi^*(E_{1+}^*M_{1+})....\} \qquad (6)$$

The asymmetries show peak structure around Δ region for both π^+ and π^0 channels, while the sign is opposite. The magnitude of asymmetry is substantially as large as $R_T^{0y} \sim 15[\mu b/st]$ for π^+ channel compared to π^0 channel. This is because of the strong interference between E_{0+} and M_{1+} channel in π^+ channel as appears in the first term in Eqn.6. The amplitude of E_{0+} is much greater in π^+ channel compared to π^0 channel due to aforementioned Kroll-Rudermann term. Although dominant Δ amplitude, i.e. M_{1+} is even stronger in π^0 channel, this interference is relatively minor due to smallness of E_{0+} for π^0 channel.

The obtained analyzing power A_N for MAID predictions by taking the ratio of response functions $R_T^{0y}(W)$ and $R_T^{00}(W)$ are shown in Fig. 7 plotted as a function of the invariant mass W at $Q^2 = 0(\text{GeV}/c)^2$ and $\theta_\pi^* = 40°$. Note there are distinctive difference between π^+ and π^0 channels in A_N as a function of W according to the MAID model. π^+ shows remarkably large asymmetry over $A_N > 0.8$
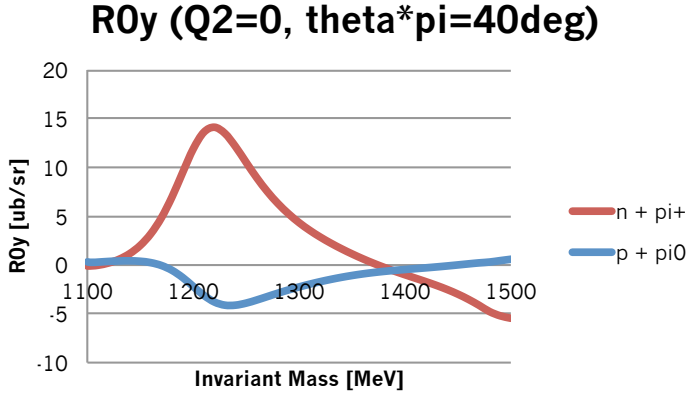
Fig. 6. (Color online) Polarized $R_T^{0y}(W)$ response function at $Q^2 = 0(\text{GeV}/c)^2$ and $\theta_\pi^* = 40°$ plotted as a function of the invariant mass W [MeV]. Red and blue curves represent MAID predictions for $\gamma^*p^\uparrow \to \pi^+ n$ and $\gamma^*p^\uparrow \to \pi^0 p$ decay channels, respectively.

just below $\Delta(1232\text{ MeV})$ due to the interference between E_{0+} of Kroll-Rudermann and Δ dipole resonance M_{1+} terms. The contribution of this invariant mass region to the observed neutron is large due to matching peak of the invariant mass yield as shown in the right panel of Fig.2.
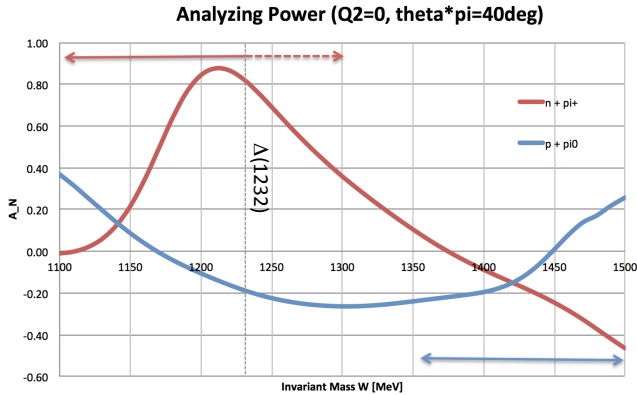
Fig. 7. (Color online) Analyzing power $A_N(W)$ at $Q^2 = 0(\text{GeV}/c)^2$ and $\theta_\pi^* = 40°$ plotted as a function of the invariant mass W [MeV]. Red and blue curves represent MAID [12] predictions for $\gamma^*p^\uparrow \to \pi^+ n$ and $\gamma^*p^\uparrow \to \pi^0 p$ decay channels, respectively.

The MAID is in general known to fit reasonably well to photo-pion production data in low to medium energy region. Shown in Fig. 8 is the analyzing power $T(= A_N)$ of MAID (red curve) fits to $\gamma^*p^\uparrow \to \pi^+ p$ reaction data observed in PHOENICS experiment at ELSA [15]. For the comparison, Argonne-Osaka [16]

model fits are also shown in blue curve. Although some model dependence is seen in higher energies $W > 1365$ MeV in the θ_π^* region where no data, two models are fairly consistent to each other in lower energies $W < 1319$ MeV. Although the ELSA data is not necessarily perfect overlap with the kinematic range of the present RHIC data, the extrapolation of data by MAID seem to give reasonable estimate since the data coverage is sufficiently large in W bins below Δ which are rather weighted for the present neutron data.
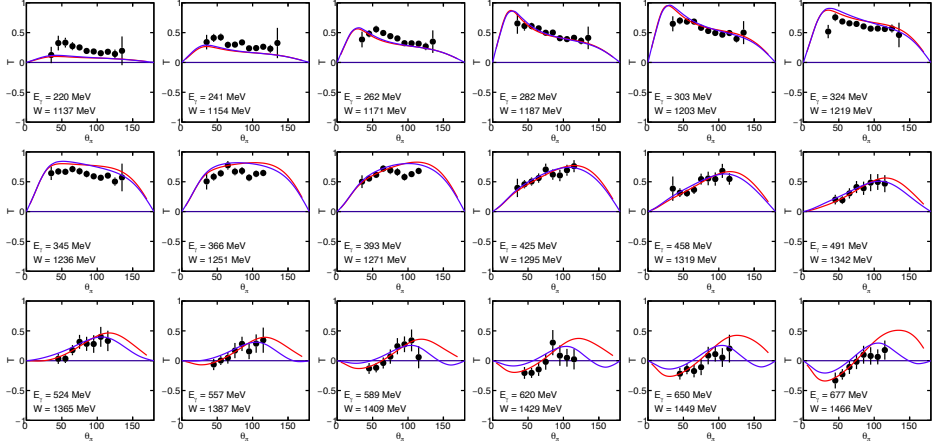
Fig. 8. (Color online) Analyzing power $T(= A_N)$ of MAID (red curve) and Argonne-Osaka [16] model (blue curve) fit to $\gamma^* p^\uparrow \to \pi^+ p$ reaction data observed in PHOENICS experiment at ELSA [15].

In reference [17], an attempt is made to evaluate average A_N within the present RHIC experiment using so evaluated MAID A_N. Shown in the left panel of the Fig.9 is the analyzing power $T(= A_N)$ as a function of pion production angle θ_π^* and the invariant mass W of $\gamma^* p^\uparrow \to \pi^+ n$. The region between thin and thick curves are the rapidity range of the present RHIC experiment and each curves corresponds to the rapidity boundaries of $\eta = 8.0$ and $\eta = 6.8$, respectively. As can be seen in the figure, the large $A_N > 0.8$ is distributed in $\theta_\pi^* < 1$ [rad] around $W \sim 1.2$ GeV and this is where the peak of the neutron yield is located as shown in the right panel of Fig.2 according to EM interaction Monte-Carlo. The yield weighted average of A_N within the acceptance between $6.8 < \eta < 8.0$ and $x_F > 0.4$ is plotted as open square in the right panel of Fig.9. The analyzing power via EM interaction are very similar between p+Al or p+Au because the slope of the photon yield as a function of photon energy is very similar. On the other hand, resulting A_N will be quite different between them due to the fraction of hadronic interaction and the EM interactions are quite different. In fact, the EM cross section grows square function of atomic number Z. The fraction of the hadronic and EM interactions are estimated by the cross section ratio of them assuming one pion exchange (OPE) for the hadronic interaction. The is simpler hadronic interaction model than the reference [5]. However, the cross section of

the hadronic interaction for the leading neutron production in this very forward rapidity range $6.8 < \eta < 8.0$ is known to be dominated by OPE [3]. On the other hand, the nuclear absorption effect is claimed to play important role in the reference [5] and is not considered in reference [17] though, the absorption effects are somewhat canceled when one take ratio between the hadronic and the EM interactions. Details are discussed in the reference [17]. So obtained hadron/EM cross section weighted A_N are plotted as open circles in the right panel of Fig.9 and are compared with experimental analyzing power data (solid symbols). Solid circle and squares are inclusive and BBC vetoed data, respectively. The calculated A_N open circles are to be compared with inclusive data points (solid circle) and they are in very good agreement.
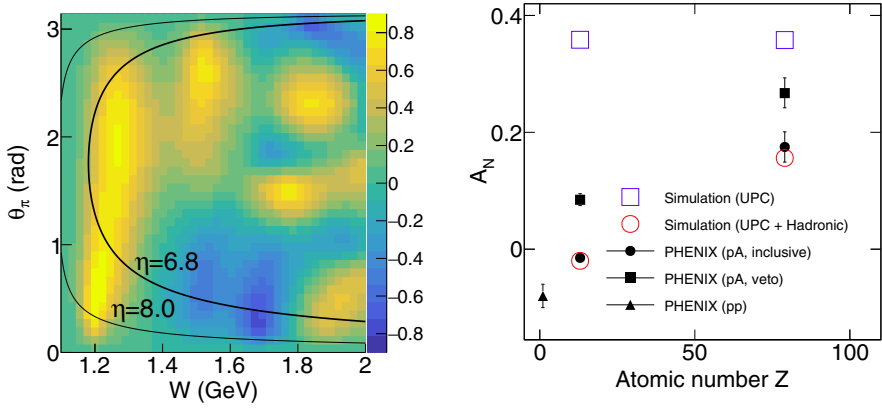
Fig. 9. (left) Analyzing power $T(= A_N)$ as a function of pion production angle in θ_π^* and the invariant mass W of $\gamma^* p^\uparrow \to \pi^+ n$. The region between thin and thick curves are the rapidity range of the present RHIC experiment and each curves corresponds to the rapidity boundaries of $\eta = 8.0$ and $\eta = 6.8$, respectively. (right) Comparison of experimental analyzing power data (solid symbols) and model predictions (open symbols) plotted as a function of atomic number Z. Solid circle and squares are inclusive and BBC vetoed data, respectively. Open square is kinematically averaged A_N prediction over RHIC acceptance by MAID. Open circles are weighted mean prediction of MAID and one pion exchange A_N for Al and Au. Both plots are quoted from reference [17].

5   Summary

A theoretical attempt was made to explain strong A-dependence in the very forward neutron asymmetry recently observed in transversely polarized proton-nucleus collision at $\sqrt{s}$=200 GeV in PHENIX experiment at RHIC [4]. The drastic A-dependence in the forward neutron asymmetry A_N cannot be explained by the conventional hadronic interaction model [5] which was successful to explain the asymmetries observed for p + p collision [3]. In this document, possible major contribution in the asymmetry from the UPC (Primakoff) effect via one photon

exchange from the nuclear Coulomb field is discussed. The Mainz unitary isobar (MAID2007) model [12] was used to estimate the asymmetry by the EM interaction which fit past $\gamma * p^{\uparrow} \rightarrow \pi^+ n$ reaction data [15] well. The MAID predicts large asymmetry below Δ region for $\pi^+ n$-channel due to the interference between non-resonance contact E_{0+} (non-spin flip) and Δ resonance M_{1+} (spin flip) amplitudes. Once kinematic average within the detector acceptance and kinematic cuts, the resulting asymmetries overshot both inclusive A_N data for both $p + Al$ and $p + Au$ data. Once these average EM asymmetries are further taken weighted mean by cross section ratio with hadronic asymmetries, the resulting asymmetries reproduced both $p + Al$ and $p + Au$ data well [17]. The importance of the interference in non-resonance and Δ resonance contradicts from the large asymmetry observed in $p^{\uparrow} + Pb \rightarrow \pi^0 + p + Pb$ at Fermi lab [7] which is interpreted mainly due to the interference between Δ and $N^*(1440)$ and higher resonances. This difference can be explained by the relatively strong Kroll-Rudermann term [14] contribution for π^+ channel, and which raises the importance of the interference below Δ unlike π^0 channel. The present EM asymmetry calculation framework is confirmed to be at least qualitatively consistent with the claim made by the authors of Fermi experiment [7].

References

1. Y. Fukao et al., Phys. Lett. B 650, 325 (2007), A. Adare et al., Phys. Rev. D 88, 032006 (2013).
2. C. Adler, A. Denisov, E. Garcia, M. J. Murray, H. Strobele, and S. N. White, Nucl. Instrum. Methods Phys. Res., A 470, 488 (2001).
3. B. Z. Kopeliovich, I. K. Potashnikova, and Ivan Schmidt, Phys. Rev. Lett. 64, 357 (1990).
4. The PHENIX collaboration, arXiv:1703.10941.
5. B. Z. Kopeliovich, I. K. Potashnikova, and Ivan Schmidt, arXiv:1702.07708.
6. I. G. Alekseev et al.: Phys. Rev. D 79, 094014 (2009).
7. D. C. Carey et al., Phys. Rev. D 79, 094014 (2009).
8. S. R. Klein, J. Nystrand, Phys. Rev. C 60, 014903 (1999), STARLIGHT webpage, http://starlight.hepforge.org/
9. A. Mucke, R. Engel, J.P. Rachen, R.J. Protheroe, and T. Stanev, Comput. Phys. Commun. 123, 290-314 (2000); SOPHIA webpage, http://homepage.uibk.ac.at/ c705282/SOPHIA.html
10. G. Mitsuka, Eur. Phys. J. C 75:614 (2015).
11. Aron M. Bernstein, Mohammad W. Ahmed, Sean Stave, Ying K. Wu, and Henry R. Weller, Annu. Rev. Nucl. Part. Sci. 2009.59:115-144.
12. D. Drechsel, S. S. Kamalov, and L. Tiator, Unitary isobar model (MAID2007), Eur. Phys. J. A 34, 69 (2007).
13. D. Drechsel and L. Tiator, J. Phys. G: Nucl. Part Phys. **18**, 449 (1992).
14. Kroll N, Ruderman, MA. Phys. Rev. 93, 233 (1954).
15. H. Dutz et al., Nucl. Phys. **A 601**, 319 (1996).
16. H. Kamano, S. X. Nakamura, T. -S. H. Lee, and T. Sato, Phys. Rev. **C 88**, 035209 (2013).
17. G. Mitsuka, Phys. Rev. **C 95**, 044908 (2017).

Single energy partial wave analyses on eta photoproduction – pseudo data

H. Osmanović[⋆][a], M. Hadžimehmedović[a], R. Omerović[a], S. Smajić[a], J. Stahov[a],
V. Kashevarov[b], K. Nikonov[b], M. Ostrick[b], L. Tiator[b], A. Švarc[c]

[a]University of Tuzla, Faculty of Natural Sciences and Mathematics, Univerzitetska 4,
75000 Tuzla, Bosnia and Herzegovina
[b]Institut für Kernphysik, Johannes Gutenberg-Universität Mainz, D-55099 Mainz,
Germany
[c]Rudjer Bošković Institute, Bijenička cesta 54, P.O. Box 180, 10002 Zagreb, Croatia

Abstract. We perform partial wave analysis of the eta photoproduction data. In an iterative procedure fixed-t amplitude analysis and a conventional single energy partial wave analysis are combined in such a way that output from one analysis is used as a constraint in another. To demonstrate the modus operandi of our method it is applied on a well defined, complete set of pseudo data generated within EtaMAID15 model.

1 Introduction

Single energy partial wave analysis (SE PWA) is a standard method used to obtain partial waves from scattering data at a given energy. Invariant amplitudes, reconstructed from partial waves by means of corresponding partial wave expansions obey a fixed-s analyticity required in Mandelstam hypothesis. It is quite general that at a given energy many different partial wave solutions equally well describe the data. The fit to the data at one energy "does not know" which solution was obtained in independent SE PWA at another, even neighboring energies. This poses a problem of finding a unique partial wave solution as a function of energy. To solve this problem and to achieve continuity of partial wave solution in energy, one has to impose some additional constraints on partial wave solutions. The aim of this paper is to demonstrate a method which imposes analyticity of invariant scattering amplitudes at fixed values of Mandelstam variable t in addition to analyticity at fixed s-value which is already achieved by partial wave expansion. In our method SE PWA and a fixed-t amplitude analysis (Ft AA) are coupled together in an iterative procedure in such a way that output from one analysis serves as a constraint in another. Detailed description of formalism and the method is given in refs. [2], [2]. Here we demonstrate how the method works. As an input we use the eta photoproduction pseudo data constructed from theoretical model EtaMAID-2015 [3]. Applying our method, we reproduced partial waves from a model which was used to generate the data fitted. This proves uniqueness of partial wave solution obtained applying our method.

⋆ Talk presented by H. Osmanović

2   Method and results

To prove uniqueness of solution obtained by use of our method, we generated a complete set of observables in the eta photoproduction process: $\{\sigma_0, \check{\Sigma}, \check{T}, \check{P}, \check{F}, \check{G}, \check{C}_{x'}, \check{O}_{x'}\}$ [4, 5]. To apply our method we need data at two different kinematical grids: energy - t (W,t) to be used in the Ft AA, and energy - scattering angle theta grid to be used in SE PWA. Our pseudo data sets are generated at 140 energies inside the physical region, each at 50 t-values with artificially small errors of 0.1%. W-t kinematical grid is shown in Fig. 1. Yellow line shows the data used in the
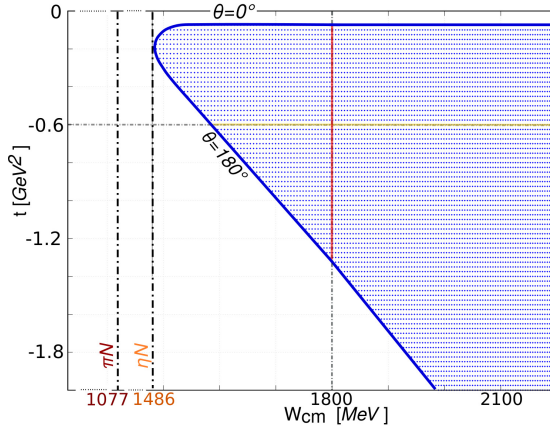
Fig. 1. (Color online) (W_{cm}, t) diagram for η photoproduction. Points represent pseudo-data generated by EtaMAID2015a model in physical range. Yellow line symbolizes fixed-t analysis, and red line symbolizes fixed-s (SE) analysis.

Ft AA ($t = -0.6 GeV^2$), while the data along red line ($W = 1800 MeV$) are used in the SE PWA. Iterative procedure in our method is shown in Fig. 2. χ^2_{SEdata} and
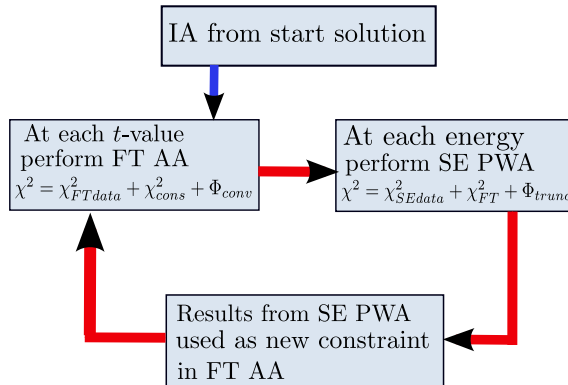
Fig. 2. Iterative procedure in a combined single energy partial wave analysis and fixed-t amplitude analysis.

χ^2_{FTdata} are standard quadratic forms used in fitting the data, Φ_{conv} is convergence test function which is integral part of Pietarinen expansion method used in Ft AA [6–10], while Φ_{trunc} makes a soft cut off of higher multipoles at lower energies in SE PWA (for technical details see refs [2], [2]). The two analyses, SE PWA and Ft AA, are coupled by terms χ^2_{Ft} and χ^2_{SE} which measure deviations of values of invariant amplitudes obtained in SE PWA from corresponding ones obtained in Ft AA and vice versa. After several iterations, usually not more than three, results from both analyses agree reasonably well. Figure 3 and Figure 4 show importance of constraint from Ft AA in obtaining a unique partial wave solution in SE PWA. In Figure 3 are shown partial waves obtained in unconstrained SE
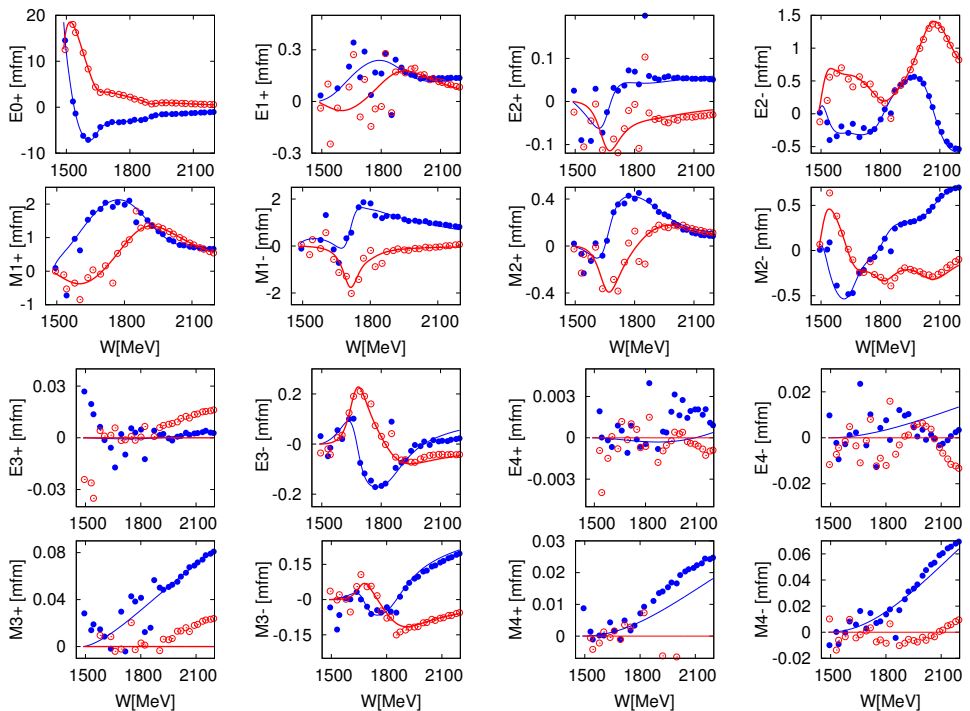
Fig. 3. (Color online) The result of on unconstrained single-energy fit described in the text. The blue and red points show the real and imaginary parts of the multipoles obtained in the fit compared to the "true" multipoles from the underlying EtaMAID-2015 model (blue and red solid lines).

PWA. Even if a complete set of data with small errors is used in analysis, unique solution is not obtained- input partial waves solution from which the data is generated is not reconstructed. Figure 4 shows results of PWA using our method with the same input data after two iterations. Starting solution is reconstructed with a high accuracy.
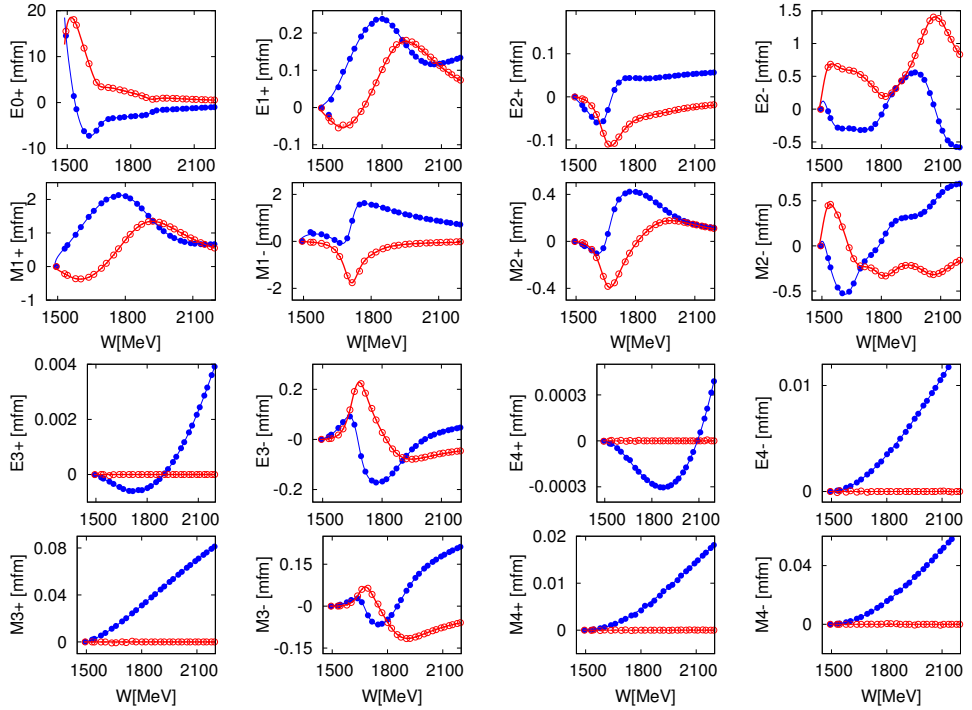
Fig. 4. (Color online) Real (blue) and imaginary (red) parts of electric and magnetic multi-poles up to L = 4. The points are the result of the analytically constrained single-energy fit to the pseudo data and are compared to the multipoles of the underlying EtaMAID-2015 model, shown as solid lines.

3   Conclusions

In order to achieve unique and continuous solution in energy, additional constraint in an partial wave analysis is needed. It is shown that a unique solution may be obtained using only analytic properties of invariant scattering amplitudes at fixed values of Mandelstam variables s and t as constraint.

References

1. H. Osmanović, M. Hadžimehmedović, R. Omerović, J. Stahov,V. Kashevarov, K. Nikonov, M. Ostrick, L. Tiator, and A. Švarc, arXiv:1707.07891 [nucl-th]
2. M. Hadžimehmedović, V. Kashevarov, K. Nikonov, R. Omerović, H. Osmanović, M. Ostrick, J. Stahov, A. Švarc, L. Tiator, Bled Workshops Phys., 16, 40 (2015).
3. V. L. Kashevarov, L. Tiator, M. Ostrick, Bled Workshops Phys., 16, 9 (2015).
4. Y. Wunderlich, R. Beck and L. Tiator, Phys. Rev. C **89**, no. 5, 055203 (2014).
5. W. T. Chiang and F. Tabakin, Phys. Rev. C **55**, 2054 (1997).
6. E. Pietarinen, Nuovo Cimento Soc. Ital. Fis. **12A**, 522 (1972).
7. E. Pietarinen, Nucl. Phys. **B 107** 21 (1976).

8. E. Pietarinen, University of Helsinki Preprint, HU-TFT-78-23, (1978).

9. J. Hamilton, J. L. Petersen, *New development in Dispersion Theory*, Vol. 1. Nordita, Copenhagen, 1973.

10. G. Höhler, *Pion Nucleon Scattering*, Part 2, Landolt-Börnstein: Elastic and Charge Exchange Scattering of Elementary Particles, Vol. 9b (Springer-Verlag, Berlin, 1983).

Cluster Separability in Relativistic Few Body Problems[*]

N. Reichelt[a], W. Schweiger[a], and W.H. Klink[b]

[a]Institute of Physics, University of Graz, A-8010 Graz, Austria
[b]Department of Physics and Astronomy, University of Iowa, Iowa City, USA

Abstract. A convenient framework for dealing with hadron structure and hadronic physics in the few-GeV energy range is relativistic quantum mechanics. Unlike relativistic quantum field theory, one deals with a fixed, or at least restricted number of degrees of freedom while maintaining relativistic invariance. For systems of interacting particles this is achieved by means of the, so called, "Bakamjian-Thomas construction", which is a systematic procedure for implementing interaction terms in the generators of the Poincaré group such that their algebra is preserved. Doing relativistic quantum mechanics in this way one, however, faces a problem connected with the physical requirement of cluster separability as soon as one has more than two interacting particles. Cluster separability, or sometimes also termed "macroscopic causality", is the property that if a system is subdivided into subsystems which are then separated by a sufficiently large spacelike distance, these subsystems should behave independently. In the present contribution we discuss the problem of cluster separability and sketch the procedure to resolve it.

1 Introduction to relativistic quantum mechanics

It is a widespread opinion that a relativistically invariant quantum theory of interacting particles has to be a (local) quantum field theory. Therefore we first have to specify what we mean by "relativistic quantum mechanics". Relativistic quantum mechanics is based on a theorem by Bargmann which basically states that [1,2]:

A quantum mechanical model formulated on a Hilbert space preserves probabilities in all inertial coordinate systems if and only if the correspondence between states in different inertial coordinate systems can be realized by a single-valued unitary representation of the covering group of the Poincaré group.

According to this theorem one has succeeded in constructing a relativistically invariant quantum mechanical model, if one has found a representation of the (covering group of the) Poincaré group in terms of unitary operators on an appropriate Hilbert space. Equivalently one can also look for a representation of the generators of the Poincaré group in terms of self-adjoint operators acting on this Hilbert space. These self-adjoint operators should then satisfy the Poincaré

---

[*] Talk presented by N. Reichelt and by W. Schweiger

algebra

$$[J^i, J^j] = \imath\,\epsilon^{ijk} J^k\,, \quad [K^i, K^j] = -\imath\,\epsilon^{ijk} J^k\,, \quad [J^i, K^j] = \imath\,\epsilon^{ijk} K^k\,,$$
$$[P^\mu, P^\nu] = 0\,, \quad [K^i, P^0] = -\imath\,P^i\,, \quad [J^i, P^0] = 0\,,$$
$$[J^i, P^j] = \imath\,\epsilon^{ijk} P^k\,, \quad [K^i, P^j] = -\imath\,\delta_{ij}\,P^0\,. \tag{1}$$

P^0 and P^i generate time and space translations, respectively, J^i rotations and K^i Lorentz boosts. From the last commutation relation it is quite obvious that, if P^0 contains interactions, K^i or P^j (or both) have to contain interactions too. The form of relativistic dynamics is then characterized by the interaction dependent generators. Dirac [3] identified three prominent forms of relativistic dynamics, the *instant form* (interactions in P^0, K^i, $i = 1, 2, 3$), the *front form* (interactions in $P^- = P^0 - P^3$, $F^1 = K^1 - J^2$, $F^2 = K^2 + J^1$) and the *point form* (interactions in P^μ, $i = 0, 1, 2, 3$). In what follows we will stick to the point form, where P^μ, the generators of space-time translations, contain interactions and $\mathbf{J}$, $\mathbf{K}$, the generators of Lorentz transformations, are interaction free. The big advantage of this form is that boosts and the addition of angular momenta become simple.

For a single free particle and also for several free particles it is quite easy to find Hilbert-space representations of the Poincaré generators in terms self-adjoint operators that satisfy the algebra given in Eq. (1), but what about interacting systems? Local quantum field theories provide a relativistic invariant description of interacting systems, but then one has to deal with a complicated many-body theory. It is less known that interacting representations of the Poincaré algebra can also be realized on an N-particle Hilbert space and one does not necessarily need a Fock space. A systematic procedure for implementing interactions in the Poincaré generators of an N-particle system such that the Poincaré algebra is preserved, has been suggest long ago by Bakamjian and Thomas [4]. In the point form this procedure amounts to factorize the four-momentum operator of the interaction-free system into a four-velocity operator and a mass operator and add then interaction terms to the mass operator:

$$P^\mu = M V_{\text{free}}^\mu = (M_{\text{free}} + M_{\text{int}}) V_{\text{free}}^\mu\,. \tag{2}$$

Since the mass operator is a Casimir operator of the Poincaré group, the constraints on the interaction terms that guarantee Poincaré invariance become simply that M_{int} should be a Lorentz scalar and that it should commute with V_{free}^μ, i.e. $[M_{\text{int}}, V_{\text{free}}^\mu] = 0$. Remarkably, this kind of construction allows for instantaneous interactions ("interactions at a distance"). Similar procedures can also be carried out in the instant and front forms of relativistic dynamics such that the physical equivalence of all three forms is guaranteed in the sense that the different descriptions are related by unitary transformations [5].

A very convenient basis for representing Bakajian-Thomas (BT) type mass operators consists of velocity states

$$|v; \mathbf{k}_1, \mu_1; \mathbf{k}_2, \mu_2; \ldots; \mathbf{k}_N, \mu_N\rangle\,, \qquad \sum_{i=1}^{N} \mathbf{k}_i = 0\,. \tag{3}$$

These specify the state of an N-particle system by its overall velocity $\boldsymbol{v}$, the particle momenta $\boldsymbol{k}_i$ in the rest frame of the system and the spin projections μ_i of the individual particles. The physical momenta of the particles are then given by $\boldsymbol{p}_i = \overrightarrow{B(\boldsymbol{v})k_i}$, where $B(\boldsymbol{v})$ is a canonical (rotationless) boost with the overall system velocity $\boldsymbol{v}$. Associated with this kind of boost is also the notion of "canonical spin" which fixes the spin projections μ_i. N-particle velocity states, as introduced above, are eigenstates of the free N-particle velocity operator V^μ_{free} and the free mass operator

$$M_{\text{free}} |\boldsymbol{v}; \boldsymbol{k}_1, \mu_1; \boldsymbol{k}_2, \mu_2; \dots \rangle = (\omega_1 + \omega_2 + \dots) |\boldsymbol{v}; \boldsymbol{k}_1, \mu_1; \boldsymbol{k}_2, \mu_2; \dots \rangle, \quad (4)$$

with $\omega_i = \sqrt{m_i^2 + \boldsymbol{k}_i^2}$. The overall velocity factors out in velocity-state matrix elements of BT-type mass operators,

$$\begin{aligned}
\langle \boldsymbol{v}'; \boldsymbol{k}'_1, \mu_1; \boldsymbol{k}'_2, \mu_2; \dots |M| \boldsymbol{v}; \boldsymbol{k}_1, \mu_1; \boldsymbol{k}_2, \mu_2; \dots \rangle \\
\propto v^0 \, \delta^3(\boldsymbol{v}' - \boldsymbol{v}) \, \langle \boldsymbol{k}'_1, \mu_1; \boldsymbol{k}'_2, \mu_2; \dots \|M\| \boldsymbol{k}_1, \mu_1; \boldsymbol{k}_2, \mu_2; \dots \rangle, \quad (5)
\end{aligned}$$

leading to the separation of overall and internal motion of the system.

2 Cluster separability

A central requirement for local relativistic quantum field theories is "microscopic causality", i.e. the property that field operators at space-time points x and y should commute or anticommute, depending on whether they describe bosons or fermions, if these space-time points are space-like separated, i.e.

$$[\Psi(x), \Psi(y)]_\pm = 0 \quad \text{for} \quad (x - y)^2 < 0. \quad (6)$$

The crucial point here is that this must hold for arbitrarily small space-like distances. This condition requires an infinite number of degrees of freedom and can therefore not be satisfied in relativistic quantum mechanics with only a finite number of degrees of freedom. What replaces microscopic causality in the case of relativistic quantum mechanics is the physically more sensible requirement of "macroscopic causality", or also often called "cluster separability". It roughly means that subsystems of a quantum mechanical system should behave independently, if they are sufficiently space-like separated.

In order to phrase cluster separability in more mathematical terms, we start with an N-particle state $|\Phi\rangle$ with wave function $\phi(\boldsymbol{p}_1, \boldsymbol{p}_2, \dots, \boldsymbol{p}_N)$ and decompose this N-particle system into two subclusters (A) and (B). Next one introduces a separation operator $U^{(A)(B)}_\sigma$ with the property that

$$\lim_{\sigma \to \infty} \langle \Phi | U^{(A)(B)}_\sigma | \Phi \rangle = 0. \quad (7)$$

The role of the separation operator will become clearer by means of an example. Let us consider (space-like) separation by a canonical boost. In this case subsystem (A) is boosted with velocity $\boldsymbol{v}$ and subsystem (B) with velocity $-\boldsymbol{v}$. The action on the wave function is then

$$\left(U^{(A)(B)}_{\boldsymbol{v}} \phi\right)(\boldsymbol{p}_{i \in (A)}, \boldsymbol{p}_{j \in (B)}) = \phi\left(\overrightarrow{B(-\boldsymbol{v})p}_{i \in (A)}, \overrightarrow{B(\boldsymbol{v})p}_{j \in (B)}\right) \quad (8)$$

and one has to consider the limit $\sigma = |\boldsymbol{v}| \to \infty$ in Eq. (7).

Having introduced a separation operator we are now able to formulate cluster separability in a more formal way. In the literature one can find different notions of it. A comparably weak, but physically plausible requirement, is cluster separability of the scattering operator:

$$\text{s} - \lim_{\sigma \to \infty} U_\sigma^{(A)(B)\dagger} \, S \, U_\sigma^{(A)(B)} = S^{(A)} \otimes S^{(B)} \,. \tag{9}$$

It means that the scattering operator should factorize into the scattering operators of the subsystems after separation. For three-particle systems it has been demonstrated that this type of cluster separability can be achieved by a BT construction [6].

A stronger requirement is that the Poincaré generators become additive, when the clusters are separated. In a weaker version this means for the four-momentum operator that

$$\lim_{\sigma \to \infty} \langle \Phi | U_\sigma^{(A)(B)\dagger} \left(P^\mu - P^\mu_{(A)} \otimes I_{(B)} - I_{(A)} \otimes P^\mu_{(B)} \right) U_\sigma^{(A)(B)} | \Phi \rangle = 0 \,, \tag{10}$$

the stronger version is that

$$\lim_{\sigma \to \infty} \left\| \left(P^\mu - P^\mu_{(A)} \otimes I_{(B)} - I_{(A)} \otimes P^\mu_{(B)} \right) U_\sigma^{(A)(B)} | \Phi \rangle \right\| = 0 \,. \tag{11}$$

The BT construction violates both conditions already in the 2+1-body case (i.e. particles 1 and 2 interacting and particle 3 free) [2, 7]. The reason for the failure can essentially be traced back in this case to the fact that the BT-type mass operator and the mass operator of the separated 2+1-particle system differ in the velocity conserving delta functions. In the BT-case it is the overall three-particle velocity which is conserved, in the separated case it is rather the velocity of the interacting two-particle system. The separation, however, is done by boosting with the velocity of the interacting two-particle system.

One may now ask, whether wrong cluster properties lead to observable physical consequences. From our studies of the electromagnetic structure of mesons we have to conclude that this is indeed the case [8–10]. In these papers electron scattering off a confined quark-antiquark pair was treated within relativistic point form quantum mechanics starting from a BT-type mass operator in which the dynamics of the photon is also fully included. The meson current can then be identified in a unique way from the resulting one-photon-exchange amplitude which has the usual structure, i.e. electron current contracted with the meson current and multiplied with the covariant photon propagator. The covariant analysis of the resulting meson current, however, reveals that it exhibits some unphysical features which most likely can be ascribed to wrong cluster properties. For pseudoscalar mesons, e.g., its complete covariant decomposition takes on the form

$$\tilde{J}^\mu(\mathbf{p}'_M; \mathbf{p}_M) = (p_M + p'_M)^\mu \, f(Q^2, s) + (p_e + p'_e)^\mu \, g(Q^2, s) \,. \tag{12}$$

It is still conserved, transforms like a four-vector, but exhibits an unphysical dependence on the electron momenta which manifests itself in form of an additional covariant (and corresponding form factor) and a spurious Mandelstam-s dependence of the form factors. Although unphysical, these features do not

spoil the relativistic invariance of the electron-meson scattering amplitude. The Mandelstam-s dependence of the physical and spurious form factors f and g is shown in Fig. 1. Since the spurious form factor g is seen to vanish for large s and the s-dependence of the physical form factor f becomes also negligible in this case it is suggestive to extract the physical form factor in the limit $s \to \infty$. This strategy was pursued in Refs. [8–10] where it lead to sensible results. It gives a simple analytical expression for the physical form factor $F(Q^2) = \lim_{s \to \infty} f(Q^2, s)$ which agrees with corresponding front form calculations in the $q_\perp = 0$ frame. Similar effects of wrong cluster properties on electromagnetic form factors were also observed in model calculations done within the framework of front form quantum mechanics [11].
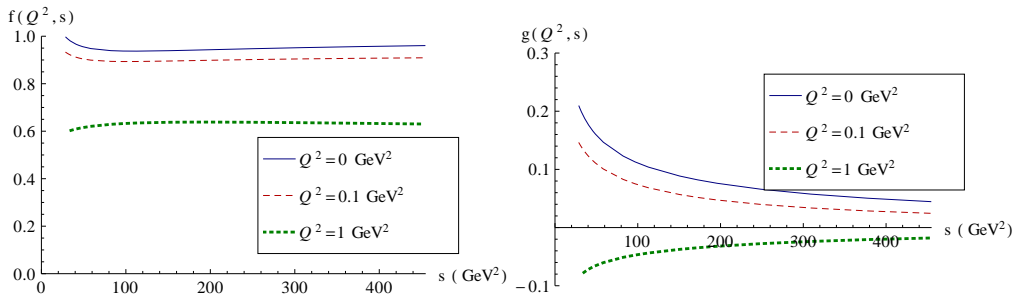
Fig. 1. Mandelstam-s dependence of the physical and spurious B meson electromagnetic form factors f and g for various values of the (negative) squared four-momentum transfer Q^2 [9]. The result has been obtained with a harmonic-oscillator wave function with parameters $a = 0.55$ GeV, $m_b = 4.8$ GeV, $m_{u,d} = 0.25$ GeV.

3   Restoring cluster separability

It is obviously the BT-type structure of the four-momentum operator (see Eq. (2)) which guarantees Poincaré invariance on the one hand, but leads to wrong cluster properties on the other hand (if one has more than two particles). In order to show, how this conflict may be resolved, let us consider a three-particle system with pairwise two-particle interactions. To simplify matters we will consider spinless particles and neglect internal quantum numbers. We start with the four-momentum operators of the two-particle subsystems,

$$P^\mu_{(ij)} = M_{(ij)} V^\mu_{(ij)}, \quad i, j = 1, 2, 3, \quad i \neq j, \tag{13}$$

which have a BT-type structure (i.e. $V^\mu_{(ij)}$ is free of interactions). Cluster separability holds for these subsystems, if the two-particle interaction is sufficiently short ranged. The third particle can now be added by means of the usual tensor-product construction

$$\tilde{P}^\mu_{(ij)(k)} = P^\mu_{(ij)} \otimes I_{(k)} + I_{(ij)} \otimes P^\mu_{(k)}. \tag{14}$$

The individual four-momentum operators $\tilde{P}^\mu_{(ij)(k)}$ describe 2+1-body systems in a Poincaré invariant way and exhibit also the right cluster properties. One may now think of adding all these four momentum operators, to end up with a four momentum operator for a three particle system with pairwise interactions:

$$\tilde{P}^\mu_3 = \tilde{P}^\mu_{(12)(3)} + \tilde{P}^\mu_{(23)(1)} + \tilde{P}^\mu_{(31)(2)} - 2P^\mu_{3\,\text{free}}\,. \tag{15}$$

But the components of the resulting four-momentum operator do not commute,

$$[\tilde{P}^\mu_3, \tilde{P}^\nu_3] \neq 0 \quad \text{since} \quad [M_{(ij)\,\text{int}}, V^\mu_{(j)}] \neq 0\,. \tag{16}$$

One can, of course, write the individual $\tilde{P}^\mu_{(ij)(k)}$ in the form

$$\tilde{P}^\mu_{(ij)(k)} = \tilde{M}_{(ij)(k)}\,\tilde{V}^\mu_{(ij)(k)} \quad \text{with} \quad \tilde{M}^2_{(ij)(k)} = \tilde{P}_{(ij)(k)} \cdot \tilde{P}_{(ij)(k)}\,, \tag{17}$$

but the four-velocities $\tilde{V}^\mu_{(ij)(k)}$ contain interactions and differ for different clusterings, so that an overall four-velocity cannot be factored out of $\tilde{P}^\mu_3$. The key observation is now that all four-velocity operators have the same spectrum, namely $\mathbb{R}^3$. This implies that there exist unitary transformations which relate the four-velocity operators. One can find, in particular, unitary operators $U_{(ij)(k)}$ such that

$$\tilde{V}^\mu_{(ij)(k)} = U_{(ij)(k)} V^\mu_3 U^\dagger_{(ij)(k)}\,. \tag{18}$$

With these unitary operators one can now define new three-particle momentum operators for a particular clustering,

$$\begin{aligned}
P^\mu_{(ij)(k)} &:= U^\dagger_{(ij)(k)} \tilde{P}^\mu_{(ij)(k)} U_{(ij)(k)} = U^\dagger_{(ij)(k)} \tilde{M}_{(ij)(k)} U_{(ij)(k)} U^\dagger_{(ij)(k)} \tilde{V}^\mu_{(ij)(k)} U_{(ij)(k)} \\
&= M_{(ij)(k)} V^\mu_3\,,
\end{aligned} \tag{19}$$

which have already BT-structure, i.e. with the free three-particle velocity factored out. From Eq. (19) it can be seen that the unitary operators $U_{(ij)(k)}$ obviously "pack" the interaction dependence of the four-velocity operators $\tilde{V}^\mu_{(ij)(k)}$ into the mass operator $M_{(ij)(k)}$. Therefore they were called "packing operators" by Sokolov in his seminal paper on the formal solution of the cluster problem [12]. The sum $(P^\mu_{(12)(3)} + P^\mu_{(23)(1)} + P^\mu_{(31)(2)} - 2P^\mu_{3\,\text{free}})$ describes a three-particle system with pairwise interactions, it has now BT-structure and satisfies thus the correct commutation relation. However, it still violates cluster separability. The solution is a further unitary transformation of the whole sum by means of $U = \prod U_{(ij)(k)}$, assuming that $U_{(ij)(k)} \to 1$ for separations $(ki)(j)$, $(jk)(i)$ and $(i)(j)(k)$. The final expression for the three-particle four-momentum operator, that has all the properties it should have, is:

$$\begin{aligned}
P^\mu_3 &:= U \left[P^\mu_{(12)(3)} + P^\mu_{(23)(1)} + P^\mu_{(31)(2)} + P^\mu_{(123)\,\text{int}} - 2P^\mu_{3\,\text{free}} \right] U^\dagger \\
&= U \left[M_{(12)(3)} + M_{(12)(3)} + M_{(12)(3)} + M_{(123)\,\text{int}} - 2M_{3\,\text{free}} \right] V^\mu_3 U^\dagger \\
&= U\,M_3\,V^\mu_3\,U^\dagger\,.
\end{aligned} \tag{20}$$

If U commutes with Lorentz transformations, it can be shown that such a "generalized BT construction" will satisfy relativity and cluster separability for N-particle systems. In addition to the three-body force induced by U, which is of

purely kinematical origin, we have also allowed for a genuine three-body inter-action $M_{(123)\,int}$. Since the $U_{(ij)(k)}$ will, in general, not commute, U depends on the order of the $U_{(ij)(k)}$ in the product. For identical particles one should even take some kind of symmetrized product, for which also different possibilities exist [2, 12]. This means that P_3^μ is, apart of the newly introduced free-body interaction $M_{(123)\,int}$, not uniquely determined by the two-body momentum operators $P_{(ij)}^\mu$. There are even different ways to construct the packing operators $U_{(ij)(k)}$. All the unitary transformations leave, however, the on-shell data (binding energies, scattering phase shifts, etc.) of the two-particle subsystems untouched, they only affect their off-shell behavior.

The kind of procedure just outlined formally solves the cluster problem for three-body systems. Generalizations to $N > 3$ particles and particle production have also been considered [13]. Its practical applicability, however, depends strongly on the capability to calculate the packing operators for a particular system. A possible procedure can also be found in Sokolov's paper. The trick is to split the packing operator further

$$U_{(ij)(k)} = W^\dagger(M_{(ij)})W(M_{(ij)\,free}) \tag{21}$$

into a product of unitary operators which depend on the corresponding two-particle mass operators in a way to be determined. With this splitting one can rewrite Eq. (18) in the form

$$W(M_{(ij)\,free})V_3^\mu W^\dagger(M_{(ij)\,free}) = W(M_{(ij)})\tilde{V}_{(ij)(k)}^\mu W^\dagger(M_{(ij)}) \,. \tag{22}$$

Since this equation should hold for any interaction the right- and left-hand sides can be chosen to equal some simple four-velocity operator, for which $V_{(ij)}^\mu \otimes I_k$ is a good choice. In order to compute the action of W it is then convenient to take bases in which matrix elements of V_3^μ, $V_{(ij)}^\mu \otimes I_k$ and $\tilde{V}_{(ij)(k)}^\mu$ can be calculated. This is the basis of (mixed) velocity eigenstates

$$|v_{(12)}; \tilde{k}_1, \tilde{k}_2, p_3\rangle = |v_{(12)}; \tilde{k}_1, \tilde{k}_2\rangle \otimes |p_3\rangle \tag{23}$$

of $M_{(ij)(k)\,free}$ if one wants to calculate the action of $W(M_{(ij)\,free})$ and corresponding eigenstates of $M_{(ij)(k)}$ if one wants to calculate the action of $W(M_{(ij)})$. It turns out that the effect of these operators is mainly to give the two-particle subsystem (ij) the velocity $v_{(ij)(k)}$ of the whole three-particle system. After some calculations one finds out that the whole effect of the packing operator $U_{(ij)(k)}$ on the mass operator $\tilde{M}_{(ij)(k)}$ is just the replacement

$$\frac{1}{m_{(ij)}^{\prime\,3/2} m_{(ij)}^{3/2}} v_{(ij)}^0 \delta^3(v_{(ij)}^\prime - v_{(ij)})$$

$$\rightarrow \frac{\sqrt{v_{(ij)}^\prime \cdot v_{(ij)(k)}}}{m_{(ij)(k)}^{\prime\,3/2}} \frac{\sqrt{v_{(ij)} \cdot v_{(ij)(k)}}}{m_{(ij)(k)}^{3/2}} v_{(ij)(k)}^0 \delta^3(v_{(ij)(k)}^\prime - v_{(ij)(k)}) \tag{24}$$

in the mixed velocity-state matrix elements. Here $m_{(ij)}$ and $m_{(ij)(k)}$ are the invariant masses of the free two-particle subsystem and the free three-particle system, $v_{(ij)}$ and $v_{(ij)(k)}$ the corresponding four-velocities.

4   Summary and outlook

We have given a short introduction into the field of relativistic quantum mechanics. It has been shown that the Bakamjian-Thomas construction, the only known systematic procedure to implement interactions such that Poincaré invariance of a quantum mechanical system is guaranteed, leads to problems with cluster separability for systems of more than two particles. Cluster separability is a physically sensible requirement for quantum mechanical systems which replaces microcausality in relativistic quantum field theories. We have discussed the physical consequences of wrong cluster properties, e.g., unphysical contributions in electromagnetic currents of bound states. Following the work of Sokolov we have sketched how a three-particle mass operator with pairwise interactions and correct cluster properties can be constructed. This is accomplished by a set of unitary transformations called packing operators. For the simplest case of three spinless particles we have explicitly calculated these packing operators. In a next step it is planned to use these results to see whether the problems encountered with electromagnetic bound-state currents can be cured by starting with a mass operator that has the correct cluster properties.

References

1. V. Bargmann, Ann. Math. **59**, 1 (1954)
2. B.D. Keister and W.N. Polyzou, Adv. Nucl. Phys. **20**, 225 (1991)
3. P.A.M. Dirac, Rev. Mod. Phys. **21**, 392 (1949)
4. B. Bakamjian and L. H. Thomas, Phys. Rev. **92**, 1300 (1953)
5. S.N. Sokolov and A.N. Shatnii, Theor. Math. Phys. **37**, 1029 (1978)
6. F. Coester, Helv. Phys. Acta **38**, 7 (1965)
7. U. Mutze, J. Math. Phys. **19**, 231 (1978)
8. E.P. Biernat, W. Schweiger, K. Fuchsberger and W.H. Klink, Phys. Rev. C **79**, 055203 (2009)
9. M. Gomez-Rocha and W. Schweiger, Phys. Rev. D **86**, 053010 (2012)
10. E.P. Biernat and W. Schweiger, Phys. Rev. C **89**, 055205 (2014)
11. B.D. Keister and W.N. Polyzou, Phys. Rev. C **86**, 014002 (2012)
12. S.N. Sokolov, Theor. Math. Phys. **36**, 682 (1978)
13. F. Coester and W.N. Polyzou, Phys. Rev. D **26, 1348 (1982)**

Baryon Masses and Structures
Beyond Valence-Quark Configurations⋆

R.A. Schmidt, W. Plessas, and W. Schweiger

Theoretical Physics, Institute of Physics, University of Graz, A-8010 Graz, Austria

Abstract. In order to describe baryon resonances realistically it has turned out that three-quark configurations are not sufficient. Rather explicit couplings to decay channels are needed. This means that additional degrees of freedom must be foreseen. We report results from a study of the nucleon ground state and the Delta resonance by including explicit pionic effects.

All current approaches to quantum chromodynamics (QCD) struggle with a proper description of hadron resonances. For baryons one has found that in case of ground states at low energies three-quark configurations can still provide a reasonable picture. For instance, in a relativistic constituent-quark model relying on $\{QQQ\}$ configurations only, the masses of all ground-state baryons as well as their electromagnetic and axial structures can be well reproduced [1]. In this framework, however, the resonant states are afflicted with severe shortcomings. While the characteristics of the mass spectra can still be yielded to some extent, the reaction properties of baryon resonances fall short, especially with respect to their strong decays. Obviously the reason is that with three-quark configurations only the resonances are described as excited bound states with real eigenvalues rather than genuine resonant states with complex eigenvalues. Consequently, the corresponding wave functions or amplitudes show a completely distinct behaviour.

We have started to include beyond $\{QQQ\}$ configurations explicit mesonic degrees of freedom. In the first instance, we have studied pionic effects in the N and the Δ masses. We have done so by considering π-loop effects on the hadronic as well as the microscopic quark levels. Our program aims at developing a coupled-channels relativistic constituent-quark model that can generate consistently the strong vertex form factors, the baryon ground-state and resonant masses as well as their electroweak structures. It will contain mesonic degrees of freedom such as $\{QQQ\pi\}$, $\{QQQ\rho\}$, and eventually $\{QQQ\pi\pi\}$ etc.

Here we discuss results obtained from π-dressing of the N and the Δ on the hadronic level. We have investigated the most important one-π-loop effects and several higher-order diagrams. A first account of this study was given already in Ref. [2], where also the formalism and details of the calculation are explained. In this context one has in the first instance to solve an eigenvalue equation, which

---

⋆ Talk presented by W. Plessas

results from coupling of a bare $\widetilde{N}$ and a bare $\widetilde{\Delta}$ to a single π according to the diagrams in Fig. 1. It yields the bare and dressed masses, where the latter is real for the N ground state and becomes complex for the Δ resonance. The only input into the calculation are the prescriptions for the $\pi\widetilde{N}\widetilde{N}$ and $\pi\widetilde{N}\widetilde{\Delta}$ form factors at the strong-interaction vertices. For that we have employed models existing in the literature [3–5]. Beyond the results already produced in Ref. [2] we give here in addition values for the dressing effects by using the more recent form-factor parametrization by Kamano et al. [6] derived from a coupled-channels meson-nucleon model. The different form factors are parametrized through the formulae

$$F_{\pi\widetilde{N}\widetilde{B}}(k_\pi^2) = \frac{1}{1 + (\frac{k_\pi}{\lambda_1})^2 + (\frac{k_\pi}{\lambda_2})^4} \qquad \text{or} \qquad F_{\pi\widetilde{N}\widetilde{B}}(k_\pi^2) = \exp^{-k_\pi^2/2\lambda^2}$$

$$\text{or} \qquad F_{\pi\widetilde{N}\widetilde{B}}(k_\pi^2) = \left(\frac{\lambda^2}{k_\pi^2 + \lambda^2}\right)^2, \tag{1}$$

where $\widetilde{B}$ stands either for $\widetilde{N}$ or $\widetilde{\Delta}$. The values of the various cut-off parameters are given in Tab. 1 together with the corresponding coupling constants.

Table 1. Parameters of the bare $\pi\widetilde{N}\widetilde{N}$ and $\pi\widetilde{N}\widetilde{\Delta}$ vertex form factors. The first three columns correspond to the multipole type as in the first formula of Eq. (1), the fourth column to the Gaussian type as in the second formula of Eq. (1), and the last column to the dipole type as in the third formula of Eq. (1). The corresponding parametrizations are taken from Refs. [3], [5] and [6], respectively. All (bare) coupling constants belong to $k_\pi^2 = 0$. RCQM refers to the predictions of the relativistic constituent-quark model [7] in Ref. [3], SL to the πN meson-exchange model by Sato and Lee [4], PR to the Nijmegen soft-core model of Polinder and Rijken [5], and KNLS to the coupled-channels meson-nucleon model of Kamano, Nakamura, Lee, and Sato. All cut-off parameters are in GeV.

		RCQM	SL	PR multipole	PR Gaussian	KNLS
	$f_{\pi\widetilde{N}\widetilde{N}}^2/4\pi$	0.0691	0.08	0.013	0.013	0.08
	λ_1	0.451	0.453	0.940		
$\pi\widetilde{N}\widetilde{N}$	λ_2	0.931	0.641	1.102		
	λ				0.665	0.656
	$f_{\pi\widetilde{N}\widetilde{\Delta}}^2/4\pi$	0.188	0.334	0.167	0.167	0.126
	λ_1	0.594	0.458	0.853		
$\pi\widetilde{N}\widetilde{\Delta}$	λ_2	0.998	0.648	1.014		
	λ				0.603	0.709

For the $\pi\widetilde{N}\widetilde{N}$ vertex the momentum dependences of the form factors from the five different models are shown in Fig. 2. With these ingredients the π-dressing effects in the N mass are yielded as in Tab. 2. The mass shifts are basically of the same order of magnitude for all form-factor models employed, even though
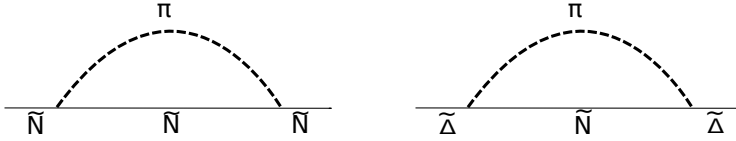
Fig. 1. π-loop diagrams considered for the dressing of a bare $\widetilde{N}$ and a bare $\widetilde{\Delta}$.
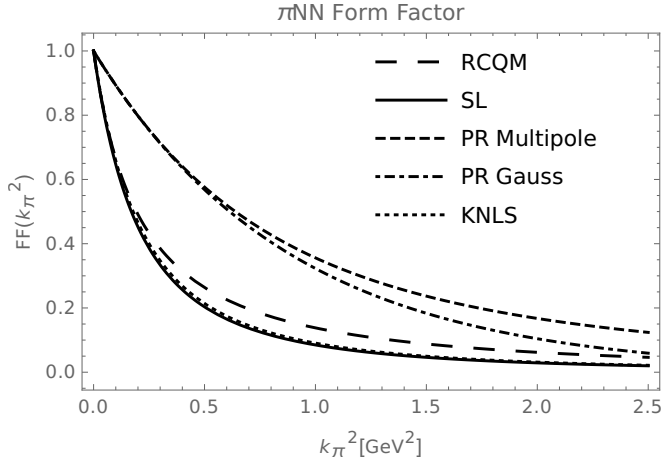

Fig. 2. Dependences on the π three-momentum squared k_π^2 of the different (bare) form-factor models for the $\pi\widetilde{N}\widetilde{N}$ system.

the momentum dependences are quite different as seen from Fig. 2. However, the net effect is gained from an interplay of the momentum dependence of each form factor and the corresponding $\pi\widetilde{N}\widetilde{N}$ coupling constant (cf. Tab. 1). The largest dressing effect is obtained in case of the RCQM.

Table 2. π-loop effects in the N mass $m_N = 0.939$ GeV according to the l.h.s. diagram of Fig. 1.

		RCQM	SL	PR multipole	PR Gaussian	KNLS
$m_{\widetilde{N}}$	[GeV]	1.067	1.031	1.051	1.025	1.037
$m_{\widetilde{N}} - m_N$	[GeV]	0.128	0.092	0.112	0.086	0.098

For the $\pi\widetilde{N}\widetilde{\Delta}$ vertex the momentum dependences of the form factors from the five different models are shown in Fig. 3. With these ingredients the π-dressing effects in the Δ mass are yielded as in Tab. 3. It is immediately evident that the Δ mass gets complex. The real part corresponds to resonance position in the πN channel and the complex part to (half) the hadronic Δ decay width. While the π-dressing effects in the real part are of about the same magnitudes as in the N, in

all cases the decay widths are much too small as compared to the empirical value of about 0.117 GeV.
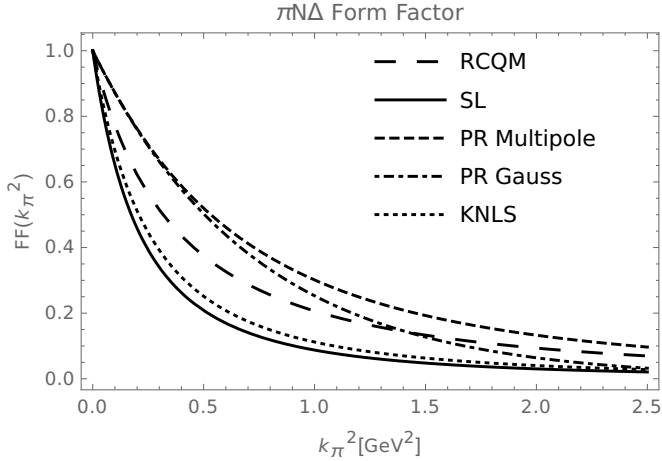

Fig. 3. Dependences on the π three-momentum squared k_π^2 of the different (bare) form-factor models for the $\pi\widetilde{N}\widetilde{\Delta}$ system.

Table 3. π-loop effects in the Δ mass Re $(m_\Delta)= 1.232$ GeV and in the π-decay width Γ according to the r.h.s. diagram of Fig. 1, where the bare $\widetilde{N}$ masses $m_{\widetilde{N}}$ in the intermediate states are the same as in Table 2.

		RCQM	SL	PR multipole	PR Gaussian	KNLS
$m_{\widetilde{\Delta}}$	[GeV]	1.300	1.290	1.335	1.321	1.259
$m_{\widetilde{\Delta}} - \mathrm{Re}\,(m_\Delta)$	[GeV]	0.068	0.058	0.103	0.089	0.027
$\Gamma = 2\,\mathrm{Im}\,(m_\Delta)$	[GeV]	0.004	0.023	0.008	0.016	0.007

An improvement in the $\Delta \to \pi N$ decay width Γ is achieved by replacing the bare $\widetilde{N}$ in the intermediate state by the dressed N like in Fig. 4. Thereby the phase space for the strong decay is enlarged, and the situation may be closer to the realistic one. The π-dressing effect in the real part is slightly raised in all cases, as compared to the values in Tab. 3, however, the changes achieved for the decay width Γ are respectable. Now, they reach about 50% of the phenomenological value, except for the KNLS form-factor model. Still, the results appear to be unsatisfactory.

Therefore we have investigated higher-order effects, i.e. two-π loops, where the ones with π-π interactions in the intermediate state can be effectively described by σ and ρ mesons. The corresponding dressing effects turned to be marginal. Their inclusions do not help much to improve the Δ decay width.
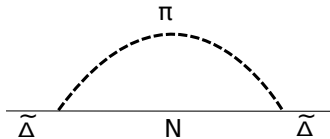
Fig. 4. π-loop diagram considered for the dressing of a bare $\widetilde{\Delta}$, where in the intermediate state a physical N with mass $m_N = 0.939$ GeV is employed.

Table 4. π-loop effects in the Δ mass $\mathrm{Re}\,(m_\Delta) = 1.232$ GeV and in the π-decay width Γ according to the diagram in Fig. 4, where in the intermediate state always $m_N = 0.939$ GeV.

		RCQM	SL	PR multipole	PR Gaussian	KNLS
$m_{\widetilde{\Delta}}$	[GeV]	1.309	1.288	1.347	1.328	1261
$m_{\widetilde{\Delta}} - \mathrm{Re}\,(m_\Delta)$	[GeV]	0.077	0.056	0.114	0.096	0.029
$\Gamma = 2\,\mathrm{Im}\,(m_\Delta)$	[GeV]	0.047	0.064	0.052	0.051	0.027

We are now in the course of investigating explicit pionic effects on the microscopic level, i.e. along a relativistic coupled-channels constituent-quark model. This will also help us to get rid of inputs of vertex form factors foreign to the quark model, because in such an approach one can determine within the same framework both the mass dressings as well as the vertex form factors consistently.

Acknowledgment

References

1. W. Plessas, Int. J. Mod. Phys. A **30**, 1530013 (2015)
2. R. A. Schmidt, L. Canton, W. Plessas, and W. Schweiger, Few-Body Syst. **58**, 34 (2017)
3. T. Melde, L. Canton, and W. Plessas, Phys. Rev. Lett. **102**, 132002 (2009)
4. T. Sato and T.-S. H. Lee, Phys. Rev. C **54**, 2660 (1996)
5. H. Polinder and T. A. Rijken, Phys. Rev. C **72**, 065210 (2005); ibid. 065211
6. H. Kamano, S. X. Nakamura, T.-S. H. Lee, and T. Sato, Phys. Rev. C **88**, 035209 (2013)
7. L. Y. Glozman, W. Plessas, K. Varga and R. F. Wagenbrunn, Phys. Rev. D **58**, 094030 (1998)

Single energy partial wave analyses on eta photoproduction – experimental data

J. Stahov[*][a], H. Osmanović[a], M. Hadžimehmedović[a], R. Omerović[a],
V. Kashevarov[b], K. Nikonov[b], M. Ostrick[b], L. Tiator[b], A. Švarc[c]

[a]University of Tuzla, Faculty of Natural Sciences and Mathematics, Univerzitetska 4,
75000 Tuzla, Bosnia and Herzegovina
[b]Institut für Kernphysik, Johannes Gutenberg-Universität Mainz, D-55099 Mainz,
Germany
[c]Rudjer Bošković Institute, Bijenička cesta 54, P.O. Box 180, 10002 Zagreb, Croatia

Abstract. Free, unconstrained, single channel, single energy partial wave analysis of η photoproduction is discontinuous in energy. We achieve point-to-point continuity by enforcing fixed-t analyticity on model independent way using available experimental data, and show that present database is insufficient to produce a unique solution. The fixed-t analyticity in the fixed-t amplitude analysis is imposed by using Pietarinen's expansion method known from Karlsruhe-Helsinki analysis of pion-nucleon scattering data. We present an analytically constrained partial wave analysis using experimental data for four observables recently measured at MAMI and GRAAL in the energy range from threshold to $\sqrt{s} = 1.85$ GeV.

1 Introduction

In another contribution of our group [1] to the Mini Workshop, we applied iterative procedure with the fixed-t analyticity constraints to a partial wave analysis of eta photoproduction pseudo data. In this paper we apply our method to a partial wave analysis of experimental data considering some limitations due to use of real data instead of idealised pseudo one. Presently, we have an incomplete set of experimental data consisting of differential cross section σ_0, single target polarisation asymmetry T, double beam-target polarisation with circular polarized photons F, and single beam polarisation Σ. Statistical and systematic errors of experimental data are much larger than 0.1% used in our analysis with pseudodata. There is also limitation in kinematical coverage. Unpolarized differential cross section has the best coverage in energy and scattering angles. Good coverage is also available for the polarisation data (Σ, T, F) up to total c.m. energy $W = 1.85 GeV$. More details about formalism and our method may be found in ref. [2].

---

[*] Talk presented by J. Stahov

2   Input preparation and results

The list of data which we used in our PWA analysis with experimental data is given in Table 1.

Table 1. Experimental data from A2@MAMI and GRAAL used in our PWA.

Obs	N	E_{lab} [MeV]	N_E	θ_{cm} [^{0}]	N_θ	Reference
σ_0	2400	$710 - 1395$	120	$18 - 162$	20	A2@MAMI(2010,2017) [3,4]
Σ	150	$724 - 1472$	15	$40 - 160$	10	GRAAL(2007) [5]
T	144	$725 - 1350$	12	$24 - 156$	12	A2@MAMI(2014) [6]
F	144	$725 - 1350$	12	$24 - 156$	12	A2@MAMI(2014) [6]

As it may be seen from the table, in our data base we have data for differential cross sections at much more energies then for polarisation observables. To perform partial wave analysis, all observables are needed at the same kinematical points. Experimental values of double-polarisation asymmetry F, target asymmetry T, and beam asymmetry Σ for given scattering angles have to be interpolated to the energies where the σ_0 data are available (fixed-s data binning). We have used a spline smoothing method as a standard method for interpolation and data smoothing [7] (Fortran code available on request). In the Ft AA part of our method, we have to build a data base at fixed t-values using measured angular distribution at a fixed value of variable s (fixed-t data binning). This has been done using again spline interpolation and smoothing method. We have performed Ft AA at t-values in the range $-1.00 GeV^2 < t < -0.09 GeV^2$ at 20 equidistant values. When working with real data, uniqueness means that the partial wave solution does not depend on starting solution. We start with two different MAID solutions: Solution I (EtaMAID-2016, [8]) and Solution II (EtaMAID-2017, [3]). Although significantly different, both solutions describe experimental data very well as might be seen in Figure 1 for two values of variable t (predictions from these two solutions can not be distinguished in the plots).

In our truncated PWA we fitted partial waves up to L_{max}=5. As in the case of pseudo data, procedure has converged fast. Resulting multipoles up to L=2, obtained after three iterations, are shown in Figure 2. Almost no differences can be observed for the dominant S waves, what is to be expected while this wave is similar in both starting solutions. Other partial waves are consistent within their error bands. Considerable differences still exist in certain kinematical regions, mainly at higher energies. It is a strong indication that for some multipoles a unique solution in this kinematical regions was not achieved (See ImE_{1+}, ImE_{2-}, and ReM_{2-} for example). There are different reasons for nonuniqueness observed. First of all, we have as an input an incomplete set of four observables. Secondly, our fixed- t constraint loses its constraining power at higher energies, especially at larger scattering angles. In addition, less kinematical points are experimentally accessible for higher negative t- values. From partial wave analysis
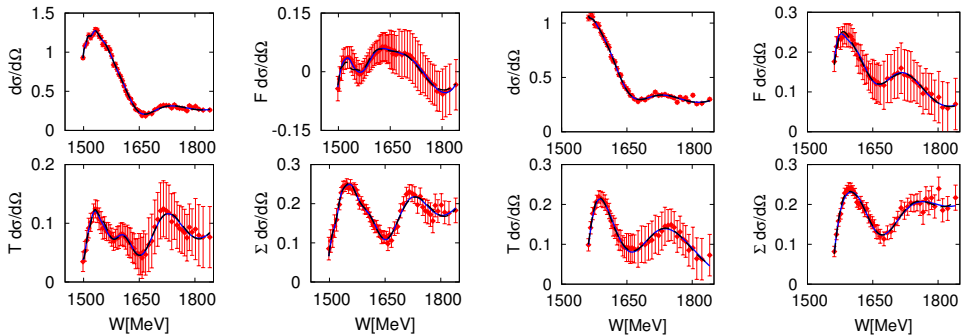
Fig. 1. Pietarinen fit of the interpolated data at $t = -0.2\,\mathrm{GeV}^2$ and $t = -0.5\,\mathrm{GeV}^2$. The dashed (black) and solid (blue) curves are the results starting with solutions I and II respectively and are on top of each other.
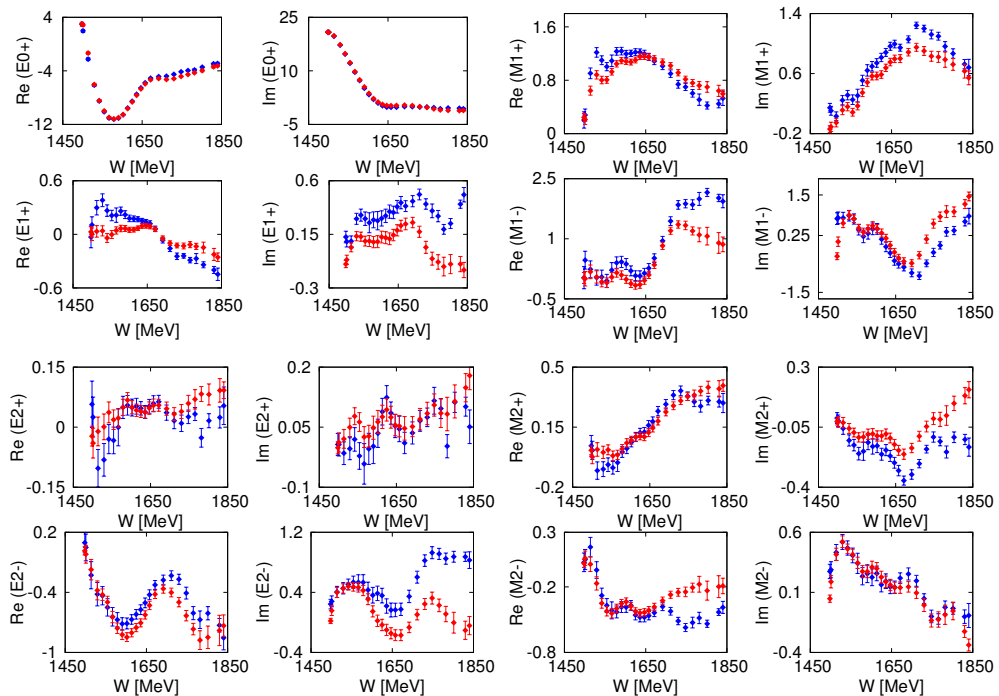
Fig. 2. (Color online) Real and imaginary parts of the S-, P- and D-wave multipoles obtained in the final step after three iterations using analytical constraints from helicity amplitudes obtained from initial solutions I (blue) and II (red).

of pseudo data we learned that a complete set of data results in unique solution. From that reason, we presume that new data from ELSA, JLAB and MAMI, which are expected soon, will help to resolve remaining ambiguities.

3   Conclusions

We applied iterative procedure with the fixed-t analyticity constraints to a partial wave analysis of eta photoproduction experimental data. In truncated PWA we obtained multipoles up to L_{max}=5. Ambiguities still remain in some multipoles, mainly at higher energies. New data, expected soon, will significantly expand our database, improve reliability of our results, and resolve remaining ambiguities.

References

1. H. Osmanović, M. Hadžimehmedović, R. Omerović, S. Smajic, J. Stahov,V. Kashevarov, K. Nikonov, M. Ostrick, L. Tiator, and A. Švarc, paralel publication in the same issue (Proceedings-Bled2017).
2. H. Osmanović, M. Hadžimehmedović, R. Omerović, J. Stahov,V. Kashevarov, K. Nikonov, M. Ostrick, L. Tiator, and A. Švarc, arXiv:1707.07891 [nucl-th]
3. V. L. Kashevarov et al., Phys. Rev. Lett. **118**, 212001 (2017).
4. E. F. McNicoll *et al.* [Crystal Ball at MAMI Collaboration], Phys. Rev. C **82**, 035208 (2010). Erratum: [Phys. Rev. C **84**, 029901 (2011)]
5. O. Bartalini *et al.* [GRAAL Collaboration], Eur. Phys. J. A **33**, 169 (2007).
6. C. S. Akondi *et al.*, [A2 Collaboration at MAMI], Phys. Rev. Lett. **113**, 102001 (2014).
7. C. de Boor, *A Practical Guide to Splines*, Springer-Verlag, Heidelberg, 1978, revised 2001.
8. V. L. Kashevarov, L. Tiator, M. Ostrick, JPS Conf. Proc. **13**, 020029 (2017).

Exclusive pion photoproduction on bound neutrons

I. Strakovsky

The George Washington University

Abstract. An overview of the GW SAID group effort to analyze pion photoproduction on the neutron target was given. The disentangling of the isoscalar and isovector EM couplings of N^* and Δ^* resonances requires compatible data on both proton and neutron targets. The final-state interactions play a critical role in the state-of-the-art analysis in extraction of the $\gamma n \to \pi N$ data from the deuteron target experiments. Then resonance couplings determined by the SAID PWA technique are compared to previous findings. The neutron program is an important component of the current JLab, MAMI-C, SPring-8, ELSA, and ELPH studies.

# Resonances and strength functions of few-body systems

Y. Suzuki

Department of Physics, Niigata University, Niigata 950-2181, Japan
RIKEN Nishina Center, Wako 351-0198, Japan

Abstract. A resonance offers a testing ground for few-body dynamics. Two types of resonances are discussed in detail. One is very narrow Hoyle resonance in ^{12}C that plays a crucial role in producing that element in stars. The other includes broad high-lying negative-parity resonances in $A = 4$ nuclei, ^{4}H, ^{4}He, ^{4}Li. The former is dominated by the Coulomb force of three-α particles at large distances, while the latter are by short-ranged nuclear forces. The structure of these resonances is described by different approaches, adiabatic hyperspherical method and correlated Gaussians used for strength function calculations. The localization of the resonance is successfully realized by a complex absorbing potential and a complex scaling method, respectively.

1 Hoyle resonance

The synthesis of ^{12}C is essential to ^{12}C-based life and its process at low temperatures is sequential via a narrow resonance of ^{8}Be:

$$\alpha + \alpha \rightarrow \, ^8\text{Be}, \quad \alpha + \, ^8\text{Be} \rightarrow \, ^{12}\text{C} + \gamma. \tag{1}$$
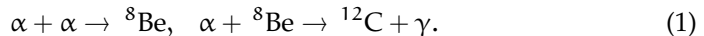
As predicted by Hoyle, however, an existence of a very narrow resonance at around $E_x =$7.7 MeV is vital to explain the abundance of ^{12}C element. The resonance is found to be just 0.38 MeV above 3α threshold with its width of 8.5 eV.

Since nobody has ever succeeded in reproducing the Hoyle resonance width, we have undertaken to tackle this problem in the adiabatic hyperspherical method [1, 2]. This study has further been motivated by the fact that there exists huge discrepancy in the rate of triple-α reactions, $\alpha + \alpha + \alpha \rightarrow \, ^{12}\text{C} + \gamma$, calculated by several authors [3–5].

In contrast to two-body resonances, the Hoyle resonance is characterized by the followings: (1) 3α particles interact via long-ranged Coulomb force even at large distances. (2) no asymptotic wave function is known. (3) 2α subsystem forms a sharp resonance, which causes successive avoided crossings with three-particle continuum states.

The detail of our approach is given in Refs. [1, 2]. The three-body system is completely specified by six coordinates excluding the center-of-mass coordinate. Among six coordinates one is chosen to be the hyperradius of length dimension, and other five coordinates are hyperangles. Among the five angle coordinates

three are Euler angles and two are used to specify the geometry of the three body system. By changing the geometry as much as possible, we can study the adiabatic potential curve of the three-body system as a function of the hyperradius. A resonance can be confined by introducing a complex absorbing potential [6] at large distances of the hyperradius. This method works excellently for quantitatively reproducing the very narrow width of the Hoyle resonance as well as predicting the triple-α reaction rate at low temperatures without relying on any ambiguous ansatz.

2 Resonances in $A = 4$ nuclei

^{4}He nucleus is doubly magic and its 0^+ ground state is strongly bound. The first excited state of ^{4}He is not a negative-party but again 0^+. The negative-parity excited states appear above the ^{3}He+p threshold. Seven negative-parity states are known and some of them have very broad widths. There exist isobar resonances in ^{4}H and ^{4}Li that are also very broad. Most of these resonances are identified by R-matrix phenomenology.

These resonances offer typical four-body resonances governed by the nuclear force. The decay channels include not only two-body but three-body systems. To describe the resonance we have employed correlated Gaussians [7,8] that provide us with efficient and accurate performance as few-body basis functions. A general form of the correlated Gaussians is

$$[\theta_L \times \chi_S]_{JM} \exp\left[-\sum_{i<j} a_{ij}(\mathbf{r}_i - \mathbf{r}_j)^2 \right]\eta_{TM_T}, \tag{2}$$

where θ_L, χ_S, η_T stand for the functions of orbital angular momentum, spin, isospin parts. a_{ij} are variational parameters that control the spatial configuration of the system. See also Ref. [9] for recent review on the correlated Gaussians.

The negative-parity resonances may be studied by analyzing strength functions for electromagnetic excitations from the ground state of ^{4}He. Actually we have considered the spin-dipole operator specified by type p and $\lambda\mu$ tensor (λ=0,1,2)

$$\mathcal{O}^p_{\lambda\mu} = \sum_{i=1}^{4} [(\mathbf{r}_i - \mathbf{R}) \times \boldsymbol{\sigma}_i]_{\lambda\mu} T^p_i \tag{3}$$

where the center-of-mass coordinate of $A = 4$ nucleus, $\mathbf{R}$, is subtracted from the position coordinate $\mathbf{r}_i$ to make sure excitations of intrinsic motion only and T^p_i distinguishes different types of isospin operators (t_x, t_y, t_z)

$$T^p_i = \begin{cases} 1 & \text{Isoscalar} \\ 2t_z(i) & \text{Isovector} \\ t_x(i) \pm it_y(i) & \text{Charge} - \text{exchange} \end{cases} \tag{4}$$

We calculate the strength function $S^p_\lambda(E)$ corresponding to the response of the ^{4}He ground state Ψ_0 induced by $\mathcal{O}^p_{\lambda\mu}$

$$S^p_\lambda(E) = \mathcal{S}_{\mu f}|\langle\Psi_f|\mathcal{O}^p_{\lambda\mu}|\Psi_0\rangle|^2\delta(E_f - E_0 - E), \tag{5}$$

where $\mathcal{S}_{\mu f}$ denotes a sum over all possible final states This strength function can be computed by using the complex scaling method. The important thing for accurate evaluation of $S_\lambda^p(E)$ is to span possible final configurations as much as possible.

We have studied three negative-parity states with isospin 0 in ^{4}He and four negative-parity states with isospin1 in ^{4}He, ^{4}H, ^{4}Li [10–12]. Some of the resonance widths are very broad, and thus it is hard to identify their resonance parameters on the complex plane. However, the strength functions calculated above clearly indicate peaks near the resonance energies. We have confirmed that even the broad resonance can be identified with this calculation.

Acknowledgments

References

1. H. Suno, Y. Suzuki, and P. Descouvemont, Phys. Rev. C **91**, 014004 (2015).
2. H. Suno, Y. Suzuki, and P. Descouvemont, Phys. Rev. C **94**, 054607 (2016).
3. K. Ogata, M. Kan, and M. Kamimura, Prog. Theor. Phys. 122, 1055 (2009).
4. N. B. Nguyen, F. M. Nunes, and I. J. Thompson, Phys. Rev. C 87, 054615 (2013).
5. S. Ishikawa, Phys. Rev. C 87, 055804 (2013).
6. D. E. Manolopoulos, J. Chem. Phys. **117**, 9552 (2002).
7. K. Varga and Y. Suzuki, Phys. Rev. C **52**, 2885 (1995).
8. Y. Suzuki and K. Varga, *Stochastic Variational Approach to Quantum-Mechanical Few-Body Problems*, Lecture Notes in Physics, m **54**, Springer, Berlin, 1998.
9. J. Mitroy, S. Bubin, W. Horiuchi, Y. Suzuki, L. Adamowicz, W. Cencek, K. Szalewicz, J. Komasa, D. Blume, and K. Varga, Rev. Mod. Phys. **85**, 693 (2013).
10. W. Horiuchi and Y. Suzuki, Phys. Rev. C **78**, 034305 (2008).
11. W. Horiuchi and Y. Suzuki, Phys. Rev. C **85**, 054002 (2012).
12. W. Horiuchi and Y. Suzuki, Phys. Rev. C **87**, 034001 (2013).

From Experimental Data to Pole Parameters in a Model Independent Way
(Angle Dependent Continuum Ambiguity and Laurent + Pietarinen Expansion)

Alfred Švarc

Rudjer Bošković Institute, Bijenička cesta 54, P.O. Box 180, 10002 Zagreb, Croatia

Abstract. It is well known that unconstrained single-energy partial wave analysis (USEPWA) gives many equivalent discontinuous solutions, so a constraint to some theoretical model must be used to ensure the uniqueness. It can be shown that it is a direct consequence of not specifying the angle-dependent part of continuum ambiguity phase which mixes multipoles, and by choosing this phase we restore the uniqueness of USEPWA, and obtain the solution in a model independent way. Up to now, there was no reliable way to extract pole parameters from so obtained SE partial waves, but a new and simple single-channel method (Laurent + Pietarinen expansion) applicable for continuous and discrete data has been recently developed. It is based on applying the Laurent decomposition of partial wave amplitude, and expanding the non-resonant background into a power series of a conformal-mapping, quickly converging power series obtaining the simplest analytic function with well-defined partial wave analytic properties which fits the input. The generalization of this method to multi- channel case is also developed and presented. Unifying both methods in succession, one constructs a model independent procedure to extract pole parameters directly from experimental data without referring to any theoretical model.

1 Introduction

It is well known that unconstrained single-energy partial wave analysis (USEPWA) gives many equivalent discontinuous solutions, so a constraint to some theoretical model must be used to ensure the uniqueness. It can be shown that it is a direct consequence of not specifying the angle-dependent part of continuum ambiguity phase which mixes multipoles, and by choosing this phase we restore the uniqueness of USEPWA, and obtain the solution in a model independent way [1]. Up to now, there was no reliable way to extract pole parameters from so obtained SE partial waves, but a new and simple single-channel method (Laurent + Pietarinen expansion) applicable for continuous and discrete data has been recently developed [2–4]. It is based on applying the Laurent decomposition of partial wave amplitude, and expanding the non-resonant background into a power series of a conformal-mapping, quickly converging power series obtaining the simplest analytic function with well-defined partial wave analytic properties which fits the

input. The method is particularly useful to analyse partial wave data obtained directly from experiment because it works with minimal theoretical bias since it avoids constructing and solving elaborate theoretical models, and fitting the final parameters to the input, what is the standard procedure now. The generalization of this method to multi- channel case is also developed and presented.

2   Angular dependent continuum ambiguity

Let us recall that observables in single-channel reactions are given as a sum of products involving one (helicity or transversity) amplitude with the complex conjugate of another, so that the general form of any observable is $\mathcal{O} = f(H_k \cdot H_l^*)$, where f is a known, well-defined real function. The direct consequence is that any observable is invariant with respect to the following simultaneous phase transformation of all amplitudes:

$$H_k(W, \theta) \to \tilde{H}_k(W, \theta) = e^{i\,\phi(W,\theta)} \cdot H_k(W, \theta)$$
$$\text{for all } k = 1, \cdots, n \tag{1}$$

where n is the number of spin degrees of freedom (n=1 for the 1-dim toy model, n=2 for pi-N scattering and n=4 for pseudoscalar meson photoproduction), and $\phi(W, \theta)$ is an arbitrary, real function which is the same for all contributing amplitudes.

As resonance properties are usually the goal of such studies, and these are identified with poles of the partial-wave (or multipole) amplitudes, we must analyze the influence of the continuum ambiguity not upon helicity or transversity amplitudes, but upon their partial wave decompositions. To simplify the study we introduce partial waves in a simplified version than those found in Ref. [5]:

$$A(W, \theta) = \sum_{\ell=0}^{\infty} (2\ell + 1) A_\ell(W) P_\ell(\cos\theta) \tag{2}$$

where $A(W, \theta)$ is a generic notation for any amplitude $H_k(W, \theta)$, $k = 1, \cdots n$. The complete set of observables remains unchanged when we make the following transformation:

$$A(W, \theta) \to \tilde{A}(W, \theta) = e^{i\,\phi(W,\theta)}$$
$$\times \sum_{\ell=0}^{\infty} (2\ell + 1) A_\ell(W) P_\ell(\cos\theta)$$
$$\tilde{A}(W, \theta) = \sum_{\ell=0}^{\infty} (2\ell + 1) \tilde{A}_\ell(W) P_\ell(\cos\theta) \tag{3}$$

We are interested in rotated partial wave amplitudes $\tilde{A}_\ell(W)$, defined by Eq.(3), and are free to introduce the Legendre decomposition of an exponential function as:

$$e^{i\,\phi(W,\theta)} = \sum_{\ell=0}^{\infty} L_\ell(W) P_\ell(\cos\theta). \tag{4}$$

After some manipulation of the product $P_\ell(x)P_k(x)$ (see refs. [6, 7] for details of the summation rearrangement) we obtain:

$$\tilde{A}_\ell(W) = \sum_{\ell'=0}^{\infty} L_{\ell'}(W) \cdot \sum_{m=|\ell'-\ell|}^{\ell'+\ell} \langle \ell', 0; \ell, 0|m, 0\rangle^2 \, A_m(W) \tag{5}$$

where $\langle \ell', 0; \ell, 0|m, 0\rangle$ is a standard Clebsch-Gordan coefficient.

To get a better insight into the mechanism of multipole mixing, let us expand Eq. (5) in terms of phase-rotation Legendre coefficients $L_{\ell'}(W)$:

$$\tilde{A}_0(W) = \mathbf{L_0(W)A_0(W)} + L_1(W)A_1(W) + L_2(W)A_2(W) + \ldots, \tag{6}$$

$$\tilde{A}_1(W) = \mathbf{L_0(W)A_1(W)} + L_1(W)\left[\frac{1}{3}A_0(W) + \frac{2}{3}A_2(W)\right]$$

$$+ L_2(W)\left[\frac{2}{5}A_1(W) + \frac{3}{5}A_3(W)\right] + \ldots,$$

$$\tilde{A}_2(W) = \mathbf{L_0(W)A_2(W)} + L_1(W)\left[\frac{2}{5}A_1(W) + \frac{3}{5}A_3(W)\right]$$

$$+ L_2(W)\left[\frac{1}{5}A_0(W) + \frac{2}{7}A_2(W) + \frac{18}{35}A_4(W)\right] + \ldots.$$

$$\vdots$$

The consequence of Eqs. (5) and (6) is that angular-dependent phase rotations mix multipoles.

Conclusion:

Without fixing the free continuum ambiguity phase $\phi(W, \theta)$, the partial wave decomposition $A_\ell(W)$ defined in Eq. (2) is non-unique. Partial waves get mixed, and identification of resonance quantum numbers might be changed. To compare different partial-wave analyses, it is essential to match the continuum ambiguity phase; otherwise the mixing of multipoles is yet another, uncontrolled, source of systematic errors. Observe that this phase rotation does not create new pole positions, but just reshuffles the existing ones among several partial waves.

3   Using angular-dependent phase ambiguity to obtain up-to-a-phase unique, unconstrained, single-energy solution in η photoproduction

We perform unconstrained, $L_{max} = 5$ truncated single-energy analyses on a complete set of observables for η photoproduction given in the form of pseudo-data created using the ETA-MAID15a model [8]: $d\sigma/d\Omega$, $\Sigma\, d\sigma/d\Omega$, $T\, d\sigma/d\Omega$, $F\, d\sigma/d\Omega$, $G\, d\sigma/d\Omega$, $P\, d\sigma/d\Omega$, $C_{x'}\, d\sigma/d\Omega$, and $O_{x'}\, d\sigma/d\Omega$. All higher multipoles

are put to zero. The fitting procedure finds solutions which are non-unique, and we obtain many solutions depending on the choice of initial parameters in the fit. In Fig. 1 we show a complete set of pseudo-data with the error of 1 % created at 18 angles (red symbols), and the typical SE fit (full line) at one representative energy of $W = 1769.80$ MeV.
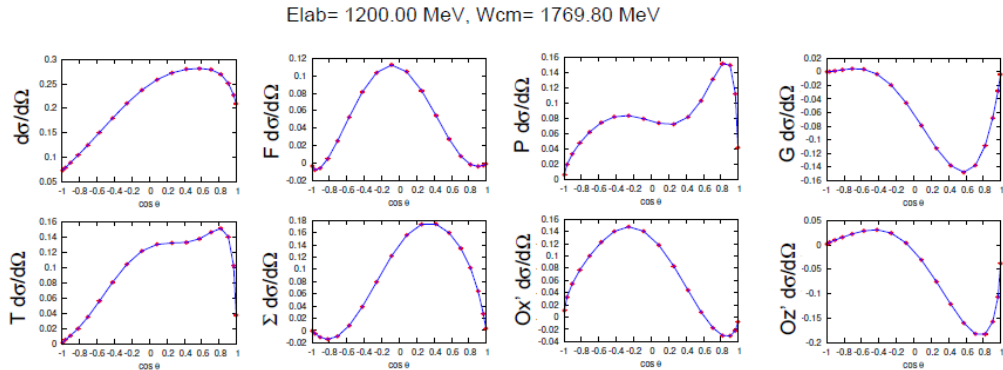
Fig. 1. (Color online) Complete set of observables for η photoproduction given in the form of pseudo-data created at 18 angles with the error bar of 1 % using the ETA-MAID15a model (red symbols) and a typical fit to the data (full line).

In Fig. 2 we show an example of three very different sets of multipoles which fit the complete pseudo-data set equally well to a high precision: two discrete and discontinuous ones obtained by setting the initial fitting values to the ETA-MAID16a [9] (SE^{16a}) and Bonn-Gatchina [10] (SE^{BG}) model values (blue and red symbols respectively), and the generating ETA-MAID15a model [8] which is displayed as full and dashed black continuous lines.

We know from Eq.(1) that equivalent fits to a complete set of data must be produced by helicity amplitudes with different phases. Therefore, in Fig. 3, we construct the helicity amplitudes corresponding to all three sets of multipoles from Fig. 2 at one randomly chosen energy $W = 1660.4$ MeV.
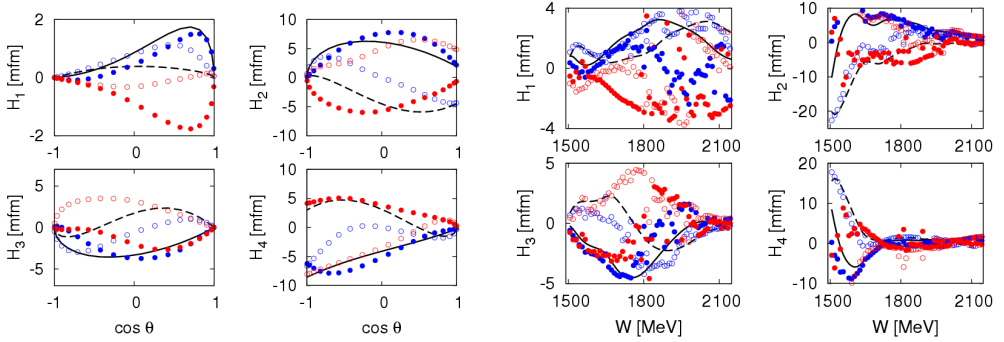
We see that all three sets of helicity amplitudes are indeed different, but the discontinuity of multipole amplitudes, observed in Fig. 2-left is not reflected in a plot of helicity amplitudes at a fixed single energy. If instead we plot an excitation curve of all four helicity amplitudes at a randomly chosen angle, which is arbitrarily set to the value $\cos\theta = 0.2588$, we obtain the result shown in Fig. 3-right.

We see that the excitation curve of helicity amplitudes in this case remains continuous only for the generating model ETA-MAID15a. For both single-energy solutions it is different, and at the same time shows notable discontinuities between neighbouring energy points. This leads to the following understanding of this, apparently very different multipole solutions:
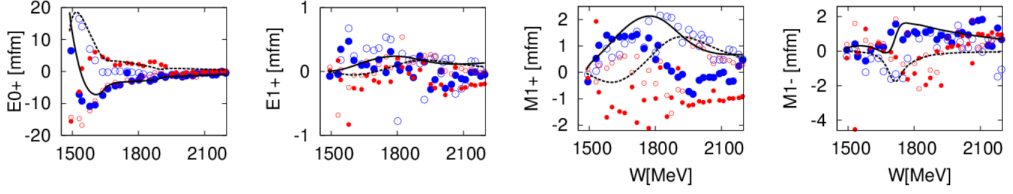
Fig. 2. (Color online) Plots of the E_{0+}, M_{1-}, E_{1+}, and M_{1+} multipoles. Full and dashed black lines give the real and imaginary part of the ETA-MAID15a generating model. Discrete blue and red symbols are obtained with the unconstrained, $L_{max} = 5$ fits of a complete set of observables generated as numeric data from the ETA-MAID15a model of ref. [8], with the initial fitting values taken from the ETA-MAID16a [9] and the Bonn-Gatchina [10] models respectively. Filled symbols represent the real parts and open symbols give the imaginary parts.

Fig. 3. (Color online) Left we show three sets of helicity amplitudes for all three sets of multipoles at one randomly chosen energy $W = 1660.4$ MeV, and right for we show the excitation curves for all three sets of multipoles, at one randomly chosen value of $\cos\theta = 0.2588$ MeV. The figure coding is the same as in Fig. 2.

When we perform an unconstrained SE PWA, each minimization is performed independently at individual energies, and the phase is chosen randomly. So, at each energy the fit chooses a different angle dependent phase, and creates different, discontinuous numerical values for each helicity amplitude, producing discontinuous sets of multipoles.

However, the invariance with respect to phase rotations offers a possible solution. Let us show the procedure.

We introduce the following angle-dependent phase rotation simultaneously for all four helicity amplitudes:

$$\tilde{H}_k^{SE}(W, \theta) = H_k^{SE}(W, \theta) \cdot e^{i\,\Phi_{H_2}^{15a}(W,\theta) - i\,\Phi_{H_2}^{SE}(W,\theta)}$$
$$k = 1, \ldots, 4 \tag{7}$$

where $\Phi_{H_2}^{SE}(W, \theta)$ is the phase of any single-energy solution and $\Phi_{H_2}^{15a}(W, \theta)$ is the phase of generating solution ETA-MAID15a. Applying this rotation we replace

the discontinuous $\Phi_{H_2}^{SE}(W, \theta)$ phase from any SE solution with the continuous $\Phi_{H_2}^{15a}(W, \theta)$ ETA-MAID15a phase.
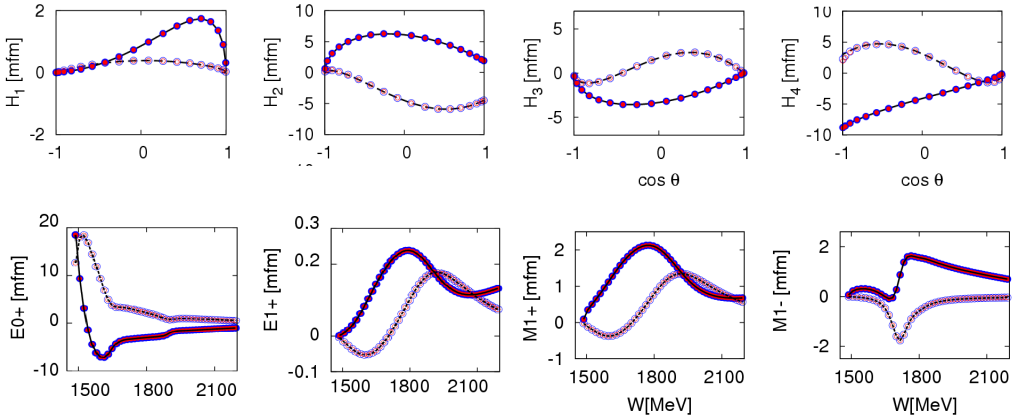
Fig. 4. (Color online) Up we show all three sets of rotated helicity amplitudes at one randomly chosen energy $W = 1660.4$ MeV, and down three sets of rotated multipoles. The figure coding is the same as in Fig. 2.

The resulting rotated single-energy helicity amplitudes are compared with generating ETA-MAID15a amplitudes in Fig. 4.

We see that rotated helicity amplitudes of both single-energy solutions are now identical to the generating ETA-MAID15a helicity amplitudes.

Thus, the previously different sets of discrete, discontinuous single-energy multipoles different from the generating solution ETA-MAID15a and given in Fig. 2, are after phase rotation transformed into continuous multipoles now identical to the generating solution, and given in lower part of Fig. 4.

So, we have constructed a way to generate up-to-a-phase unique solutions in an unconstrained PWA of a complete set of observables generated as pseudo-data.

4 Laurent + Pietarinen expansion

The driving concept behind the Laurent-Pietarinen (L+P) expansion was the aim to replace an elaborate theoretical model by a local power-series representation of partial wave amplitudes [2]. The complexity of a partial-wave analysis model is thus replaced by much simpler model-independent expansion which just exploits analyticity and unitarity. The L+P approach separates pole and regular part in the form of a Laurent expansion, and instead of modeling the regular part in some physical model it uses the conformal mapping to expand it into a rapidly converging power series with well defined analytic properties. So, the method replaces the regular part calculated in a model by the simplest analytic function

which has correct analytic properties of the analyzed partial wave (multipole), and fits the data. In such an approach the model dependence is minimized, and is reduced to the choice of the number and location of branch-points used in the model.

The L+P expansion is based on the Pietarinen expansion used in some former papers in the analysis of pion-nucleon scattering data [11–14], but for the L+P model the Pietarinen expansion is applied in a different manner. It exploits the Mittag-Leffler expansion[1] of partial wave amplitudes near the real energy axis, representing the regular, but unknown, background term by a conformal-mapping-generated, rapidly converging power series called a Pietarinen expansion[2]. The method was used successfully in several few-body reactions [3, 4, 17], and recently generalized to the multi-channel case [18]. The formulae used in the L+P approach are collected in Table 1. In the fits, the regular background part is represented by three Pietarinen expansion series, all free parameters are fitted. The first Pietarinen expansion with branch-point x_P is restricted to an unphysical energy range and represents all left-hand cut contributions. The next two Pietarinen expansions describe the background in the physical range with branch-points x_Q and x_R respecting the analytic properties of the analyzed partial wave. The second branch-point is mostly fixed to the elastic channel branch-point, the third one is either fixed to the dominant channel threshold, or left free. Thus, only rather general physical assumptions about the analytic properties are made like the number of poles and the number and the position of branch-points, and the simplest analytic function with a set of poles and branch-points is constructed. The method is applicable to both, theoretical and experimental input, and represents the first reliable procedure to extract pole positions from experimental data, with minimal model bias.

The generalization of the L+P method to a multichannel L+P method is performed in the following way: i) separate Laurent expansions are made for each channel; ii) pole positions are fixed for all channels, iii) residua and Pietarinen coefficients are varied freely; iv) branch-points are chosen as for the single-channel model; v) the single-channel discrepancy function D_{dp}^a (see Eq. (5) in ref. [17]) which quantifies the deviation of the fitted function from the input is generalized to a multi-channel quantity D_{dp} by summing up all single-channel contributions, and vi) the minimization is performed for all channels in order to obtain the final solution.

The formulae used in the L+P approach are collected in Table 1.

---

[1] Mittag-Leffler expansion [15]. This expansion is the generalization of a Laurent expansion to a more-than-one pole situation. For simplicity, we will simply refer to this as a Laurent expansion.

[2] A conformal mapping expansion of this particular type was introduced by Ciulli and Fisher [11, 12], was described in detail and used in pion-nucleon scattering by Esco Pietarinen [13, 14]. The procedure was denoted as a Pietarinen expansion by G. Höhler in [16].

Table 1. Formulae defining the Laurent+Pietarinen (L+P) expansion.

$$T^a(W) = \sum_{j=1}^{N_{pole}} \frac{x_j^a + \iota\, y_j^a}{W_j - W} + \sum_{k=0}^{K^a} c_k^a\, X^a(W)^k + \sum_{l=0}^{L^a} d_l^a\, Y^a(W)^l + \sum_{m=0}^{M^a} e_m^a\, Z^a(W)^m$$

$$X^a(W) = \frac{\alpha^a - \sqrt{x_P^a - W}}{\alpha^a + \sqrt{x_P^a - W}}\ ;\qquad Y^a(W) = \frac{\beta^a - \sqrt{x_Q^a - W}}{\beta^a + \sqrt{x_Q^a - W}}\ ;\qquad Z^a(W) = \frac{\gamma^a - \sqrt{x_R^a - W}}{\gamma^a + \sqrt{x_R^a - W}}$$

$$D_{dp}^a = \frac{1}{2\,N_W^a - N_{par}^a} \sum_{i=1}^{N_W^a} \left\{ \left[\frac{\mathrm{Re}\,T^a(W^{(i)}) - \mathrm{Re}\,T^{a,exp}(W^{(i)})}{Err_{i,a}^{Re}} \right]^2 \right.$$

$$\left. + \left[\frac{\mathrm{Im}\,T^a(W^{(i)}) - \mathrm{Im}\,T^{a,exp}(W^{(i)})}{Err_{i,a}^{Im}} \right]^2 \right\} + \mathcal{P}^a$$

$$\mathcal{P}^a = \lambda_c^a \sum_{k=1}^{K^a} (c_k^a)^2\, k^3 + \lambda_d^a \sum_{l=1}^{L^a} (d_l^a)^2\, l^3 + \lambda_e^a \sum_{m=1}^{M^a} (e_m^a)^2\, m^3\ ;\qquad D_{dp} = \sum_a^{all} D_{dp}^a$$

a ... channel index N_{pole} ... number of poles $W_j, W \in \mathbb{C}$

$x_i^a, y_i^a, c_k^a, d_l^a, e_m^a, \alpha^a, \beta^a, \gamma^a \ldots \in \mathbb{R}$

$K^a, L^a, M^a \ldots \in \mathbb{N}$ number of Pietarinen coefficients in channel *a*.

D_{dp}^a ... discrepancy function in channel a

N_W^a ... number of energies in channel a

N_{par}^a ... number of fitting parameters in channel a

$\mathcal{P}^a$ ... Pietarinen penalty function

$\lambda_c^a, \lambda_d^a, \lambda_e^a$ ... Pietarinen weighting factors

$x_P^a, x_Q^a, x_R^a \in \mathbb{R}$ (or $\in \mathbb{C}$).

$Err_{i,a}^{Re,\,Im}$ ... minimization error of real and imaginary part respectively.

Acknowledgements

References

1. A. Svarc, https://indico.cern.ch/event/591374/contributions/2477135/ , PWA9/ATHOS4: The International Workshop on Partial Wave Analyses and Advanced Tools for Hadron Spectroscopy, Bad Honnef near Bonn (Germany) from March 13 to 17, 2017.
2. A. Svarc, M. Hadzimehmedovic, H. Osmanovic, J. Stahov, L. Tiator, and R. L. Workman, Phys, Rev. C88, 035206 (2013).
3. A. Svarc, M. Hadzimehmedovic, R. Omerovic, H. Osmanovic, and J. Stahov, Phys, Rev. C89, 0452205 (2014).
4. A. Svarc, M. Hadzimehmedovic, H. Osmanovic, J. Stahov, L. Tiator, and R. L. Workman, Phys, Rev. C89, 65208 (2014).
5. L. Tiator, D. Drechsel, S. S. Kamalov and M. Vanderhaeghen, Eur. Phys. J. ST **198**, 141 (2011).
6. J. Dougall, Glasgow Mathematical Journal, **1** (1952) 121-125.

7. Y. Wunderlich, A. Švarc, R. L. Workman, L. Tiator, and R. Beck, arXiv:1708.06840[nucl-th].

8. V. L. Kashevarov, L. Tiator, M. Ostrick, Bled Workshops Phys., 16, 9 (2015).

9. V. L. Kashevarov, l. Tiator, M. Ostrick, JPS Conf. Proc. 13, 020029 (2017).

10. http://pwa.hiskp.uni-bonn.de/

11. S. Ciulli and J. Fischer in Nucl. Phys. 24, 465 (1961).

12. I. Ciulli, S. Ciulli, and J. Fisher, Nuovo Cimento **23**, 1129 (1962).

13. E. Pietarinen, Nuovo Cimento Soc. Ital. Fis. **12A**, 522 (1972).

14. E. Pietarinen, Nucl. Phys. **B107**, 21 (1976).

15. Michiel Hazewinkel: *Encyclopaedia of Mathematics*, Vol.6, Springer, 31. 8. 1990, pg.251.

16. G. Höhler and H. Schopper, "Numerical Data And Functional Relationships In Science And Technology. Group I: Nuclear And Particle Physics. Vol. 9: Elastic And Charge Exchange Scattering Of Elementary Particles. B: Pion Nucleon Scattering. Pt. 2: Methods And Results and Phenomenology," *Berlin, Germany: Springer (1983) 601 P. (Landolt-Boernstein. New Series, I/9B2).*

17. A. Švarc, M. Hadžimehmedović, H. Osmanović, J. Stahov, and R. L. Workman, Phys. Rev. **C91**, 015207 (2015).

18. A. Švarc, M. Hadžimehmedović, H. Osmanović, J. Stahov, L. Tiator, R. L. Workman, Phys. Lett. **B755** (2016) 452455.

Baryon transition form factors from space-like into time-like regions

L. Tiator

Institut für Kernphysik, Johannes Gutenberg Universität Mainz, Germany

Pion electroproduction is the main source for investigations of the transition form factors of the nucleon to excited N^* and Δ baryons. After early measurements of the G_M^* form factor of the $N\Delta$ transition, in the 1990s a large program was running at Mainz, Bonn, Bates Brookhaven and JLab in order to measure the E/M ratio of the $N\Delta$ transition and the Q^2 dependence of the E/M and S/M ratios in order to get information on the internal quadrupole deformations of the nucleon and the Δ. Only at JLab both the energy and the photon virtuality were available to measure transition form factors for a set of nucleon resonances up to $Q^2 \approx 5$ GeV^2. Two review articles on the electromagnetic excitation of nucleon resonances, which give a very good overview over experiment and theory, were published a few years ago [1, 2].

In the spirit of the dynamical approach to pion photo- and electroproduction, the t-matrix of the unitary isobar model MAID is set up by the ansatz [1]

$$t_{\gamma\pi}(W) = t_{\gamma\pi}^B(W) + t_{\gamma\pi}^R(W)\,, \tag{1}$$

with a background and a resonance t-matrix, each of them constructed in a unitary way. Of course, this ansatz is not unique. However, it is a very important prerequisite to clearly separate resonance and background amplitudes within a Breit-Wigner concept also for higher and overlapping resonances. For a specific partial wave $\alpha = \{j, l, \ldots\}$, the background t-matrix is set up by a potential multiplied by the pion-nucleon scattering amplitude in accordance with the K-matrix approximation,

$$t_{\gamma\pi}^{B,\alpha}(W, Q^2) = \nu_{\gamma\pi}^{B,\alpha}(W, Q^2)\,[1 + it_{\pi N}^\alpha(W)]\,, \tag{2}$$

where the on-shell part of pion-nucleon rescattering is maintained in the non-resonant background and the off-shell part from pion-loop contributions is absorbed in the phenomenological renormalized (dressed) resonance contribution. In the latest version MAID2007 [3], the S, P, D, and F waves of the background contributions are unitarized as explained above, with the pion-nucleon elastic scattering amplitudes $t_{\pi N}^\alpha$ described by phase shifts and inelasticities taken from the GWU/SAID analysis [4].
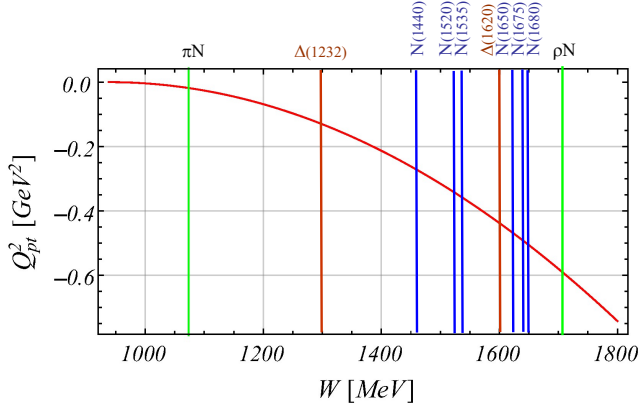
Fig. 1. The W dependence of the pseudo-threshold, where the Siegert theorem strictly holds and which also limits the physical region, where time-like form factors can be obtained from Dalitz decays $N\pi \to Ne^+e^-$. At πN threshold, the pseudo-threshold value is $Q_{pt}^2 = -m_\pi^2 = -0.018$ GeV^2, at $W = 1535$ MeV, $Q_{pt}^2 = -0.356$ GeV^2. The vertical lines denote the pion threshold and nucleon resonance positions, where space-like transition form factors have been analyzed from electroproduction experiments.

For the resonance contributions we follow Ref. [3] and assume Breit-Wigner forms for the resonance shape,

$$t_{\gamma\pi}^{R,\alpha}(W, Q^2) = \bar{\mathcal{A}}_\alpha^R(W, Q^2) \frac{f_{\gamma N}(W)\Gamma_{tot}(W)\, M_R\, f_{\pi N}(W)}{M_R^2 - W^2 - iM_R\,\Gamma_{tot}(W)}\, e^{i\phi_R(W)}, \qquad (3)$$

where $f_{\pi N}(W)$ is a Breit-Wigner factor describing the decay of a resonance with total width $\Gamma_{tot}(W)$. The energy dependence of the partial widths and of the γNN^* vertex can be found in Ref. [3]. The phase $\phi_R(W)$ in Eq. (3) is introduced to adjust the total phase such that the Fermi-Watson theorem is fulfilled below two-pion threshold.

In most cases, the resonance couplings $\bar{\mathcal{A}}_\alpha^R(W, Q^2)$ are assumed to be independent of the total energy and a simple Q^2 dependence is assumed for $\bar{\mathcal{A}}_\alpha(Q^2)$. Generally, these resonance couplings, taken at the Breit-Wigner mass $W = M_R$ are called transition form factors $\bar{\mathcal{A}}_\alpha(Q^2)$. In the literature, baryon transition form factors are defined in three different ways as helicity form factors $A_{1/2}(Q^2)$, $A_{3/2}(Q^2)$, $S_{1/2}(Q^2)$, Dirac form factors $F_1(Q^2)$, $F_2(Q^2)$, $F_3(Q^2)$ and Sachs form factors $G_E(Q^2)$, $G_M(Q^2)$, $G_C(Q^2)$. For detailed relations among them see Ref. [1]. In MAID they are parameterized in an ansatz with polynomials and exponentials, where the free parameters are determined in a fit to the world data of pion photo- and electroproduction.

In the case of the $N\Delta$ transition, the form factors are usually discussed in the Sachs definition and are denoted by $G_E^*(Q^2)$, $G_M^*(Q^2)$, $G_C^*(Q^2)$. While the G_M^* form factor by far dominates the $N \to \Delta$ transition, the electric and Coulomb transitions are usually presented as E/M and S/M ratios. In pion electroproduction they are defined as the ratios of the multipoles. Within our ansatz they can
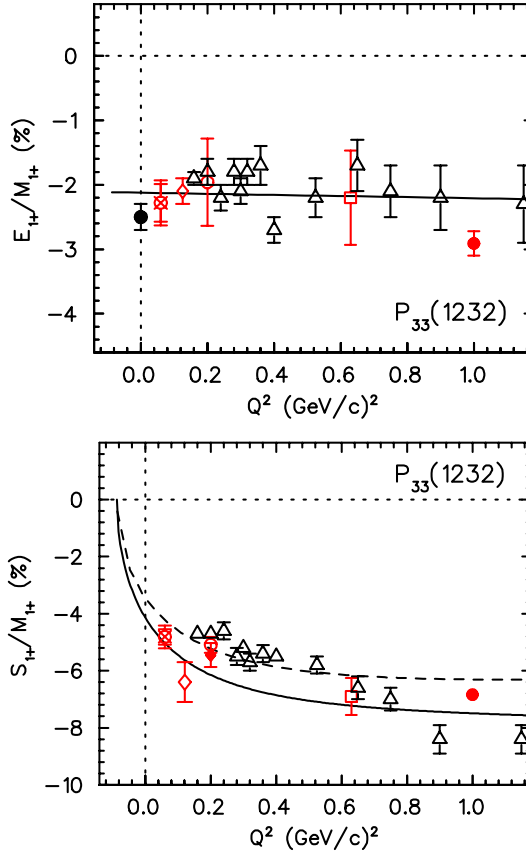
be expressed in terms of the NΔ transition form factors by

$$R_{EM}(Q^2) = -\frac{G_E^\star(Q^2)}{G_M^\star(Q^2)}, \tag{4}$$

$$R_{SM}(Q^2) = -\frac{k(M_\Delta, Q^2)}{2M_\Delta}\frac{G_C^\star(Q^2)}{G_M^\star(Q^2)}, \tag{5}$$

with the virtual photon 3-momentum

$$k(W, Q^2) = \sqrt{((W - M_N)^2 + Q^2)(W + M_N)^2 + Q^2)}/(2W).$$

Fig. 2. The Q^2 dependence of the E/M and S/M ratios of the $\Delta(1232)$ excitation for low Q^2. The data are from Mainz, Bonn, Bates and JLab. For details see Ref. [1]. The behavior of the S/M ratio at low Q^2 and in particular for $Q^2 < 0$ in the unphysical region is a consequence of the Siegert theorem.

Whereas in photo- and electroproduction, data are only available for space-like momentum transfers, $Q^2 = -k_\mu k^\mu \geq 0$, the inelastic form factors can be extended into the time-like region, $Q^2 \leq 0$, down to the so-called pseudo-threshold, Q^2_{pt}, which is defined as the momentum transfer, where the 3-momentum of the virtual photon vanishes,

$$k(W, Q^2_{pt}) = 0 \quad \rightarrow \quad Q^2_{pt} = -(W - M_N)^2. \tag{6}$$

This time-like region is called the Dalitz decay region. The energy dependence of this region is shown in Fig. 1. At pion threshold, the Dalitz decay region is very small and extends only down to $Q^2_{pt} = -0.018\,\text{GeV}^2$, for transitions to the $\Delta(1232)$ resonance down to $-0.086\,\text{GeV}^2$ and to the Roper resonance $N(1440)$ down to $-0.252\,\text{GeV}^2$.

In Fig. 2 we have extended our parametrization of the E/M and S/M ratios for $N \rightarrow \Delta$ from space-like to time-like regions and show a comparison to the data obtained from photo- and electroproduction [1,2].

In general, the extrapolation of the transverse form factors G_E and G_M into the time-like region is more reliable than the extrapolation of the longitudinal form factor G_C, which can not be measured at $Q^2 = 0$ with photoproduction. For longitudinal transitions, the photon point is only reachable asymptotically, and in practise, only at MAMI-A1 in Mainz, momentum transfers as low as $Q^2 \simeq 0.05\,\text{GeV}^2$ are accessible. Therefore, the longitudinal form factors become already quite uncertain in the real-photon limit $Q^2 = 0$.

Because of this practical limitation, the Siegert Theorem, already derived in the 1930s, give a powerful constraint for longitudinal form factors. In the long-wavelength limit, where $k \rightarrow 0$, all three components of the e.m. current become identical, $J_x = J_y = J_z$, because of rotational symmetry. As a consequence, excitations as $N \rightarrow \Delta(1232)3/2^+$ or $N \rightarrow N(1535)1/2^-$ obtain charge form factors that are proportional to the electric form factors. For the $N \rightarrow N(1440)1/2^+$ transition, where no electric form factor exists, still a minimal constraint remains, namely

$$S_{1/2}(Q^2) \sim k(Q^2), \tag{7}$$

forcing the longitudinal helicity form factor to vanish at the pseudo-threshold. This is a requirement for all $S_{1/2}$ transition form factors to any nucleon resonance. In Fig. 3 the longitudinal transition form factor for the Roper resonance transition is shown. Different model predictions are compared to previous data of the JLab-CLAS analysis and a new data point measured at MAMI-A1 for $Q^2 = 0.1\,\text{GeV}^2$ [5]. Only the MAID prediction comes close to the new measurement because of the build-in constraint from the Siegert theorem.

The study of baryon resonances is still an exciting field in hadron physics. With the partial wave analyses from MAID and the JLab group of electroproduction data a series of transition form factors has been obtained in the space-like region. We have shown that with the help of the long-wavelength limit (Siegert Theorem) extrapolations to the time-like region can be obtained satisfying minimal constraints at the pseudo-threshold. In this time-like region, Dalitz decays in the process $N\pi \rightarrow N^*/\Delta \rightarrow Ne^+e^-$ can be measured and time-like form fac-
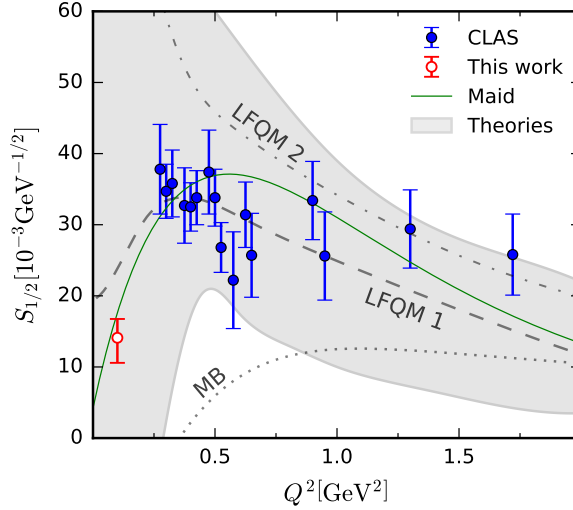
Fig. 3. Longitudinal transition form factor $S_{1/2}(Q^2)$ for the transition from the proton to the Roper resonance. The figure and the red exp. data point at $Q^2 = 0.1$ GeV^2 are from Štajner et al. [5], the blue data points are from the CLAS collaboration. The MAID model prediction which satisfies the Siegert's Theorem in the time-like region is in very good agreement with the new data point. For further details, see Ref. [5].

tors can be analyzed experimentally. Such experiments are already in progress at HADES@GSI and are also planned with the new FAIR facility at GSI.

References

1. L. Tiator, D. Drechsel, S. S. Kamalov and M. Vanderhaeghen, Eur. Phys. J. ST **198**, 141 (2011).
2. I. G. Aznauryan and V. D. Burkert, Prog. Part. Nucl. Phys. **67**, 1 (2012).
3. D. Drechsel, S. S. Kamalov, and L. Tiator, Eur. Phys. J. A **34** (2007) 69; https://maid.kph.uni-mainz.de/.
4. R. A. Arndt, I. I. Strakovsky, R. L. Workman, Phys. Rev. **C53** (1996) 430-440; (SP99 solution of the GW/SAID analysis); http://gwdac.phys.gwu.edu/.
5. S. Štajner *et al.*, Phys. Rev. Lett. **119**, no. 2, 022001 (2017).

Mathematical aspects of phase rotation ambiguities in partial wave analyses

Y. Wunderlich

Helmholtz-Institut für Strahlen- und Kernphysik, Universität Bonn, Nussallee 14–16, 53115 Bonn, Germany

Abstract. The observables in a single-channel 2-body scattering problem remain invariant once the amplitude is multiplied by an overall energy- and angle-dependent phase. This invariance is known as the continuum ambiguity. Also, mostly in truncated partial wave analyses (TPWAs), discrete ambiguities originating from complex conjugation of roots are known to occur. In this note, it is shown that the general continuum ambiguity mixes partial waves and that for scalar particles, discrete ambiguities are just a subset of continuum ambiguities with a specific phase. A numerical method is outlined briefly, which can determine the relevant connecting phases.

1 Introduction

We assume the well-known partial wave decomposition of the amplitude $A(W, \theta)$ for a $2 \rightarrow 2$-scattering process of spinless particles

$$A(W, \theta) = \sum_{\ell=0}^{\infty} (2\ell + 1) A_\ell(W) P_\ell(\cos \theta). \tag{1}$$

The *data* out of which partial waves shall be extracted are given by the differential cross section, which is (ignoring phase-space factors)

$$\sigma_0(W, \theta) = |A(W, \theta)|^2. \tag{2}$$

Making a *complete experiment analysis* [1] for this simple example, we see that the cross section constrains the amplitude to a circle for each energy and angle: $|A(W, \theta)| = +\sqrt{\sigma_0(W, \theta)}$. Thus, one energy- and angle-dependent phase is in principle unknown when based on data alone. The other side of the medal in this case is given by the fact that the amplitude itself can be rotated by an arbitrary energy- and angle-dependent phase and the cross section does not change. This invariance is known as the *continuum ambiguity* [2]:

$$A(W, \theta) \rightarrow \tilde{A}(W, \theta) := e^{i\Phi(W, \theta)} A(W, \theta). \tag{3}$$

Another concept known in the literature on partial wave analyses is that of so-called *discrete ambiguities* [2–4]. Suppose the full amplitude $A(W, \theta)$ can be split

into a product of a linear-factor of the angular variable, for instance $\cos\theta$, and a remainder-amplitude $\hat{A}(W,\theta)$ [3]:

$$A(W,\theta) = \hat{A}(W,\theta)\,(\cos\theta - \alpha)\,. \tag{4}$$

This is generally the case whenever the amplitude is a polynomial (i.e. the series (1) is truncated), but it may also be possible for infinite partial wave models. Then, it is seen quickly that the cross section (2) is invariant under complex conjugation of the root α, which causes the discrete ambiguity

$$\alpha \longrightarrow \alpha^{*}\,. \tag{5}$$

Figure 1 shows a schematic illustration of the meaning of the terms *continuum*- vs. *discrete ambiguities*. In this proceeding, the purely mathematical mechanisms (3) and (5) are investigated. Of course, constraints from physics may reduce the amount of ambiguity encountered. For instance, unitarity is a very powerful constraint which, for elastic scatterings, leaves only one remaining non-trivial so-called *Crichton*-ambiguity [5]. This is believed to be true independent of any truncation-order L of the partial wave expansion [2]. However, in energy-regimes where the scattering becomes inelastic, so-called *islands of ambiguity* are known to exist [6].
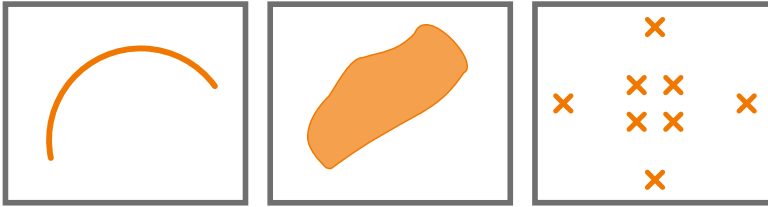
Fig. 1. Three schematic pictures are shown in order to distinguish the terms *discrete-* and *continuum* ambiguities. The grey colored box depicts in each case the higher-dimensional parameter-space composed by the partial wave amplitudes, be it for infinite partial wave models, or for truncated ones.
Left: One-dimensional (for instance circular) arcs can be traced out by continuum ambiguity transformations, both for infinite and truncated models.
Center: Connected continua in amplitude space, containing an infinite number of points with identical cross section, can be generated by use of angle-dependent rotations (3) (however, only in case the partial wave series goes to infinity). The connected patches are also called *islands of ambiguity* [2,6].
Right: Discrete ambiguities refer to cases where the cross section is the same for discretely located points in amplitude space. These ambiguities are most prominent in TPWAs [2,4]. However, two-fold discrete ambiguities can also appear for infinite partial wave models, once elastic unitarity is valid [2].
These figures have been published in reference [8].

Although here we focus just on the scalar example, ambiguities have become a topic of interest in the quest for so-called *complete experiments* in reactions with spin, for instance photoproduction of pseudoscalar mesons [1,7].

This proceeding is a briefer version of the more detailed publication [8]. The arXiv-reference [9] also treats very similar issues, as does the contribution of Alfred Švarc to these proceedings.

2   The effect of continuum ambiguity transformations on partial wave decompositions

We let the general transformation (3) act on $A(W, \theta)$ and assume a partial wave decomposition for the original as well as the rotated amplitude

$$A(W, \theta) \longrightarrow \tilde{A}(W, \theta) = e^{i\Phi(W, \theta)} A(W, \theta) = e^{i\Phi(W, \theta)} \sum_{\ell=0}^{\infty} (2\ell + 1) A_\ell(W) P_\ell(\cos \theta)$$

$$\equiv \sum_{\ell=0}^{\infty} (2\ell + 1) \tilde{A}_\ell(W) P_\ell(\cos \theta). \tag{6}$$

Out of the infinitely many possibilities to parametrize the angular dependence of the phase-rotation, the convenient choice of a Legendre-series is employed

$$e^{i\Phi(W, \theta)} = \sum_{k=0}^{\infty} L_k(W) P_k(\cos \theta). \tag{7}$$

In case this form of the rotation is inserted into the partial wave projection integrals of the general rotated waves $\tilde{A}_\ell$ (cf. equation (6)), the following *mixing formula* emerges [10]

$$\boxed{\tilde{A}_\ell(W) = \sum_{k=0}^{\infty} L_k(W) \sum_{m=|k-\ell|}^{k+\ell} \langle k, 0; \ell, 0 | m, 0 \rangle^2 A_m(W).} \tag{8}$$

Here, $\langle j_1, m_1; j_2, m_2 | J, M \rangle$ is just a usual Glebsch-Gordan coefficient.

Some more remarks should be made on the formula (8): first of all, although it's derivation is not difficult, this author has (at least up to this point) not found this expression in the literature, at least in this particular form. However, mixing-phenomena have been pointed out for πN-scattering [11] and for photoproduction [12].

Secondly, in can be seen quickly from the mixing formula that for angle-*in*dependent phases, i.e. when only the coefficient L_0 survives in the parametrization (7) of the rotation-functions, partial waves do not mix. Rather, in this case each partial wave is multiplied by $L_0(W) = e^{i\Phi(W)}$. However, once the phase $\Phi(W, \theta)$ carries even a weak angle-dependence, the expansion (7) directly becomes infinite and thus introduces contributions to an infinite partial wave set via the mixing-formula. There may be (a lot of) cases where the series (7) converges quickly and in these instances, it is safe to truncate the infinite equation-system (8) at some point.

It has to be stated that the mixing under very general continuum ambiguity transformations may lead to the mis-identification of resonance quantum numbers (reference [9] illustrates this fact on a toy-model example).

3   Discrete ambiguities as continuum ambiguity transformations

In case of a polynomial-amplitude, i.e. a truncation of the infinite series (1) at some finite cutoff L, the amplitude decomposes into a product of linear factors [4]

$$A(W, \theta) = \sum_{\ell=0}^{L} (2\ell + 1) A_\ell(W) P_\ell(\cos\theta) \equiv \lambda \prod_{i=1}^{L} (\cos\theta - \alpha_i), \qquad (9)$$

with a complex normalization proportional to the highest wave $\lambda \propto A_L(W)$. In case of a TPWA, one energy-dependent overall phase has to be fixed. This could be done, for instance, by choosing λ real and positive: $\lambda = |\lambda|$. Sometimes it is also customary to fix the phase of the S-wave.

Gersten [4] showed that discrete ambiguities in the TPWA can occur in case subsets of the roots $\{\alpha_i\}$ are complex conjugated. All combinatorial possibilities can be parametrized by a set of mappings $\boldsymbol{\pi}_p$, the number of which rises exponentially with L:

$$\boldsymbol{\pi}_p (\alpha_i) := \begin{cases} \alpha_i & , \mu_i (p) = 0 \\ \alpha_i^* & , \mu_i (p) = 1 \end{cases}, \ p = \sum_{i=1}^{L} \mu_i (p) \, 2^{(i-1)}, \ p = 0, \dots, (2^L - 1). \quad (10)$$

In case these maps are applied, they yield a set of 2^L polynomial-amplitudes, which all have identical cross section:

$$A^{(p)}(W, \theta) = \lambda \prod_{i=1}^{L} (\cos\theta - \boldsymbol{\pi}_p [\alpha_i]) \equiv \sum_{\ell=0}^{L} (2\ell + 1) A_\ell^{(p)}(W) P_\ell(\cos\theta). \qquad (11)$$

Since σ_0 is invariant under the discrete Gersten-ambiguities, these transformations can effectively only be rotations (because of $|A| = \sqrt{\sigma_0}$). More precisely, because one overall phase is fixed for all partial waves, discrete ambiguities can only be angle-dependent rotations. The corresponding rotation-functions are just fractions of two polynomial amplitudes

$$e^{i\varphi_p (W,\theta)} = \frac{A^{(p)}(W, \theta)}{A(W, \theta)} = \frac{(\cos\theta - \boldsymbol{\pi}_p [\alpha_1]) \dots (\cos\theta - \boldsymbol{\pi}_p [\alpha_L])}{(\cos\theta - \alpha_1) \dots (\cos\theta - \alpha_L)}. \qquad (12)$$

Therefore, discrete ambiguities mix partial waves, just as the general continuum ambiguities do. Furthermore, the expression on the right-hand-side of (12) is explicitly an infinite series in $\cos\theta$. Thus, one may expect an infinite tower of rotated partial waves $\tilde{A}_\ell$ to be non-vanishing upon consideration of the mixing-formula (8). However, in this case of course the rotation fine-tunes exact cancellations in the results of the mixing for all higher partial waves $\tilde{A}_{\ell > L}$.

Furthermore, Gersten [4] claims (without proof) that the root-conjugations *exhaust all possibilities* for discrete ambiguities of the TPWA. We have to state that we believe him.

The remainder of this proceeding is used to outline a numerical method that is *orthogonal* to the Gersten-formalism, but which can also substantiate this claim.

4   Functional minimizations show exhaustiveness of Gersten-ambiguities

We use the notation $x = \cos\theta$, introduce the complex rotation function $F(W, x) := e^{i\Phi(W,x)}$ and from now on drop the explicit energy W. The proposed numerical method assumes a truncated full amplitude $A(x)$ as a known input. Then, all possible functions $F(x)$ are scanned numerically for only those that satisfy the following two conditions:

(I) The complex solution-function $F(x)$ has to have modulus 1 for each value of x.

$$|F(x)|^2 = 1, \ \forall x \in [-1, 1]. \tag{13}$$

(II) The rotated amplitude $\tilde{A}(x)$, coming out of an amplitude $A(x)$ truncated at L, has to be truncated as well, i.e.

$$\tilde{A}_{L+k} = 0, \ \forall k = 1, \ldots, \infty. \tag{14}$$

Formally, this *scanning*-procedure can be implemented by minimizing a suitably defined *functional* of $F(x)$:

$$W[F(x)] := \sum_x \left(\text{Re}\,[F(x)]^2 + \text{Im}\,[F(x)]^2 - 1 \right)^2$$

$$+ \text{Im} \left[\frac{1}{2} \int_{-1}^{+1} dx\, F(x)A(x) \right]^2 + \sum_{k \geq 1} \left\{ \text{Re} \left[\frac{1}{2} \int_{-1}^{+1} dx\, F(x)A(x)P_{L+k}(x) \right]^2 \right.$$

$$\left. + \text{Im} \left[\frac{1}{2} \int_{-1}^{+1} dx\, F(x)A(x)P_{L+k}(x) \right]^2 \right\} \longrightarrow \min. \tag{15}$$

Here, the first term ensures the unimodularity of $F(x)$ (i.e. condition (I)), the second fixes a phase-convention on the S-wave $\tilde{A}_0$ and the big sum over k sets all higher partial wave of the rotated amplitude to zero.

   It has to be clear that for practical numerical applications, the sums over k and x have to be finite, i.e. the former is cut off and the latter is defined on a grid of x-values. Also, a general function $F(x)$ is defined by an infinite amount of real degrees of freedom, which has to be made finite as well.

   This can be achieved for instance by using a finite Legendre-expansion, i.e. a truncated version of equation (7) (with possibly large cutoff $\mathcal{L}_{\text{cut}}$), or by discretizing $F(x)$ on a finite grid of points $\{x_n\} \in [-1, 1]$. More details on the numerical minimizations can be found in reference [8].

   The only non-redundant solutions of this procedure are, in the end, the Gersten-rotation functions (12). Figures 2 to 5 illustrate this fact for the simple toy-model [8] (partial waves given in arbitrary units):

$$A(x) = \sum_{\ell=0}^{2} (2\ell + 1)A_\ell P_\ell(x) = A_0 + 3A_1 P_1(x) + 5A_2 P_2(x)$$

$$= 5 + 3(0.4 + 0.3\,i)x + \frac{5}{2}(0.02 + 0.01\,i)(3x^2 - 1). \tag{16}$$
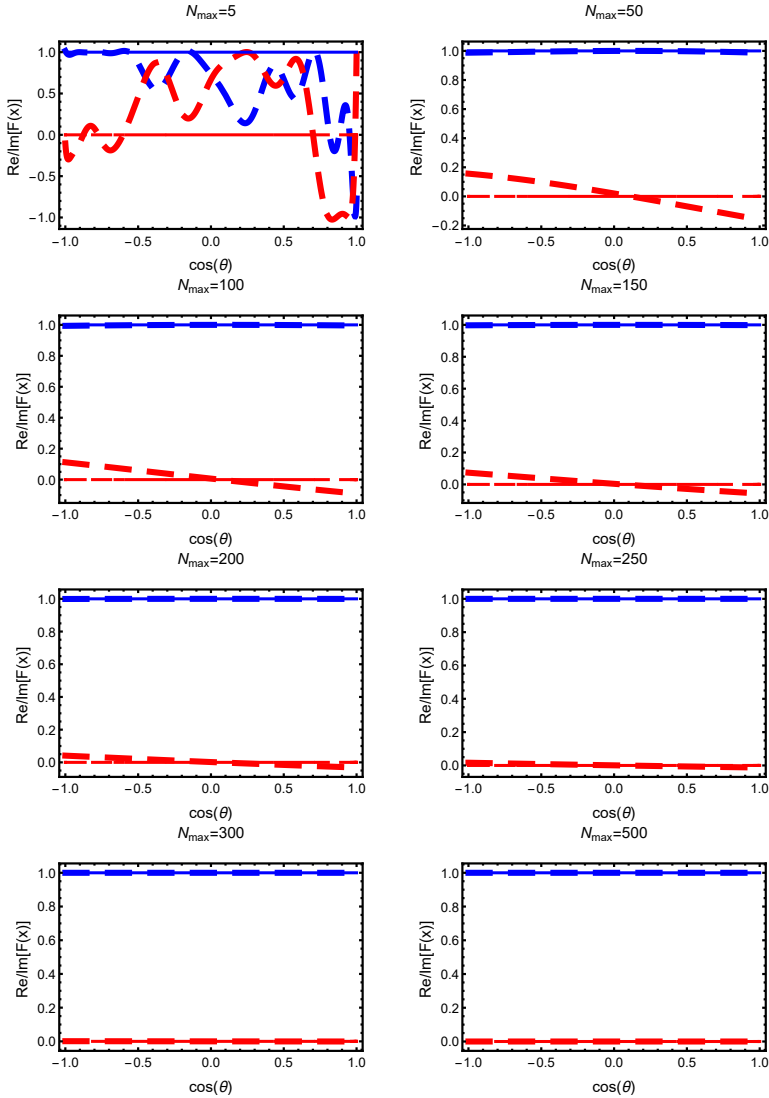
$$e^{i\varphi_0(x)}$$

Fig. 2. (Color online) The convergence of the functional minimization procedure is illustrated in these plots. For the discrete ambiguities $e^{i\varphi_0(x)}$ and $e^{i\varphi_1(x)}$ of the toy-model (16), two randomly drawn initial functions have been chosen from an applied ensemble of initial conditions in the search. These initial conditions then converged to these two respective Gersten-rotations. Results are shown for different values of the maximal number of iterations N_{max} of the minimizer, as indicated. Numbers range from $N_{max} = 5$ up to $N_{max} = 500$. In all plots, the real- and imaginary parts of the precise Gersten-ambiguity are drawn as blue and red solid lines. The results of the functional minimizations up to N_{max} are drawn as thick dashed lines, having the same color-coding for real- and imaginary parts (color online). These figures have already been published in reference [8].

$$e^{i\varphi_1(x)}$$
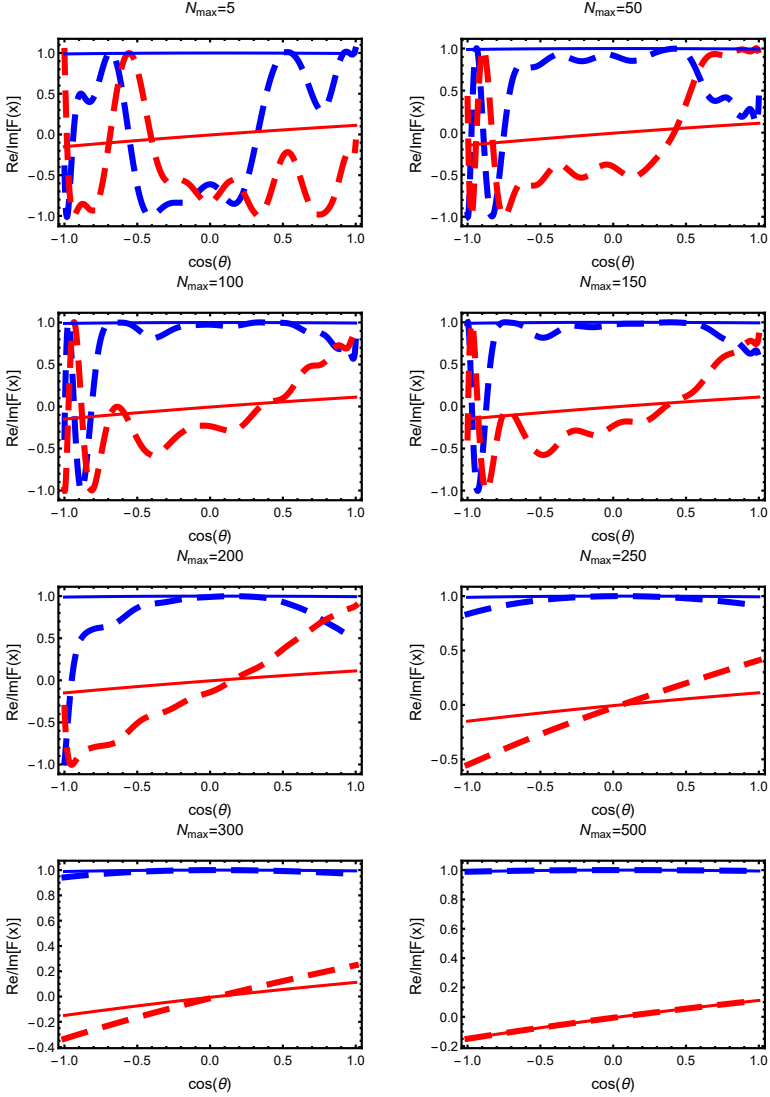
Fig. 3. These plots are the continuation of Figure 2. The convergence of the numerical minimization of the functional (15) is shown for the phase $e^{i\varphi_1(x)}$, which generates discrete ambiguities of the toy-model (16).
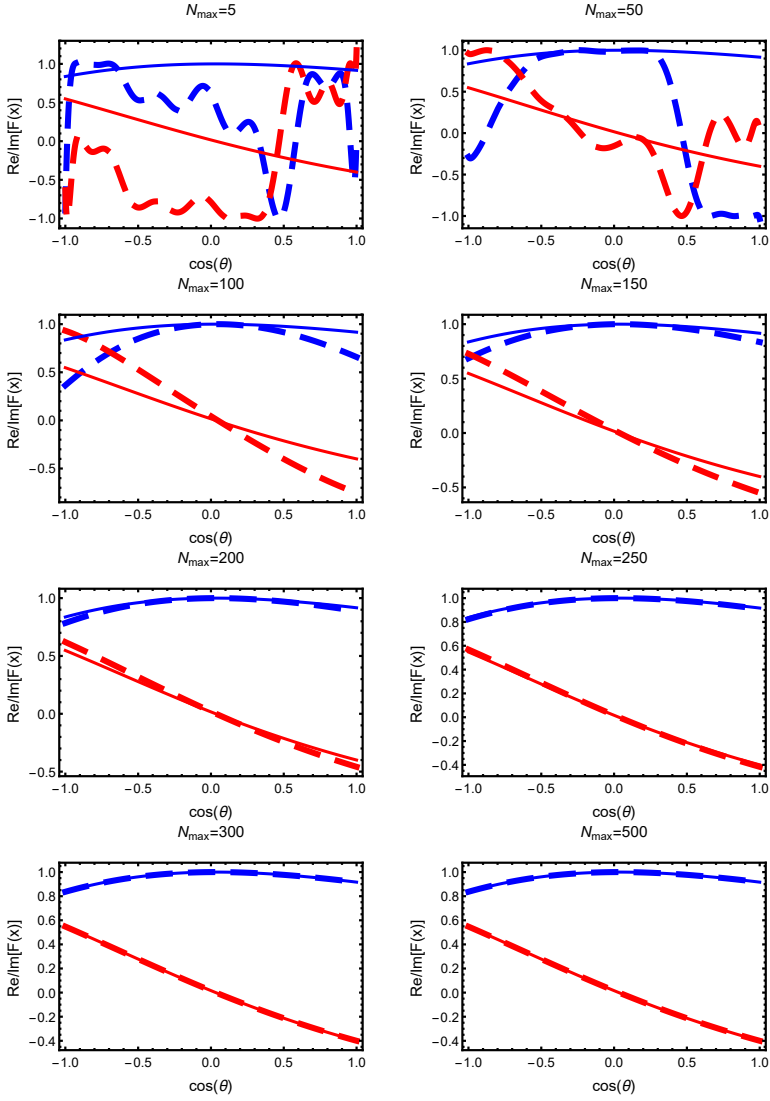
$$e^{i\varphi_2(x)}$$

Fig. 4. Same as before, but for the phase $e^{i\varphi_2(x)}$.
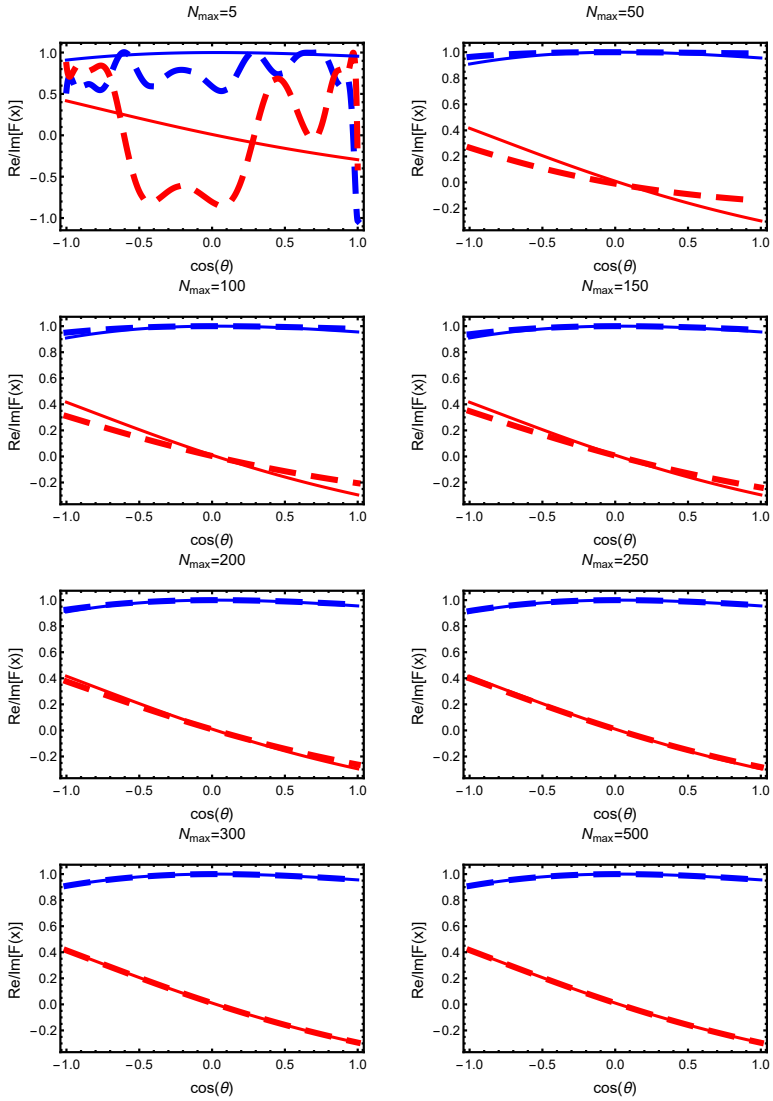
$$e^{i\varphi_3(x)}$$

Fig. 5. Same as before, but for the phase $e^{i\varphi_3(x)}$.

This model is truncated at L = 2. Thus it has two roots (α_1, α_2) and $2^2 = 4$ Gersten-ambiguities. The latter are generated by four phase-rotation functions: $e^{i\varphi_0(x)} = 1$, $e^{i\varphi_1(x)}$, $e^{i\varphi_2(x)}$ and $e^{i\varphi_3(x)}$. Figures 2 to 5 demonstrate the con-vergence-process of the functional minimization towards a particular Gersten-rotation, for very general initial functions. The fact that always one of the four Gersten-rotations is found is *in*dependent of the choice of the initial function.

5   Conclusions & Outlook

We have seen that general continuum ambiguity transformations, as well as dis-crete Gersten-ambiguities, are in the end manifestations of the same thing: angle-dependent phase-rotations. Therefore, they both mix partial waves.

The rotations belonging to the Gersten-symmetries have the following defin-ing property: they are the only rotations which, if applied to an original truncated model, leave the truncation order L untouched. In order to demonstrate this fact, a (possibly) new numerical method has been outlined capable of determining all continuum ambiguity transformations satisfying pre-defined constraints.

A possible further avenue of reserach may consist off the generalization of these findings to reactions with spin, for instance pseudoscalar meson photopro-duction. Here, the massive amount of new polarization data gathered over the last years have renewed interest in questions of the uniqueness of partial wave decompositions. However, once one transitions to the case with spin, some open issues still exist, as have already been discussed during the workshop.

References

1. R.L. Workman, L. Tiator, Y. Wunderlich, M. Döring, H. Haberzettl, Phys. Rev. C **95** no.1, 015206 (2017).
2. J. E. Bowcock and H. Burkhardt, Rep. Prog. Phys. **38**, 1099 (1975).
3. L.P. Kok., *Ambiguities in Phase Shift Analysis*,
   In ∗Delhi 1976, Conference On Few Body Dynamics∗, Amsterdam 1976, 43-46.
4. A. Gersten, Nucl. Phys. B **12**, p. 537 (1969).
5. J. H. Crichton, *Nuovo Cimento*, A **45**, 256 (1966).
6. D. Atkinson, L. P. Kok, M. de Roo and P. W. Johnson, Nucl. Phys. B **77**, 109 (1974).
7. Y. Wunderlich, R. Beck and L. Tiator, Phys. Rev. C **89**, no. 5, 055203 (2014).
8. Y. Wunderlich, A. Švarc, R. L. Workman, L. Tiator and R. Beck, arXiv:1708.06840 [nucl-th].
9. A. Švarc, Y. Wunderlich, H. Osmanović, M. Hadžimehmedović, R. Omerović, J. Stahov, V. Kashevarov, K. Nikonov, M. Ostrick, L. Tiator, and R. Workman, arXiv:1706.03211 [nucl-th].
10. One just has to use the re-expansion

$$P_k(x)P_\ell(x) = \sum_{m=|k-\ell|}^{k+\ell} \begin{pmatrix} k & l & m \\ 0 & 0 & 0 \end{pmatrix}^2 (2m+1)P_m(x)$$

$$= \sum_{m=|k-\ell|}^{k+\ell} \langle k,0;\ell,0|m,0 \rangle^2 P_m(x). \tag{17}$$

   For the first equality, see the reference:
   W. J. Thompson, *Angular Momentum*, John Wiley & Sons (2008).
   The second equality uses a well-known relation between 3j-symbols and Clebsch-Gordan coefficients.
11. N. W. Dean and P. Lee, Phys. Rev. D **5**, 2741 (1972).
12. A. S. Omelaenko, Sov. J. Nucl. Phys. **34**, 406 (1981).

Recent Belle Results on Hadron Spectroscopy

M. Bračko

University of Maribor, Smetanova ulica 17, SI-2000 Maribor, Slovenia and Jožef Stefan Institute, Jamova cesta 39, SI-1000 Ljubljana, Slovenia

Abstract. Recent results on hadron spectroscopy from the Belle experiment are reviewed in this contribution. Results are based on experimental data sample collected by the Belle detector, which was in operation between 1999 and 2010 at the KEKB asymmetric-energy e^+e^- collider in the KEK laboratory in Tsukuba, Japan. As a result of the size and quality of collected Belle experimental data, new measurements are still being performed now, almost a decade after the end of the Belle detector operation. Results from recent Belle publications on hadron spectroscopy, selected for this review, are within the scope of this workshop and reflect the interests of the participants.

1 Introduction

During its operation between 1999 and 2010, the Belle detector [1] at the asymmetric-energy e^+e^- collider KEKB [2] accumulated an impressive sample of data, corresponding to more than 1 ab^{-1} of integrated luminosity. The KEKB collider, called a *B Factory*, was operating mostly around the $\Upsilon(4S)$ resonance, but also at other Υ resonances, like $\Upsilon(1S)$, $\Upsilon(2S)$, $\Upsilon(5S)$ and $\Upsilon(6S)$, as well as in the nearby continuum [3]. With succesful accelerator operation and excellent detector performance, the collected experimental data sample was suitable for various measurements, including the ones in hadron spectroscopy, like discoveries of new charmonium(-like) and bottomonium(-like) hadronic states, together with studies of their properties.

2 Charmonium and Charmonium-like states

Around the year 2000, when the two B Factories started their operation [4], the charmonium spectroscopy was a well established field: the experimental spectrum of $c\bar{c}$ states below the $D\overline{D}$ threshold was in good agreement with theoretical prediction (see e.g. ref. [5]), and the last remaining $c\bar{c}$ states below the open-charm threshold were soon to be discovered [6].

2.1 The X(3872)-related news

However, the field experienced a true renaissance by discoveries of the so-called "XYZ" states—new charmonium-like states outside of the conventional charmo-

nium picture. This fascinating story began in 2003, when Belle collaboration reported on $B^+ \rightarrow K^+ J/\psi \pi^+ \pi^-$ analysis[1], where a new state decaying to $J/\psi \pi^+ \pi^-$ was discovered [7]. The new state, called X(3872), was confirmed by the CDF, DØ, *BABAR* collaborations [8], and later also by the LHC experiments [9]. The properties of this narrow state ($\Gamma = (3.0^{+1.9}_{-1.4} \pm 0.9)$ MeV) with a mass of (3872.2 ± 0.8) MeV, which is very close to the $D^0 \bar{D}^{*0}$ threshold [10], have been intensively studied by Belle and other experiments [11]. These studies determined the $J^{PC} = 1^{++}$ assignment, and suggested that the X(3872) state is a mixture of the conventional $2^3 P_1$ $c\bar{c}$ state and a loosely bound $D^0 \bar{D}^{*0}$ molecular state.

If one wants to better understand the structure of X(3872), further studies of production and decay modes for this narrow exotic state are necessary. A recent example of these experimental studies at Belle is the search for X(3872) production via the $B^0 \rightarrow X(3872) K^+ \pi^-$ and $B^+ \rightarrow X(3872) K^0_S \pi^+$ decay modes, where X(3872) decays to $J/\psi \pi^+ \pi^-$ [12]. The results, obtained on a data sample containing 772×10^6 $B\bar{B}$ events, show that $B^0 \rightarrow X(3872) K^*(892)^0$ does not dominate the $B^0 \rightarrow X(3872)(K^+ \pi^-)$ decay, which is in clear contrast to charmonium behaviour in the $B \rightarrow \psi(2S) K \pi$ case.

Another consequence of the $D^0 \bar{D}^{*0}$ molecular hypothesis of X(3872) is an existence of "X(3872)-like" molecular states with different quantum numbers. Searches for some of these states were performed in another recent Belle analysis [13], using final states containing the η_c meson. A state $X_1(3872)$, a $D^0 \bar{D}^{*0} - \bar{D}^0 D^{*0}$ combination with $J^{PC} = 1^{+-}$, and two states with $J^{PC} = 0^{++}$, X(3730) (combination of $D^0 \bar{D}^0 + \bar{D}^0 D^0$) and X(4014) (combination of $D^{*0} \bar{D}^{*0} + \bar{D}^{*0} D^{*0}$), were searched for. Additionally, neutral partners of the $Z(3900)^{\pm}$ [14] and $Z(4020)^{\pm}$ [15], and a poorly understood state X(3915) were also included in the search. No signal was observed in B decays to selected final states with the η_c meson for any of these exotic states, so only 90% confidence-level upper limits were set.

The interpretation of X(3872) being an admixture state of a $D^0 \bar{D}^{*0}$ molecule and a $\chi_{c1}(2P)$ charmonium state was also compatible with results of the recent Belle study of multi-body B decay modes with χ_{c1} and χ_{c2} in the final state, using the full Belle data sample of 772×10^6 $B\bar{B}$ events [16]. This study is important to understand the detailed dynamics of B meson decays, but at the same time these decays could be exploited to search for charmonium and charmonium-like exotic states in one of the intermediate final states such as $\chi_{cJ} \pi$ and $\chi_{cJ} \pi \pi$.

These recent results were already obtained with the complete Belle data sample, so more information about the nature of mentioned exotic states could only be extracted from the larger data sample, which will be available at the Belle II experiment [17].

2.2 Alternative $\chi_{c0}(2P)$ candidate

The charmonium-like state X(3915) was observed by the Belle Collaboration in $B \rightarrow J/\psi \omega K$ decays [18]; originally it was named Y(3940). Subsequently, it was

---

[1] Throughout the document, charge-conjugated modes are included in all decays, unless explicitly stated otherwise.

also observed by the *BABAR* Collaboration in the same B decay mode [19] and by both Belle and *BABAR* in the process $\gamma\gamma \to X(3915) \to J/\psi\omega$ [20]. The quantum numbers of the X(3915) were measured to be $J^{PC} = 0^{++}$, and as a result, the X(3915) was identified as the $\chi_{c0}(2P)$ in the 2014 PDG tables [21].

However, many properties of the X(3915) state were found to be inconsistent with this identification. For example, the $\chi_{c0}(2P) \to D\overline{D}$ decay mode is expected to be dominant, but has not yet been observed experimentally for the X(3915). Also, the measured X(3915) width of (20 ± 5) MeV is much smaller than expected $\chi_{c0}(2P)$ width of $\Gamma \gtrsim 100$ MeV [22]. A later reanalysis [23] of the data from Ref. [20] showed that both $J^{PC} = 0^{++}$ and 2^{++} assignments are possible. As a result of these considerations, the X(3915) was no longer identified as the $\chi_{c0}(2P)$ in the 2016 PDG tables [10]; and there was enough motivation for Belle Collaboration to perform an updated analysis of the process $e^+e^- \to J/\psi D\overline{D}$.

This latest analysis [24] used the 980 fb^{-1} data sample, collected at or near the $\Upsilon(1S)$, $\Upsilon(2S)$, $\Upsilon(3S)$, $\Upsilon(4S)$ and $\Upsilon(5S)$ resonances. In addition to this 1.4 times increased statistics with respect to previous measurement, a sophisticated multi-variate method was used to improve the discrimination of the signal and back-ground events, and an amplitude analysis was performed to study the J^{PC} quantum numbers of the $D\overline{D}$ system. As a result of this analysis, a new charmonium-like state, the $X^*(3860)$, was observed in the process $e^+e^- \to J/\psi D\overline{D}$. The mass of this state is determined to be (3862^{+26+40}_{-32-13}) MeV and its width is $(201^{+154+88}_{-67-82})$ MeV. The $X^*(3860)$ quantum number hypotheses $J^{PC} = 0^{++}$ and 2^{++} are compared using MC simulation. Monte Carlo pseudoexperiments are generated according to the fit result with the 2^{++} $X^*(3860)$ signal in data and then fitted with the 2^{++} and 0^{++} signals (see Figure 1). The $J^{PC} = 0^{++}$ hypothesis is favoured over the 2^{++} hypothesis at the level of 2.5σ.

The new state $X^*(3860)$ seems to be a better candidate for the $\chi_{c0}(2P)$ charmonium state than the X(3915): the measured $X^*(3860)$ mass is close to potential model prediction for the $\chi_{c0}(2P)$, while the preferred quantum numbers are $J^{PC} = 0^{++}$, although the 2^{++} hypothesis is not excluded.

2.3   Study of $J^{PC} = 1^{--}$ states using ISR

Initial-state radiation (ISR) has proven to be a powerful tool to search for $J^{PC} = 1^{--}$ states at B-factories, since it allows one to scan a broad energy range of $\sqrt{s}$ below the initial e^+e^- centre-of-mass (CM) energy, while the high luminosity compensates for the suppression due to the hard-photon emission. Three charmonium-like 1^{--} states were discovered at B factories via initial-state radiation in the last decade: the Y(4260) in $e^+e^- \to J/\psi\pi^+\pi^-$ [25,26], and the Y(4360) and Y(4660) in $e^+e^- \to \psi(2S)\pi^+\pi^-$ [27,28]. Together with the conventional charmonium states $\psi(4040)$, $\psi(4160)$, and $\psi(4415)$, there are altogether six vector states; only five of these states are predicted in the mass region above the DD threshold by the potential models [29]. It is thus very likely, that some of these states are not charmonia, but have exotic nature—they could be multiquark states, meson molecules, quark-gluon hybrids, or some other structures. In order to understand the structure and behaviour of these states, it is therefore necessary to study them in many decay channels and with largest possible data samples available.
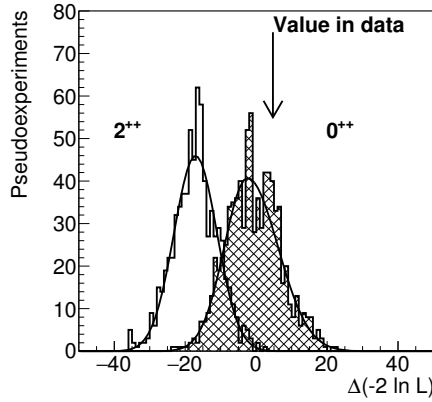
Fig. 1. Comparison of the 0^{++} and 2^{++} hypotheses in the default model (constant nonresonant amplitude). The histograms are distributions of $\Delta(-2\ln L)$ in MC pseudoexperiments generated in accordance with the fit results with 2^{++} (open histogram) and 0^{++} (hatched histogram) signals.

Recent paper from Belle collaboration [30] reports on the experimental study of the process $e^+e^- \to \gamma\chi_{cJ}$ (J=1, 2) via initial-state radiation using the data sample of 980 fb^{-1}, collected at and around the $\Upsilon(nS)$ (n=1, 2, 3, 4, 5) resonances. For the CM energy between 3.80 and 5.56 GeV, no significant $e^+e^- \to \gamma\chi_{c1}$ and $\gamma\chi_{c2}$ signals were observed except from $\psi(2S)$ decays, therefore only upper limits on the cross sections were determined at the 90% credibility level. Reported upper limits in this CM-energy interval range from few pb to a few tens of pb. Upper limits on the decay rate of the vector charmonium [$\psi(4040)$, $\psi(4160)$, and $\psi(4415)$] and charmonium-like [Y(4260), Y(4360), and Y(4660)] states to $\gamma\chi_{cJ}$ were also reported in this study (see Table 1). The obtained results could help in better understanding the nature and properties of studied vector states.

	χ_{c1} (eV)	χ_{c2} (eV)
$\Gamma_{ee}[\psi(4040)] \times \mathcal{B}[\psi(4040) \to \gamma\chi_{cJ}]$	2.9	4.6
$\Gamma_{ee}[\psi(4160)] \times \mathcal{B}[\psi(4160) \to \gamma\chi_{cJ}]$	2.2	6.1
$\Gamma_{ee}[\psi(4415)] \times \mathcal{B}[\psi(4415) \to \gamma\chi_{cJ}]$	0.47	2.3
$\Gamma_{ee}[Y(4260)] \times \mathcal{B}[Y(4260) \to \gamma\chi_{cJ}]$	1.4	4.0
$\Gamma_{ee}[Y(4360)] \times \mathcal{B}[Y(4360) \to \gamma\chi_{cJ}]$	0.57	1.9
$\Gamma_{ee}[Y(4660)] \times \mathcal{B}[Y(4660) \to \gamma\chi_{cJ}]$	0.45	2.1

Table 1. Upper limits on $\Gamma_{ee} \times \mathcal{B}(R \to \gamma\chi_{cJ})$ at the 90% C.L.

Initial-state radiation technique was also used in the new Belle measurement of the exclusive $e^+e^- \to D^{(*)\pm}D^{*\mp}$ cross sections as a function of the center-of-mass energy from the $D^{(*)\pm}D^{*\mp}$ threshold through $\sqrt{s} = 6.0$ GeV [31]. The

analysis is based on a Belle data sample collected with an integrated luminosity of 951 fb^{-1}. The accuracy of the cross section measurement is increased by a factor of two over the previous Belle study, due to the larger data set, the improved track reconstruction, and the additional modes used in the D and D* reconstruction. The complex shape of the $e^+e^- \rightarrow D^{*+}D^{*-}$ cross sections can be explained by the fact that its components can interfere constructively or destructively. The fit of this cross section is not trivial, because it must take into account the threshold and coupled-channels effects.

Finally, the first angular analysis of the $e^+e^- \rightarrow D^{*\pm}D^{*\mp}$ process was performed within this study, allowing the decomposition of the corresponding exclusive cross section into three possible components for the longitudinally, and transversely-polarized D$^{*\pm}$ mesons, as shown in Figure 2. The obtained components have distinct behaviour near the D^{*+}D^{*-} threshold. The only non-vanishing component at higher energy is the TL helicity of the D^{*+}D^{*-} final state. The measured decomposition allows the future measurement of the couplings of vector charmonium states into different helicity components, useful in identifying their nature and in testing the heavy-quark symmetry.
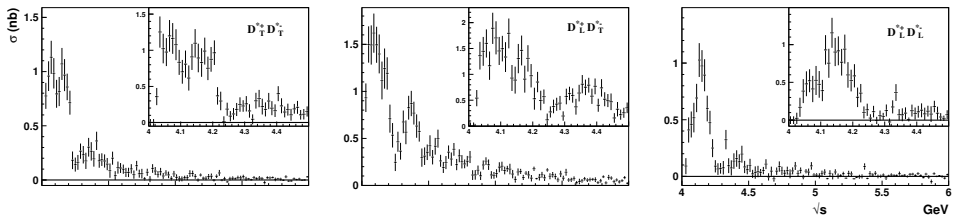

Fig. 2. The components of the $e^+e^- \rightarrow D^{*+}D^{*-}\gamma_{\text{ISR}}$ cross section corresponding to the different D$^{*\pm}$'s helicities. (The labels and units for the horizontal axis, common in all three cases, are shown only for the right plot.

3   Results on Charmed Baryons

Recently, a lot of effort in Belle has been put into studies of charmed baryons. Many of these analyses are still ongoing, but some of the results are already available. One example of such a result is the first observation of the decay $\Lambda_c^+ \rightarrow pK^+\pi^-$ using a 980 fb^{-1} data sample [32]. This is the first doubly Cabibbo-suppressed (DCS) decay of a charmed baryon to be observed, with statistical significance of 9.4 σ (fit results for invariant-mass distributions are shown in Figure 3). The branching fraction of this decay with respect to its Cabibbo-favoured (CF) counterpart is measured to be $\mathcal{B}(\Lambda_c^+ \rightarrow pK^+\pi^-)/\mathcal{B}(\Lambda_c^+ \rightarrow pK^-\pi^+) = (2.35 \pm 0.27 \pm 0.21) \times 10^{-3}$, where the uncertainties are statistical and systematic, respectively.

This year the results of the most recent baryon study were published [33]. In this study the inclusive production cross sections of hyperons and charmed
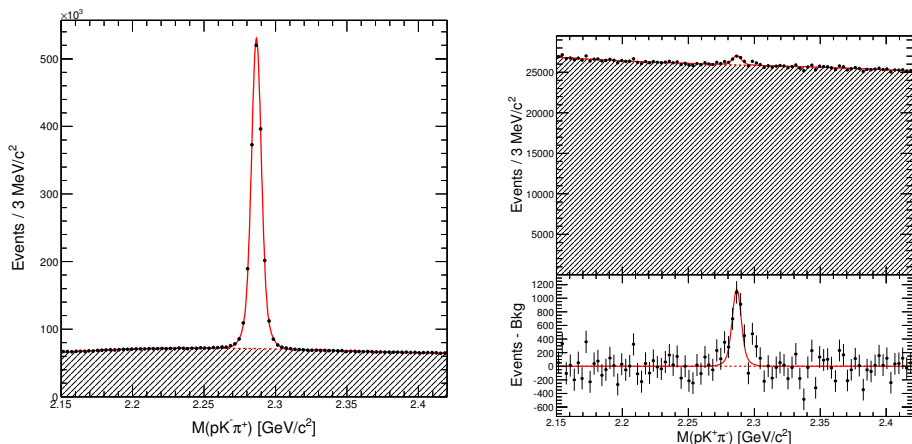
Fig. 3. Invariant mass distributions for the Λ_c^+ candidates: $M(pK^-\pi^+)$ for the CF decay mode (left) and $M(pK^+\pi^-)$ for the DCS decay mode (right, top). In the DCS case the distribution after the combinatorial-background subtraction is also shown (right, bottom). The curves indicate the fit result: the full fit model (solid) and the combinatorial background only (dashed).

.

baryons from e^+e^- annihilation were measured. The analysed sample corresponds to 800 fb^{-1} of Belle data collected around the $\Upsilon(4S)$ resonance. The feed-down contributions from heavy particles were estimated and subtracted, using the measured data. The direct production cross sestions of hyperons and charmed baryons were thus measured and presented for the first time (see Figure 4).

The production cross sections divided by the spin multiplicities for $S = -1$ hyperons follow an exponential function with a single slope parameter except for the $\Sigma(1385)^+$ resonance. A suppression for $\Sigma(1385)^+$ and $S = -2, -3$ hyperons is observed, which is likely a consequence of decuplet suppression and strangeness suppression in the fragmentation process. The production cross sections of charmed baryons are significantly higher than those of excited hyperons, and strong suppression of Σ_c with respect to Λ_c^+ is observed. The ratio of the production cross sections of Λ_c^+ and Σ_c is consistent with the difference of the production probabilities of spin-0 and spin-1 diquarks in the fragmentation process. This observation supports the theory that the diquark production is the main process of charmed baryon production from e^+e^- annihilation, and that the diquark structure exists in the ground state and low-lying excited states of Λ_c^+ baryons.

4   Summary and Conclusions

Many new particles have already been discovered during the operation of the Belle experiment at the KEKB collider, and some of them are mentioned in this report. Although the operation of the experiment finished almost a decade ago,
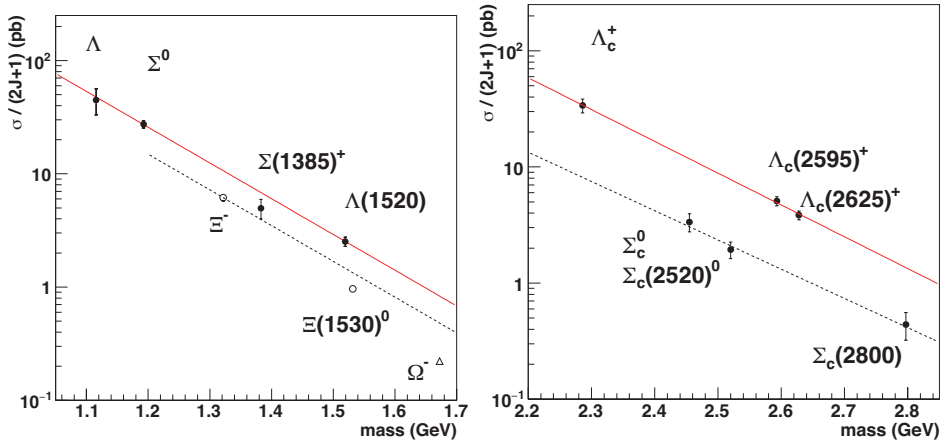
Fig. 4. Scaled direct production cross section as a function of mass of hyperons (left) and charmed baryons (right). S = −1, −2, −3 hyperons are shown with filled circles, open circles and a triangle, respectively.

data analyses are still ongoing and consequently more interesting results on charmonium(-like), bottomonium(-like) and baryon spectroscopy can still be expected from Belle in the near future. The results are eagerly awaited by the community and will be widely discussed at various occasions, in particular at workshops and conferences.

Still, the era of the Belle experiment is slowly coming to an end. Further progress towards high-precision measurements—with possible experimental surprises — in the field of hadron spectroscopy are expected from the huge experimental data sample, which will be collected in the future by the Belle II experiment [17]. This future might actually start soon, since the Belle II detector begins its operation early next year.

References

1. Belle Collaboration, *Nucl. Instrum. Methods* A **479**, 117 (2002).
2. S. Kurokawa and E. Kikutani, *Nucl. Instrum. Methods* A **499**, 1 (2003), and other papers included in this Volume.
3. J. Brodzicka *et al.*, *Prog. Theor. Exp. Phys.* , 04D001 (2012).
4. A. J. Bevan *et al.*, *Eur. Phys. J.* C **74**, 3026 (2014).
5. M. B. Voloshin, *Prog. Part. Nucl. Phys.* **61**, 455 (2008).
6. Belle Collaboration, *Phys. Rev. Lett.* **89**, 102001 (2002); Cleo Collaboration, *Phys. Rev. Lett.* **95**, 102003 (2005).
7. Belle Collaboration, *Phys. Rev. Lett.* **91**, 262001 (2003).
8. CDF Collaboration, *Phys. Rev. Lett.* **93**, 072001 (2004); DØ Collaboration, *Phys. Rev. Lett.* **93**, 162002 (2004); *BABAR* Collaboration, *Phys. Rev.* D **71**, 071103 (2005).
9. LHCb Collaboration, *Eur. Phys. J.* C **72**, 1972 (2012); CMS Collaboration, *J. High Energy Phys.* **04**, 154 (2013).
10. C. Patrignani *et al.* (Particle Data Group), *Chin. Phys. C* **40**, 100001 (2016).

11. Belle Collaboration, *Phys. Rev.* D **84**, 052004(R) (2011); CDF Collaboration, *Phys. Rev. Lett.* **103**, 152001 (2009); LHCb Collaboration, *Phys. Rev. Lett.* **110**, 222001 (2013).
12. Belle Collaboration, *Phys. Rev.* D **91**, 051101(R) (2015).
13. Belle Collaboration, *J. High Energy Phys.* **06**, 132 (2015).
14. Belle Collaboration, *Phys. Rev. Lett.* **110**, 252002 (2013); BESIII Collaboration, *Phys. Rev. Lett.* **110**, 252001 (2013); BESIII Collaboration, *Phys. Rev. Lett.* **112**, 022001 (2014); T. Xiao, S. Dobbs, A. Tomaradze and K. K. Seth, *Phys. Lett.* B **727**, 366 (2013).
15. BESIII Collaboration, *Phys. Rev. Lett.* **111**, 242001 (2013); *Phys. Rev. Lett.* **112**, 132001 (2014).
16. Belle Collaboration, *Phys. Rev.* D **93**, 052016 (2016).
17. Belle II Collaboration, Belle II Technical design report, [arXiv:1011.0352 [physics.ins-det]].
18. K. Abe *et al.* (Belle Collaboration), Phys. Rev. Lett. **94**, 182002 (2005).
19. B. Aubert *et al.* (*BABAR* Collaboration), Phys. Rev. Lett. **101**, 082001 (2008); P. del Amo Sanchez *et al.* (*BABAR* Collaboration), Phys. Rev. D **82**, 011101 (2010).
20. S. Uehara *et al.* (Belle Collaboration), Phys. Rev. Lett. **104**, 092001 (2010); J. P. Lees *et al.* (*BABAR* Collaboration), Phys. Rev. D **86**, 072002 (2012).
21. K. A. Olive *et al.* (Particle Data Group), Chin. Phys. C **38**, 090001 (2014).
22. F. K. Guo and U. G. Meissner, Phys. Rev. D **86**, 091501 (2012).
23. Z. Y. Zhou, Z. Xiao and H. Q. Zhou, Phys. Rev. Lett. **115**, 022001 (2015).
24. K. Chilikin *et al.* (Belle Collaboration), Phys. Rev. D **95**, 112003 (2017).
25. *BABAR* Collaboration, *Phys. Rev. Lett.* **95**, 142001 (2005); *Phys. Rev.* D **86**, 051102 (2012).
26. Belle Collaboration, *Phys. Rev. Lett.* **99**, 182004 (2007).
27. Belle Collaboration, *Phys. Rev. Lett.* **99**, 142002 (2007).
28. *BABAR* Collaboration, *Phys. Rev. Lett.* **98**, 212001 (2007); *Phys. Rev.* D **89**, 111103 (2014).
29. S. Godfrey and N. Isgur, *Phys. Rev.* D **32**, 189 (1985); T. Barnes, S. Godfrey and E. S. Swanson,*Phys. Rev.* D **72**, 054026 (2005); G. J. Ding, J. J. Zhu and M. L. Yan, *Phys. Rev.* D **77**, 014033 (2008).
30. Belle Collaboration, *Phys. Rev.* D **92**, 012011 (2015).
31. Belle Collaboration, arXiv:1707.09167 [hep-ex]; submitted to Phys. Rev. D.
32. Belle Collaboration, *Phys. Rev. Lett.* **117**, 011801 (2016).
33. Belle Collaboration, arXiv:1706.06791 [hep-ex]; submitted to Phys. Rev. D.

The Roper resonance – a genuine three quark or a dynamically generated resonance?

B. Golli

Faculty of Education, University of Ljubljana and Jožef Stefan Institute, 1000 Ljubljana, Slovenia

Abstract. We investigate two mechanisms for the formation of the Roper resonance: the excitation of a valence quark to the 2s state versus the dynamically generation of a quasi-bound meson-nucleon state. We use a coupled channel approach including the πN, πΔ and σN channels, fixing the pion-baryon vertices in the underlying quark model and using a phenomenological form for the s-wave sigma-baryon interaction. The Lippmann-Schwinger equation for the K matrix with a separable kernel is solved to all orders which results in the emergence of a quasi-bound state at around 1.4 GeV. Analysing the poles in the complex energy plane using the Laurent-Pietarinen expansion we conclude that the mass of the resonance is determined by the dynamically generated state, but an admixture of the $(1s)^2(2s)^1$ component is crucial to reproduce the experimental width and the modulus of the resonance pole.

This work has been done in collaboration with Simon Širca from Ljubljana, Hedim Osmanović from Tuzla and Alfred Švarc from Zagreb.

The recent results of lattice QCD simulation in the P11 partial wave by the Graz-Ljubljana group [1] including besides 3q interpolating fields also operators for πN in relative p-wave and σN in s-wave, has revived the interest in the nature of the Roper resonance. Their calculation and a similar calculation by the Adelaide group [2] show no evidence for a dominant 3q configuration below 1.65 GeV and 2.0 GeV, respectively, that could be interpreted as a three-quark Roper state, and therefore support the dynamical origin of the Roper resonance.

In our work [3] we study the interplay of the dynamically generated state and the three-quark resonant state in a simplified model incorporating the πN, πΔ and σN channels. The choice of the channels as well as of the parameters of the model is based on our previous calculations of the scattering and the meson photo- and electro-production amplitudes for several partial waves in which all relevant channels as well as most of the nucleon and Δ resonances in the intermediate energy regime have been included [5–9]. The bare octet-meson–baryon vertices are calculated in the Cloudy Bag Model while the parameters of the σ-baryon interaction are left free: apart of its strength, the Breit-Wigner mass and the width of the σ are varied. We have been able to consistently reproduce the results in the S and P partial waves; only the D waves typically require an increase in the strength of the meson-quark couplings compared to those predicted by the underlying quark model. The results presented here are obtained with the

σ mass and width both equal to 600 MeV, and only the σNN coupling is varied. Very similar results have been obtained for the mass and width of 500 MeV.

The central quantity in our approach is the half-on-shell K matrix[1] that consists of the resonant (pole) terms and the background (non-pole) term $\mathcal{D}$:

$$\chi_{\alpha\gamma}(k, k_\gamma) = \frac{V_{\gamma N}(k_\gamma)\, V_{\alpha N}(k)}{m_N - W} + \frac{V_{\gamma R}(k_\gamma)\, V_{\alpha R}(k)}{m_R - W} + \mathcal{D}_{\alpha\gamma}(k, k_\gamma)\,. \tag{1}$$

Indices α, β, γ ... denote the three channels, the first term corresponds to the nucleon pole, the second term is optional and generates an explicit resonance with the K-matrix pole at $W = m_R$. The Lippmann-Schwinger equation (LSE) for the K matrix splits into the equation for the dressed $N \to \alpha$ vertex,

$$\mathcal{V}_{\alpha N}(k) = V_{\alpha N}^{(0)}(k) + \sum_\beta \int dk' \, \frac{\mathcal{K}_{\alpha\beta}(k, k')\mathcal{V}_{\beta N}(k')}{\omega_\beta(k') + E_\beta(k') - W}\,, \tag{2}$$

and the equation for the background,

$$\mathcal{D}_{\alpha\delta}(k, k_\delta) = \mathcal{K}_{\alpha\delta}(k, k_\delta) + \sum_\beta \int dk' \, \frac{\mathcal{K}_{\alpha\beta}(k, k')\mathcal{D}_{\beta\delta}(k', k_\delta)}{\omega_\beta(k') + E_\beta(k') - W}\,. \tag{3}$$

If the resonant state is included, an equation analogous to (2) holds for the $R \to \alpha$ vertex. Let us note that the splitting of the K matrix is similar to the splitting used in approaches computing directly the T matrix, but is not equivalent. In the K-matrix approach the T matrix is obtained by solving the Heitler equation, $T = K + iKT$, which necessarily mixes the pole and the non-pole terms.

Our approximation consists of assuming a separable form for the kernel $\mathcal{K}_{\alpha\beta}$:

$$\mathcal{K}_{\alpha\beta}(k, k') = \sum_i \varphi_{\beta i}^\alpha(k)\, \xi_{\alpha i}^\beta(k')\,, \tag{4}$$

$$\varphi_{\beta i}^\alpha(k) = \frac{m_i}{E_\beta}\, (\omega_\beta + \varepsilon_{i\alpha}^\beta) \frac{V_{i\beta}^\alpha(k)}{\omega_\alpha(k) + \varepsilon_{i\beta}^\alpha}\, f_{\alpha\beta}^i\,,$$

$$\xi_{\alpha i}^\beta(k') = \frac{V_{i\alpha}^\beta(k')}{\omega_\beta(k') + \varepsilon_{i\alpha}^\beta}\,, \qquad \varepsilon_{i\alpha}^\beta = \frac{m_i^2 - m_\alpha^2 - \mu_\beta^2}{2E_\alpha}\,,$$

where i runs over intermediate N and Δ, f are the corresponding spin-isospin factors, $V_{i\beta}^\alpha$ corresponds to the decay of the baryon in channel β into the intermediate baryon and the meson in channel α, and m (E) and μ (ω) stand for the baryon and the meson mass (energy), respectively. $\mathcal{K}_{\alpha\beta}(k, k')$ reduces to the u-channel exchange potential when either k or k' takes its on-shell value. This type of approximation has been used in our previous calculations and has lead to consistent results. Let us mention that neglecting the integral terms in (2) and (3) corresponds to the so called K-matrix approximation.

---

[1] χ is proportional to the K matrix (satisfying $S = (1+iK)/(1-iK)$) by a kinematical factor which is not relevant for the present discussion.

Equation (2) and (3) can be solved exactly by the ansatz:

$$\mathcal{V}_{\alpha N}(k) = V_{\alpha N}^{(0)}(k) + \sum_{\beta i} x_{\beta i}^{\alpha} \, \varphi_{\beta i}^{\alpha}(k) \,, \tag{5}$$

$$\mathcal{D}_{\alpha\delta}(k) = \mathcal{K}_{\alpha\delta}(k, k_\delta) + \sum_{\beta i} z_{\beta i}^{\alpha\delta} \, \varphi_{\beta i}^{\alpha}(k) \,, \tag{6}$$

with coefficients x and z satisfying sets of algebraic equations of the form

$$\sum_{\gamma j} A_{\alpha i, \gamma j}^{\beta} \, x_{\gamma j}^{\beta} = b_{\alpha i}^{\beta} \,, \qquad \sum_{\gamma j} A_{\alpha i, \gamma j}^{\beta} \, z_{\gamma j}^{\beta\delta} = c_{\alpha i}^{\beta\delta} \,.$$

Note that both equations involve the same matrix $\mathsf{A} = \mathsf{I} + \mathsf{M}$, $\mathsf{M} = [M]_{\alpha i, \gamma j}^{\beta}$ where

$$M_{\alpha i, \gamma j}^{\beta} = -\int dk \, \frac{\xi_{\alpha i}^{\beta}(k) \varphi_{\gamma j}^{\beta}(k)}{\omega_\beta(k) + E_\beta(k) - W} \,. \tag{7}$$

For sufficiently strong interaction, the matrix A becomes singular and one or more poles appear in the background part of the K matrix which signals the emergence of a dynamically generated state. In fact, poles at the *same* energies appear also in the corresponding resonant terms of the K matrix, in addition to the nucleon pole and the (optional) pole at m_R. The mechanism of this process can be studied by performing the *singular value decomposition* $\mathsf{A} = \mathsf{U}\mathsf{W}\mathsf{V}^{\mathsf{T}}$ where W is a diagonal matrix containing the singular values w_i. The singular values remain close to unity with exception of one which approaches zero as the interaction increases (Fig. 1 a) and eventually becomes negative for sufficiently strong $g_{\sigma NN}$ (Fig. 2 a). We claim that it is this value, w_{min}, and the corresponding singular vector U_{min}, that determine the properties of the quasi-bound molecular state. This state is dominated by the σN component. For the invariant energies W for which w_{min} is close to zero, the solutions (5) and (6), in the absence of the resonant state R, can be cast in the form

$$\mathcal{V}_{\alpha N}(k_\alpha) \approx V_{\alpha N}^{(0)}(k_\alpha) + \frac{a_\alpha}{w_{min}} \,, \qquad \mathcal{D}_{\alpha\delta}(k_\alpha, k_\delta) \approx \mathcal{K}_{\alpha\delta}(k_\alpha, k_\delta) + \frac{d_{\alpha\delta}}{w_{min}} \,. \tag{8}$$

Similarly, the nucleon self energy acquires the form

$$\Sigma_N(W) = \sum_{\beta} \int dk \, \frac{\mathcal{V}_{\beta N}(k) V_{\beta N}^{(0)}(k)}{\omega_\beta(k) + E_\beta(k) - W} \approx (m_N - W) \left(\Sigma_N'(W) + \frac{b}{w_{min}} \right) . \tag{9}$$

Just above the πN threshold, the $\mathcal{D}$ term is dominated by the u-channel N exchange processes which is reflected in a large peak in ImT (the non-pole term in Fig. 1 b). This term has the opposite sign with respect to the nucleon-pole term; these two terms almost cancel each other. In the energy region where w_{min} reaches its minimum the second terms in (8) and (9) dominate and the leading contribution to the K matrix reads

$$K_{\alpha\delta} \approx \frac{a_\alpha a_\delta}{b} \frac{1}{(m_N - W) \, w_{min}} + \frac{d_{\alpha\delta}}{w_{min}} \,.$$

The two terms generate a resonance peak at the minimum of w_{min} (dashed-dotted line in Fig. 1 b); the real part, ReW_p, of the corresponding S-matrix pole in Table 1 appears slightly below W of the minimum of w_{min}. Increasing $g_{\sigma NN}$, w_{min} crosses zero twice and two poles of the S-matrix appear with ReW_p close to the intersections (see Fig. 1 a and Table 1 for $g_{\sigma NN} = 2.05$).

If we include the resonant state by imposing a fixed value for m_R in the second term of (1), the position of the peak almost does not change for a value of m_R as low as 1530 MeV (solid line in Fig. 1 b). The effect of the resonant state is reflected in the increased width of the resonance rather than in the change of its position. This general scenario does not change if we decrease $g_{\pi NN}$ in order to reproduce the experimental values of ReT and ImT (Fig. 2 b). While the peak in ImT moves to somewhat higher W, the position of the minimum of w_{min} as well as of the real part of the S-matrix pole stay almost at the same value (see Table 1). Also, varying the value of m_R between 1520 MeV and 2000 MeV has almost no influence on the behaviour of the amplitudes and the position of the S-matrix pole.
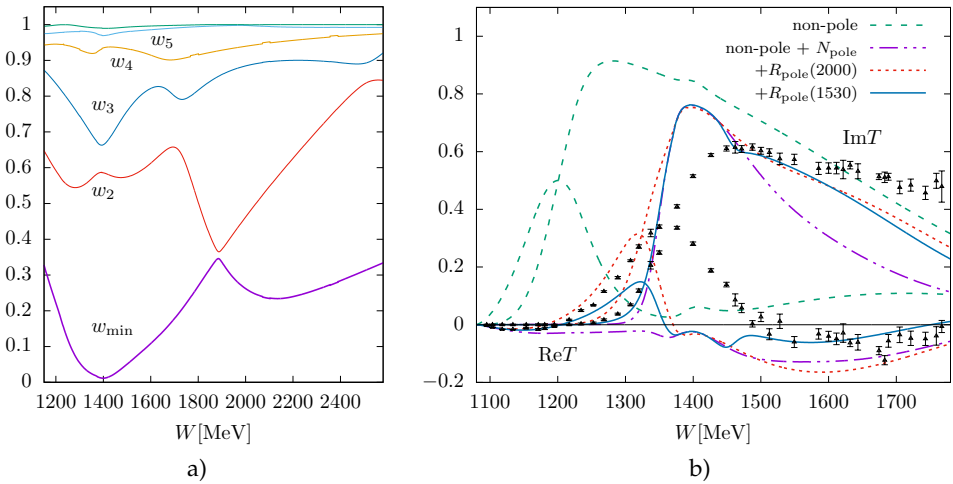
Fig. 1. (Color online) a) The six lowest singular eigenvalues of the A matrix for $g_{\sigma NN} = 2.0$. b) The real and imaginary parts of the T matrix calculated from the background (non-pole) term alone (dashed lines), from the background plus the nucleon pole term (dash-dotted lines), and from including the resonant state either at $m_R = 1530$ MeV (solid lines), or at $m_R = 2000$ MeV (short-dashed lines) for $g_{\sigma NN} = 2.0$.

We can summarize the results obtained in our simplified model as follows:

- The main mechanism for the Roper resonance formation is the dynamical generation through a quasi-bound meson-baryon state around $W \approx 1400$ MeV dominated by the σN component. Its mass is rather insensitive to variations of the $g_{\pi NN}$ coupling.
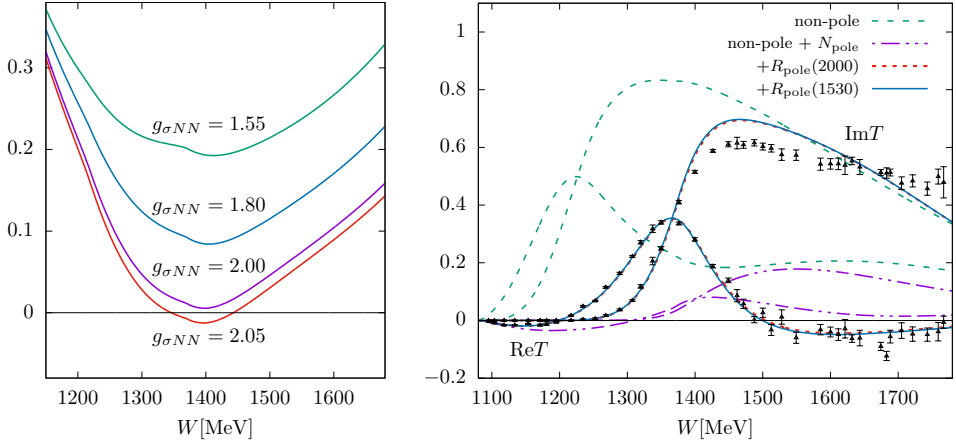
Fig. 2. (Color online) a) The lowest singular value of the W matrix, w_{min}, for four values of $g_{\sigma NN}$. b) Same as Fig. 1 b, except for $g_{\sigma NN} = 1.55$.

Table 1. S-matrix pole position and modulus for the model without the resonant state ($m_R = \infty$), and the model with the resonant state for two values of the K-matrix pole mass. The PDG values are taken from [10].

$g_{\sigma NN}$	m_R	ReW_p	$-2ImW_p$	$\lvert r \rvert$	ϑ
	[MeV]	[MeV]	[MeV]		
PDG		1370	180	46	$-90°$
1.80	∞	1397	157	11.2	$-78°$
2.00	∞	1358	111	20.6	$-81°$
2.05	∞	1331	44	7.3	$-62°$
		1438	147	18.6	$-17°$
2.00 $g_{\pi N\Delta} = 0$	∞	1342	285	18.8	$-11°$
1.55	2000	1368	180	48.0	$-87°$
1.55	1530	1367	180	47.5	$-86°$

- The real part of the S-matrix pole, ReW_p, remains close to or slightly below the mass of the quasi-bound state and is almost insensitive to the presence of a three-quark resonant state, while the PDG value of the imaginary part, ImW_p, is reproduced only if the three-quark resonant state is included.
- The S-matrix pole emerges with ReW_p close to the minimum of w_{min} even if (positive) w_{min} stays relatively far from zero; in this case the corresponding pole is not present in the K matrix.

- The mass of the quasi-bound molecular state is most strongly influenced by the σN component and lies ∼ 100 MeV below the nominal σN threshold; removing the πΔ component has little influence on the mass (see $g_{\pi N \Delta} = 0$ entry in Table 1).

References

1. C. B. Lang, L. Leskovec, M. Padmanath, S. Prelovšek, Phys. Rev. D **95**, 014510 (2017).
2. A. L. Kiratidis et al., Phys. Rev. D **95**, 074507 (2017).
3. B. Golli, H. Osmanović, S. Širca, and A. Švarc, arXiv:1709.09025 [hep-ph.]
4. P. Alberto, L. Amoreira, M. Fiolhais, B. Golli, and S. Širca, Eur. Phys. J. A **26**, 99 (2005).
5. B. Golli and S. Širca, Eur. Phys. J. A **38**, 271 (2008).
6. B. Golli, S. Širca, and M. Fiolhais, Eur. Phys. J. A **42**, 185 (2009).
7. B. Golli, S. Širca, Eur. Phys. J. A **47**, 61 (2011).
8. B. Golli, S. Širca, Eur. Phys. J. A **49**, 111 (2013).
9. B. Golli, S. Širca, Eur. Phys. J. A **52**, 279 (2016).
10. C. Patrignani et al. (Particle Data Group), Chin. Phys. C **40**, 100001 (2016) and 2017 update.

Possibilities of detecting the DD* dimesons at Belle2

Mitja Rosina

Faculty of Mathematics and Physics, University of Ljubljana, Jadranska 19, P.O. Box 2964, 1001 Ljubljana, Slovenia
and J. Stefan Institute, 1000 Ljubljana, Slovenia

Abstract. The double charm dimeson DD* represents a very interesting four-body problem since it is a delicate superposition of a molecular (dimeson) and an atomic (tetraquark) configuration. It is expected to be either weakly bound or a low resonance, depending on the model. Therefore it is a sensitive test how similar are the effective quark-quark interactions between heavy quarks and light quarks.

After the discovery of the $\Xi_{cc}^+ = ccd$ baryon at LHCb, there is a revived interest for the search of the double charm dimesons. There is, however, no such clear production and decay process available as it was for Ξ_{cc}^+. Therefore we argue that it is, compared to LHCb, a better chance for the discovery of the DD* dimeson at the upgraded Belle-2 at KEK (Tsukuba, Japan) after 2019.

1 Introduction

While the BB* dimeson (tetraquark) is expected to be strongly bound (>100 MeV) due to the smaller kinetic energy of the heavy quarks, the DD* dimeson is expected to be weakly bound (possibly at ~2 MeV) or a low resonance, depending on the model. Therefore it is a sensitive test of the effective quark-quark and quark-antiquark interactions. For example, can we assume Vuu = Vcu = Vcc = Vcū (apart from mass dependence of spin-dependent terms)?

There is no such clear production and detection process available for the DD* intermediate state as it was for Ξ_{cc}^+ which was recently discovered at LHCb analysing the resonant decay to $\Lambda_c^+ K^- \pi + \pi+$ where the Λ_c^+ baryon was reconstructed in the decay mode $pK^-\pi^+$.

Therefore we have started a study which production mechanism could enable the discovery of the DD* dimeson at the upgraded Belle-2 at KEK (Tsukuba, Japan) after 2019. For the time being, we summarize our old calculations of the DD* binding energy [1] and explain several tricky features of this interesting four-body system.

2 Comparison of charmed dimesons with the hydrogen molecule

It is interesting to compare the molecule of two heavy (charmed) mesons with the hydrogen molecule. At short distance, the two protons in the hydrogen molecule

are repelled by the electrostatic interaction, while the two heavy (charm) quarks in the mesonic molecule are attracted by the chromodynamic interaction because they can recouple their colour charges.
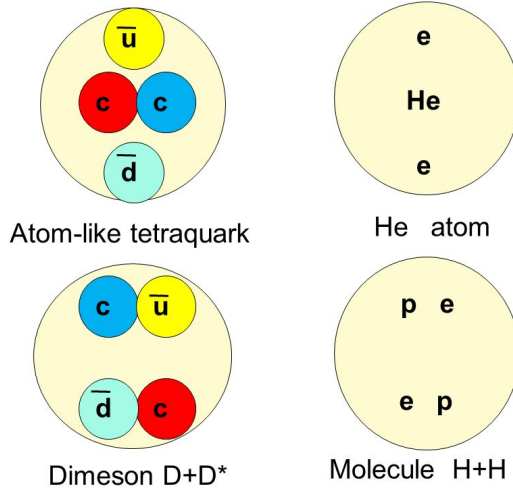

Fig. 1. Difference between atom-like and molecular configurations
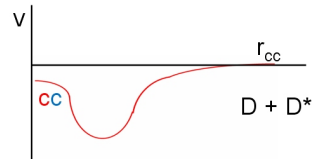
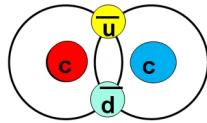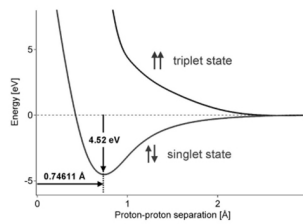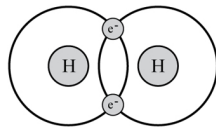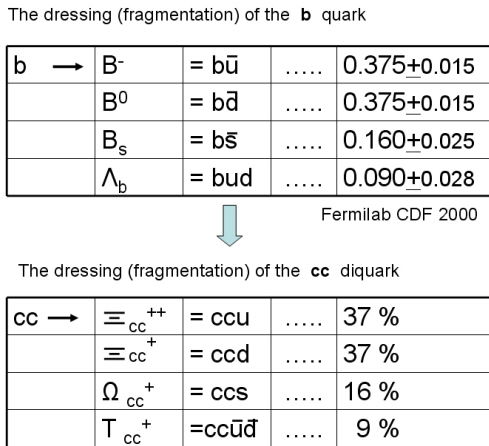**Fig. 2.**

3   Is the D+D̄* dimeson bound?

In the restricted 4-body space assuming "cc" in a bound diquark state and the u and d quarks in a general wavefunction, the energy is above the D+D* threshold. In the restricted "molecular" 4-body space with the two c quarks far apart and a general wavefunction of ū and d̄ (as assumed by several authors), the energy is also above the D+D* threshold. Only combining both spaces (we took a rich 4-body space) brings the energy below the threshold. We should verify whether it happens also for other interactions (we have used the one-gluon exchange+linear confinement [1]).

   We failed to calculate the energy of the hidden charm (charmonium-like) meson X(3872) using the same method and interaction as for DD* [2]. The reason is that a perfect variational calculation in a rather complete 4-body space finds the absolute minimum of energy which corresponds to J/psi+eta rather than DD̄∗. A demanding coupled channel calculation would be needed for a reliable result, and we have postponed it.

   It is an interesting question whether in the first step "cc" diquark is formed and later automatically dressed by u or d or ū and d̄ , or is the first step to form D + D* which merge into DD*. The later choice can profit from resonance formation, but due to the dense environment it is a danger that the D + D* system would again dissociate before really forming the dimeson. We intend to see which formalism would be appropriate for this.

The dressing (fragmentation) of the **b** quark

b $\longrightarrow$	B⁻	= bū	.....	$0.375{\pm}0.015$
	B⁰	= bd̄	.....	$0.375{\pm}0.015$
	B_s	= bs̄	.....	$0.160{\pm}0.025$
	Λ_b	= bud	.....	$0.090{\pm}0.028$

Fermilab CDF 2000

The dressing (fragmentation) of the **cc** diquark

cc $\longrightarrow$	Ξ_{cc}^{++}	= ccu	.....	37 %
	Ξ_{cc}^{+}	= ccd	.....	37 %
	Ω_{cc}^{+}	= ccs	.....	16 %
	T_{cc}^{+}	=ccūd̄	.....	9 %

Fig. 3. The estimated probability of formation of the atomic tetraquark configuration compared to the Ξ_{cc} production

   Once the "cc" diquark is formed, it is probably dressed with one light quark into the Ξ_{cc} baryon and only with about 9% probability into the "atomic" (cc)ūd̄ configuration. We have estimated this probability by analogy with the dressing of the b quark [3] into the Λ_b baryon compared to the production of B mesons (fig. 3). This percentage is further reduced by the evolution of the "atomic" configuration (cc)ūd̄ into the "molecular" configuration of DD*.

4 The decay of the DD* dimeson

The DD* dimeson is stable against a two-body decay into D+D due to its quantum numbers I=0, J=1. It can decay, however, strongly in D+D+π, or electromagnetically in D+D+γ, via the decay of D*. The strong decay is very slow (comparable to the electromagnetic decay) due to the extremely small phase space for the pion. Therefore, the DD* dimeson is "almost stable" and very suitable for detection.

We are looking for convenient methods of detection. One possibility is related to the small phase space of the pionic decay [1] (fig. 4). The ratio between the pionic and gamma decay will strongly depend on the binding or resonance energy of the dimeson.

Alternative suggestions are needed in order to have a reliable signature or tagging. We encourage the reader to come forth with new ideas!
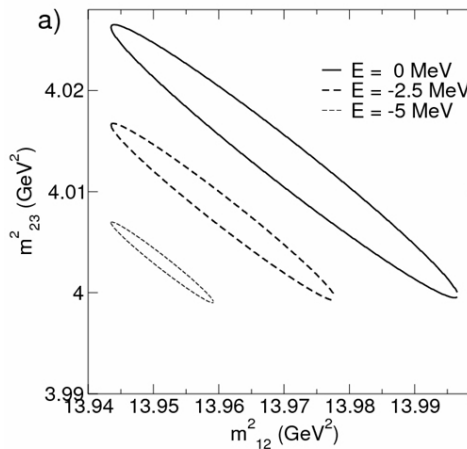
Fig. 4. Dalitz plot for the DD* decay depending on the binding or resonance energy; the area of the contours is proportional to the decay probability into pion

5 Conclusion

Considering a rather large production cross section of double $c\bar{c}$ pairs at Belle, we expect a sufficient production rate of **cc** diquarks which get dressed by a light quark into a Ξ_{cc} baryon. Once this expectation is verified, it is promising to search for the DD* dimesons, especially if they proceed via $cc + \bar{u} + \bar{d} \rightarrow (c\bar{u})(c\bar{d})$.

The motivation is twofold.

- Since the DD* dimeson is a delicate system, it is barely bound or barely unbound, it would distinguish between different models.
- Its production rate might help to understand the mechanism of the high production rate of double $c\bar{c}$ pairs at Belle.

Work is in progress to study different production and decay mechanisms in order to find a tell-tale signature in the decay products.

References

1. D. Janc and M. Rosina, Few-Body Systems **35** (2004) 175-196; also available at arXiv:hep-ph/0405208v2.
2. D. Janc, Bled Workshops in Physics **6**, No. 1 (2005) 92; also available at http://www-f1.ijs.si/BledPub.
3. T. Affolder et al. (CDF Collaboration), Phys. Rev. Lett. **84** (2000) 1663.

The study of the Roper resonance in double-polarized pion electroproduction

S. Širca[a,b]

[a] Faculty of Mathematics and Physics, University of Ljubljana, Jadranska 19, 1000 Ljubljana, Slovenia
[b] Jožef Stefan Institute, Jamova 39, 1000 Ljubljana, Slovenia

Investigations of the structure of the Roper resonance by using coincident electron scattering have been presented at several previous Mini-Workshops, and the most recent result on double-polarized pion electroproduction in the energy region of the Roper has recently been published [1]. This extended abstract is therefore just a reminder of the basic features of this experiment and just lists the highlights of that paper.

Our experimental study of the $p(e, e'p)\pi^0$ process was performed at the three spectrometer facility of the A1 Collaboration at the Mainz Microtron (MAMI). The kinematic ranges covered by our experiment were $W \approx (1440 \pm 40)\,\mathrm{MeV}$ for the invariant mass, $\theta_p^* \approx (90 \pm 15)^\circ$ and $\phi_p^* \approx (0 \pm 30)^\circ$ for the CM scattering angles and $Q^2 \approx (0.1 \pm 0.02)(\mathrm{GeV}/c)^2$ for the square of the four-momentum transfer.

We have extracted the two helicity-dependent recoil polarization components, P_x' and P_z', as well as the helicity-independent component P_y, and compared them to the values calculated by the state-of-the-art models MAID [2], DMT [3] and the partial-wave analysis SAID [4]. With the possible exception of P_y at high W which is reproduced by neither of the models, MAID is in very good agreement with the data, while DMT underestimates all three polarization components and even misses the sign of P_x'. The SAID analysis agrees less well with the P_x' data, while it exhibits an opposite trend in P_y and is completely at odds regarding P_z'. This might be a consequence of very different databases used in the analysis and calls for further investigations within these groups.

We were also able to determine the scalar helicity amplitude $S_{1/2}$ in a model-dependent manner. In contrast to its transverse counterpart, $A_{1/2}$, this amplitude is accessible only by electroproduction ($Q^2 \neq 0$) and becomes increasingly difficult to extract at small Q^2. This is a highly relevant kinematic region where many proposed explanations of the structure of the Roper resonance and mechanisms of its excitation give completely different predictions. This is also a region in which large pion-cloud effects are anticipated. In the most relevant region below $Q^2 \approx 0.5\,(\mathrm{GeV}/c)^2$ where quark-core dominance is expected to give way to

manifestations of the pion cloud — and where existing data cease — the predictions deviate dramatically.

Given that the agreement of our new recoil polarization data with the MAID model is quite satisfactory and that the transverse helicity amplitude $A_{1/2}$ is relatively much better known, we have performed a Monte Carlo simulation across the experimental acceptance to vary the relative strength of $S_{1/2}$ with respect to the best MAID value for $A_{1/2}$ and made a χ^2-like analysis with respect to our experimentally extracted P'_x, P_y and P'_z, of which P_y was the most convenient for the fit. Fixing $A_{1/2}$ to its MAID value and taking $S_{1/2}^{MAID}$ as the nominal best model value, we have been able to express $S_{1/2}$ from our fit as the fraction of $S_{1/2}^{MAID}$, yielding

$$S_{1/2} = \left(0.80^{+0.15}_{-0.20}\right) S_{1/2}^{MAID} = \left(14.1^{+2.6}_{-3.5}\right) \cdot 10^{-3} \mathrm{Ge}^{-1/2}\,.$$

This result is shown in Fig. 3 of Loather Tiator's contribution to these Proceedings.

References

1. S. Štajner et al., Phys. Rev. Lett. **119** (2017) 022001.
2. D. Drechsel, S. S. Kamalov, and L. Tiator, Eur. Phys. J. A **34** (2007) 69.
3. G. Y. Chen, S. S. Kamalov, S. N. Yang, D. Drechsel, and L. Tiator, Phys. Rev. C **76** (2007) 035206.
4. R. A. Arndt, W. J. Briscoe, M. W. Paris, and I. I. S. R. L. Workman, Chin. Phys. C **33** (2009) 1063.

Povzetki v slovenščini

Fotoprodukcija mezonov η in η′ z modelom EtaMAID upoštevajoč Reggejevo fenomenologijo

Viktor L. Kashevarov, Lothar Tiator, in Michael Ostrick

Institut für Kernphysik, Johannes Gutenberg-Universität, D-55099 Mainz, Germany

Predstavimo novo verzijo modela EtaMAID za fotoprodukcijo mezonov η in η′ na nukleonih. Model vsebuje 23 nukleonskih resonanc, ki jih opišemo z obliko Breita in Wignerja. Ozadje opišemo z izmenjavo vektorskih in aksialno-vektorskih mezonov v kanalu t upoštevajoč fenomenologijo Reggejevega reza. Parametri resonanc so bili prilagojeni znanim eksperimentalnim podatkom za fotoprodukcijo mezonov η in η′ na protonih in nevtronih. Razpravljamo o naravi najzanimivejših zapažanj.

Vloga nukleonske resonance pri asimetriji nevtronov, ki se gibljejo izrazito naprej pri trkih visokoenergijskih polariziranih protonov na jedrih

Itaru Nakagawa za kolaboracijo PHENIX

RIKEN, 2-1 Hirosawa, Wako, Saitama 351-0198, Japan

Odkrili smo presenetljivo močno odvisnost od mase pri enojni spinski asimetriji nevtronov, ki se gibljejo izrazito naprej pri trkih prečno polariziranih protonov na jedrih pri energiji 200 GeV pri eksperimentu PHENIX na pospeševalniku RHIC. Takšna drastična odvisnost prekaša vsa pričakovanja običajnih hadronskih interakcijskih modelov. Odvisnost asimetrije od mase smo skušali teoretično razložiti v okviru ultra perifernih trkov (efekt Primakoffa) z unitarnim izobarnim modelom (Mainz - MAID 2007). Računi dajo dobro ujemanje. Račune z elektromagnetno interakcijo potrjuje slika, skladna z znanimi asimetrijskimi rezultati pri procesu $p^{\uparrow} + Pb \rightarrow \pi^0 + p + Pb$ v Fermilabu.

Analiza delnih valov pri fotoprodukciji mezonov η pri dani energiji – ilustracija z namišljenimi podatki

H. Osmanović[1,*], M. Hadžimehmedović[1], R. Omerović[1], S. Smajić[1], J. Stahov[1], V. Kashevarov[2], K. Nikonov[2], M. Ostrick[2], L. Tiator[2] and A. Švarc[3]

[1] University of Tuzla, Faculty of Natural Sciences and Mathematics, Univerzitetska 4, 75000 Tuzla, Bosnia and Herzegovina
[2] Institut für Kernphysik, Johannes Gutenberg-Universität Mainz, D-55099 Mainz, Germany
[3] Rudjer Bošković Institute, Bijenička cesta 54, P.O. Box 180, 10002 Zagreb, Croatia

Z iterativnim postopkom kombiniramo analizo amplitud pri določenem t s konvencionalno analizo delnih valov pri določeni energiji na tak način, da rezultat ene analize služi kot omejitev pri drugi. Delovanje naše metode prikažemo na dobro definirani popolni zbirki namišljenih podatkov, ki smo jih proizvedli v okviru modela EtaMAID15.

Ločljivost gruč pri relativističnih problemih malo teles

Nikita Reichelt[1], Wolfgang Schweiger[1] in William H. Klink[2]

[1] Institute of Physics, University of Graz, A-8010 Graz, Austria,
[2] Department of Physics and Astronomy, University of Iowa, Iowa city, USA

Relativistična kvantna mehanika je prikladen okvir za obravnavo zgradbe in dinamike hadronov v območju energij več GeV. Drugače kot pri relativistični kvantni teorija polja zadošča tu določeno, ali vsaj omejeno, število prostostnih stopenj, da zagotovimo relativistično invarianco. Za sistem sodelujočih delcev to dosežemo s tako imenovano Bakamjian-Tomasovo konstrukcijo, ki sistematsko vgradi interakcijske člene v generatorje Poincaréjeve grupe, tako da se ohranja njihova algebra. Ta metoda pa se sooči s fizično zahtevo ločljivost gruč, čim imamo več kot dvs delca. Ločljivost gruč, včasih jo imenujejo tudi "makroskopska kavzalnost", pomeni, da se ločena podsistema na dovolj veliki razdalji obnašata avtonomno. V tem prispevku razpravljamo o tem problemu in nakažemo rešitev.

Analiza delnih valov pri fotoprodukciji mezonov η pri dani energiji – eksperimentalni podatki

J. Stahov[1,*], H. Osmanović[1,*], M. Hadžimehmedović[1], R. Omerović[1], V. Kashevarov[2], K. Nikonov[2], M. Ostrick[2], L. Tiator[2] and A. Švarc[3]

[1] University of Tuzla, Faculty of Natural Sciences and Mathematics, Univerzitetska 4, 75000 Tuzla, Bosnia and Herzegovina
[2] Institut für Kernphysik, Johannes Gutenberg-Universität Mainz, D-55099 Mainz, Germany
[3] Rudjer Bošković Institute, Bijenička cesta 54, P.O. Box 180, 10002 Zagreb, Croatia

Analiza delnih valov pri fotoprodukciji mezonov η brez omejitev, v enem kanalu, pri eni energiji vodi do nezveznosti v energiji. Zveznost od točke do točke dosežemo z zahtevo po analitičosti pri fiksnem t na modelsko neodvisen način z uporabo razpoložljivih eksperimentalnih podatkov in pokažemo, da dosedanja baza podatkov ne zadošča za enolično rešitev. Analitičost pri fiksnem t pri analizi amplitud s fiksnim t zagotovimo z metodo razvoja Pietarinena, ki je znana iz analize sipanja piona na nukleonu (Karlsruhe - Helsinki). Predstavimo analizo delnih valov z analitično omejitvijo za eksperimentalne podatke za štiri observable, ki so jih nedavno merili na pospeševalnikih MAMI in GRAAL v energijskem območju od praga do $\sqrt{s} = 1.85$ GeV.

Ekskluzivna fotoprodukcija pionov na vezanih nevtronih

Igor Strakovsky

The George Washington University, Washington, USA

Podan je bil pregled dejavnosti skupine GW SAID pri analizi fotoprodukcije pionov na nevtronski tarči. Razvozlanje izoskalarnih in izovektorskih elektromagnetnih sklopitev resonanc N* in Δ* zahteva sprejemljive podatke na obojnih, protonskih in nevtronskih tarčah. Interakcije med končnimi stanji igrajo kritično vlogo pri sodobni analizi reakcije γn → πN na devteronski tarči. Resonančne sklopitve smo določili z metodo SAID PWA in jih primerjali s prejšnimi izsledki. Reakcije na nevtronih predstavljajo znaten delež študij v laboratorijih JLab, MAMI-C, SPring-8, ELSA in ELPH.

Resonance in jakostne funkcije sistemov malo teles

Yasuyuki Suzuki

Department of Physics, Niigata University, Niigata 950-2181, Japan
and RIKEN Nishina Center, Wako 351-0198, Japan

Resonance nudijo preizkusni teren za dinamiko sistemov malo teles. Podrobno razpravljam o dveh tipih resonanc. Prva je ozka Hoylova resonanca v ^{12}C, ki igra bistveno vlogo pri sintezi ogljika v zvezdah. Drugi tip pa so široke, visoke resonance z negativno parnostjo pri jedrih z masnim številom 4: ^{4}H, ^{4}He in ^{4}Li. Pri prvem tipu je glavna coulombska sila treh delcev alfa na velikih razdaljah, pri drugem tipu pa imamo jedrske sile kratkega dosega. Strukturoteh resonanc opišem z različnimi pristopi, in sicer z adiabatsko hipersferično metodo in koreliranimi Gaussovimi funkcijam pri računih jakostnih funkcij. Resonance uspešno lokaliziramo s kompleksnim absorpcijskim potencialom, ozioma z metodo kompleksnega skaliranja.

Od modela neodvisna pot od eksperimentalnih podatkov do parametrov polov
(Večličnost kotne odvisnosti kontinuuma ter razvoj Laurenta in Pietarinena)

Alfred Švarc

Rudjer Bošković Institute, Bijenička cesta 54, P.O. Box 180, 10002 Zagreb, Croatia

Kot je znano, da neomejena analiza delnih valov z eno energijo mnogo enakovrednih nezveznih rešitev, zato rabimo omejitev povezano s primernim teoretičnim modelom. Če ne specificiramo kotne odvisnosti faze, ki povzroča večličnost kontinuuma, se mešajo multipoli; če pa izberemo fazo, rešimo enoličnost rešitve na modelsko neodvisen način. Doslej ni bilo zanesljive metode, kako izvleči parametre polov iz tako dobljenih delnih valov, vendar smo pred kratkim razvili novo preprosto metodo z enim kanalom (razvoj Laurenta in Pietarinena), ki je uporabna tako za zvezne kot diskretne podatke. Uporabimo Laurentov razvoj amplitude delnih valov, neresonantno ozadje pa razvijemo v potenčno vrsto za konformno preslikavo. Tako dobimo hitro konvergentno potenčno vrsto za preprosto analitično funkcijo z dobro definiranimi analitičnimi lastnostmi delnih valov, ki se ujemajo z vhodnimi podatki. Razvili smo tudi posplošitev na več kanalov. Če poenotimo obe metodi , lahko izpeljemo parametre polov neposredno iz eksperimentalnih podatkov brez sklicevanja na katerikoli model.

Prehodni oblikovni faktorji barionov od prostorskega pa do časovnega območja

Lothar Tiator

Institut für Kernphysik, Johannes Gutenberg-Universität Mainz, D-55099 Mainz, Germany

Predstavili smo razširitev neelastičnih oblikovnih faktorjev za foto- in elektroprodukcijo pionov na nukleonih iz območja negativnih kvadratov četvercev prenosa gibalne količine q^2 v območje s pozitivnih Q^2, vse tja do tako imenovanega psevdopraga. V teh kinematičnih režimih je mogoče določiti pomembne fizikalne omejitve za vijačnostne amplitude, ki sicer z neposredno meritvijo ne bi bile dostopne. S to metodo smo lahko nedavno določili tudi skalarno vijačnostno amplitudo $S_{1/2}$ za Roperjevo resonanco.

Matematične značilnosti večličnosti faznih zasukov pri analizah delnih valov

Yannick Wunderlich

Helmholtz-Institut für Strahlen- und Kernphysik, Universität Bonn, Germany

Observable pri sipanju dveh teles v enem kanalu se ne spremenijo, če pomnožimo amplitudo s skupno od energije in kota odvisno fazo. Ta invarianca je znana pod imenom večličnost kontinuuma. Poleg tega nastanejo znane diskretne večličnosti zaradi kompleksne konjugacije korenov, zlasti pri okrnjeni analizi delnih valov. V tem prispevku pokažem, da splošna večličnost kontinuuma meša delne valove in da so za skalarne delce diskretne večličnosti podmnožica kontinuumskih večličnosti s specifično fazo. Na kratko orišem numerično metodo, ki lahko določi ustrezne povezovalne faze.

Novejši rezultati spektroskopije hadronov pri eksperimentu Belle

Marko Bračko

Univerza v Mariboru, Smetanova ulica 17, 2000 Maribor, Slovenija
in Institut Jožef Stefan, Jamova cesta 39, 1000 Ljubljana, Slovenija

V tem prispevku so predstavljeni nekateri novejši rezultati spektroskopije hadronov pri eksperimentu Belle. Meritve so bile opravljene na vzorcu izmerjenih podatkov, ki ga je v času svojega delovanja – med letoma 1999 in 2010 – zbral eksperiment Belle, postavljen ob trkalniku elektronov in pozitronov KEKB, ki je obratoval v laboratoriju KEK v Cukubi na Japonskem. Zaradi velikosti vzorca in kakovosti izmerjenih podatkov lahko raziskovalna skupina Belle še sedaj, ko je od zaključka delovanja eksperimenta minilo že skoraj desetletje, objavlja rezultate novih meritev. Izbor novejših rezultatov, predstavljenih v tem prispevku, ustreza okviru delavnice in odraža zanimanje njenih udeležencev.

Roperjeva resonanca – trikvarkovsko ali dinamično tvorjeno resonančno stanje?

B. Golli

Pedagoška fakulteta, Univerza v Ljubljani, Ljubljana, Slovenija
in Institut J. Stefan, Ljubljana, Slovenija

Raziskujemo dva mehanizma za tvorbo Roperjeve resonance: vzbuditev valenčnega kvarka v orbitalo 2s v primerjavi z dinamično tvorbo kvazivezanega stanja mezona in nukleona. Uporabimo pristop sklopljenih kanalov s tremi kanali πN, $\pi\Delta$ in σN, pri čemer določimo v kvarkovskem modelu pionska vozlišča z barioni, za vozlišče z mezonom σ pa vzamemo fenomenološko obliko. Lippmann-Schwingerjevo enačbo s separabilnim jedrom za matriko K rešimo v vseh redih,

kar lahko vodi do nastanka kvazivezanega stanja v bližini 1.4 GeV. Pole v kompleksni energijski ravnini analiziramo z Laurent-Pietarinenovim razvojem in ugotovimo, da je masa resonance določena z dinamično tvorjenim stanjem, medtem ko je primes komponente $(1s)^2(2s)^1$ ključna za ujemanje z eksperimentalno določeno širino resonance in njenim modulom.

Možnosti za odkritje dimezona DD* na detektorju Belle2

Mitja Rosina

Fakulteta za matematiko in fiziko, Univerza v Ljubljani,
Jadranska 19, P.O.Box 2964, 1001 Ljubljana, Slovenija
in Institut Jožef Stefan, 1000 Ljubljana, Slovenija

Dvojno čarobni dimezon DD* predstavlja zelo zanimiv problem štirih teles, ker je občutljiva superpozicija molekularne (dimezonske) in atomske (tetrakvarkovske) konfiguracije. Pričakujemo, da je bodisi šibko vezan, bodisi nizka resonanca, kar je odvisno od modela. Zato je občutljivo merilo, koliko so si podobne efektivne interakcije med težkimi in lahkimi kvarki.

Po odkritju bariona $\Xi_{cc}^+ = ccd$ na velikem hadronskem trkalniku LHCb v CERNu je ponovno zaživelo zanimanje za iskanje dvojno čarobnih dimezonov. Žal pa ni na voljo tako očitnih procesov kot za produkcijo in razpad bariona Ξ_{cc}^+. Zato predlagamo, da so boljši izgledi za odkritje dimezona DD* na povečanem detektorju Belle-2 v laboratoriju KEK v Tsukubi na Japonskem, ko bodo stekle meritve leta 2019.

Študij Roperjeve resonance v dvojnopolarizirani elektroprodukciji pionov

Simon Širca

Fakulteta za matematiko in fiziko, Univerza v Ljubljani,
Jadranska 19, P.O.Box 2964, 1001 Ljubljana, Slovenija
in Institut Jožef Stefan, 1000 Ljubljana, Slovenija

Roperjeva resonanca in njena elektromagnetna struktura sodita med pomembne nerešene uganke sodobne hadronske fizike. Lastnosti tega najnižjega vzbujenega stanja nukleona z istimi kvantnimi števili so težko dostopne, saj je resonanca skrita pod velikim ozadjem sosednjih resonanc. V prispevku smo poročali o meritvi polarizacijskih komponent odrinjenega protona iz procesa $p(e, e'p)\pi^0$, in sicer od vijačnosti odvisnih P_x', P_z' ter od vijačnosti neodvisne P_y. Rezultate smo primerjali z modelskimi izračuni MAID, DMT in SAID ter ugotovili neujemanje zlasti pri slednjih dveh. Ob določenih modelskih privzetkih smo določili tudi skalarno vijačnostno amplitudo $S_{1/2}$.